DYNAMIC MODELING OF CEREBRAL BLOOD FLOW AUTOREGULATION USING ARX AND WINDKESSEL MODELS

PIYUSH GEHALOT

Presented to the Faculty of the Graduate School of

The University of Texas at Arlington in Partial Fulfillment

of the Requirements

for the Degree of

MASTER OF SCIENCE IN BIOMEDICAL ENGINEERING

THE UNIVERSITY OF TEXAS AT ARLINGTON

August 2005

DEDICATED TO MY FAMILY

ACKNOWLEDGEMENTS

I would like to express my sincere gratitude to Dr. Khosrow Behbehani, Professor and Chair, Department of Bioengineering at UTA, for providing me with the opportunity to work and for providing constant encouragement and timely guidance throughout this study.

I would also like to thank Dr. Rong Zhang, Assistant Professor, Internal Medicine – Cardiology Division, University of Texas Southwestern Medical Center at Dallas and Dr. Hanli Liu, Assistant Professor, Department of Bioengineering at UTA for helping me meet all the deadlines and providing valuable suggestions.

A special thanks to the volunteers who participated in this study. This study would not have been possible without their time and interest.

I would also like to thank Aby Mathew and my co-workers at the lab - Ganesh and Suhas for their kind co-operation. All the help and co-operation of faculty and staff of the Department of Bioengineering is also greatly appreciated.

And finally, I would like to thank my family in India for supporting me in every possible means. This would not have been possible without their and God's blessings.

July 25, 2005

ABSTRACT

DYNAMIC MODELING OF CEREBRAL BLOOD
FLOW AUTOREGULATION USING ARX
AND WINDKESSEL MODELS

Publication No. _____

Piyush Gehalot, M. S.

The University of Texas at Arlington, 2005

Supervising Professor: Khosrow Behbehani, Ph.D., P.E.

Linear lumped parameter models like ARX and Windkessel models are simple, easy to solve, and find their application in real time modeling. The present study is focused on employing single input single output ARX and Windkessel models to beat-to-beat mean arterial blood pressure (MABP, mmHg) considered as input to the model, and cerebral blood flow velocity (CBFV, cm/sec) considered as output of the model. For some models and modeling methodologies, the data consisted of cerebral perfusion pressure (CPP, mmHg, estimated from MABP) and CBFV. The data was measured from 10 healthy normal subjects while the subjects performed Valsalva maneuver with and without the ganglion blockade by the use of trimethaphan. The main objective of

this study was to examine the relative performance and limitations of the above mentioned linear modeling options and to demonstrate newer modeling methodologies for them. Also, since for linear model estimation it is required that the input be persistently exciting, the present study aimed to establish the efficacy of MABP for estimation of linear models and tested if a short data segment of 1.5 minute duration is adequate for the same, as compared to the traditional 6 minutes data.

Two ARX modeling schemes investigating up to 10^{th} order models, and three schemes for Windkessel modeling involving the 3-element model and four of its modified versions of 4 or 5 elements, were employed in the present study. Even though the study was not restricted to lower order systems or simple Windkessel models, results indicate that lower order ARX models (1^{st}, 2^{nd}, and 3^{rd} order ARX models) and the 3-element Windkessel model are adequate. Among the ARX and Windkessel methodologies, ARX modeling schemes proved more promising. The results of using CPP-CBFV data were not better than the results of using MABP-CBFV data.

It is clear that the models used for the present study had very basic mechanisms and structures, but were still able to reproduce the measured data. Also, tests involving the 1.5 minute MABP using the ARX models and results from the Monte-Carlo simulations of Windkessel models using two schemes suggest that a segment of 1.5 minute duration of MABP is effective and adequate for estimating linear models of cerebral autoregulation.

TABLE OF CONTENTS

LIST OF ILLUSTRATIONS

LIST OF TABLES

LIST OF ABBREVIATIONS

MABP……Mean Arterial Blood Pressure

CBFV……Cerebral Blood Flow Velocity

CBF……....Cerebral Blood Flow

CPP…… ....Cerebral Perfusion Pressure

VM…….....Valsalva Maneuver

HR…….....Heart Rate

MCA…… ..Middle Cerebral Artery

ECG…… ...Electrocardiogram

TCD…… ...Transcranial Doppler Ultrasonography

SNI…….....Spontaneous with No Infusion

SI…….....Spontaneous with Infusion

VNI…… ....Valsalva Maneuver with No Infusion

VI…….....Valsalva Maneuver with Infusion

MSE…… ...Mean Squared Error

FPE…… ....Final Prediction Error

FFT…… ....Fast Fourier Transform

SQP…… ....Sequential Quadratic Programming

PRBS……..Pseudo Random Binary Sequence

ICP……..Intracranial Pressure

CVP……Cerebral Venous Pressure

CHAPTER 1

INTRODUCTION

1.1 Cerebral Autoregulation

Autoregulation [3, 21] is the phenomenon wherein intrinsic, or "built-in", mechanisms within individual organs provide a localized regulation of vascular resistance and blood flow. Survival requires that the heart and brain receive an adequate supply of blood at all times. The brain is the organ that can least tolerate low rates of blood flow. Hence organs, like the brain in particular, utilize these intrinsic mechanisms to maintain relatively constant flow rates despite wide fluctuations in blood pressure. In normal range of arterial pressures, cerebral blood flow is regulated almost exclusively by autoregulation, achieved by both myogenic and metabolic mechanisms. Myogenic regulation occurs when there is variation in systemic arterial pressure. When the blood pressure falls, the cerebral arteries automatically dilate; when the pressure rises, they contract. These responses are myogenic, they are direct responses by the vascular smooth muscle and help to maintain a constant flow rate during the normal pressure variations that occur during rest, exercise, and emotional states. The myogenic regulation protects fine blood vessels in brain from being ruptured (causing cerebrovascular accident, or stroke). In metabolic regulation, the cerebral arterioles are exquisitely sensitive to local changes in metabolic activity, so that those brain regions

with the highest metabolic activity receive the most blood. The control mechanism in this case is a result of the chemical environment created by the organ's metabolism. Some of the localized chemical conditions that promote vasodilation are (1) decreased oxygen concentrations; (2) increased carbon dioxide concentrations; (3) decreased tissue pH; and (4) the release of adenosine or K^+ from the tissue cells [3]. Through these chemical changes brain signals its blood vessels of its need for increased oxygen delivery.

The cerebral autoregulation phenomenon has been well documented in animals and humans. The understanding of this phenomenon is essential for development of new strategies to prevent autonomic dysfunctions such as cognitive loss, falls, and syncope, which are major causes of morbidity and mortality in elderly people [16]. One of the means to study and analyze cerebral autoregulation is by identification of the temporal relationship between beat-to-beat changes in mean arterial blood pressure (MABP) and cerebral blood flow velocity (CBFV). Studies [18, 20, 25, 26, 28, 29, 30 and 44] of dynamic cerebral autoregulation have used different techniques to induce rapid changes in MABP. These include sudden deflation of thigh cuffs, Valsalva maneuvers, forced breathing, periodic squatting, or tilting of the whole body. Other investigations involved spontaneous fluctuations in MABP to observe corresponding transient changes in CBFV. There have been studies [13, 18, and 44] for evaluating the role of autonomic neural activity versus other non-neural factors in autoregulation by introducing ganglion blockade with trimethaphan, the infusion of which removes the autonomic neural control of dynamic autoregulation.

1.2 Valsalva Maneuver

Valsalva maneuver (VM) [3, 18, 19, 25, 26, 28, 29, and 30] is the term used to describe an expiratory effort against a closed glottis (which prevents the air from exiting the lungs) for at least 15 seconds by maintaining an expiratory pressure of approximately 30 mmHg. It is approximately 45 seconds long and is also known as Valsalva's test and Valsalva's method, after Antonio Maria Valsalva, a famous Italian anatomist. Figure 1.1 illustrates a Valsalva maneuver. The maneuver mimics commonly occurring events such as coughing, forceful defecation, or lifting of heavy weights. VM increases the intrathoracic pressure and causes the abdominal muscles to tighten up, squeezing the intestines and organs in abdominal cavity so that they press upward against the diaphragm, compressing the chest cavity even more. Contraction of thoracic cage compresses the lungs and causes a large rise in intrapleural pressure (the pressure measured in the space between the lungs and thoracic wall) from approximately -3 mmHg to >150 mmHg. This results in the compression of the thoracic veins which causes a fall in venous return and cardiac output, thus lowering arterial blood pressure. The lowering of arterial pressure then stimulates the baroreceptor reflex, resulting in tachycardia and increased total peripheral resistance. When the glottis is finally opened and the air is exhaled, the cardiac output returns to normal, however, the blood pressure is high as the total peripheral resistance is still elevated. The blood pressure is then brought back to normal by the baroreceptor reflex, which causes a slowing of the heart rate (HR).

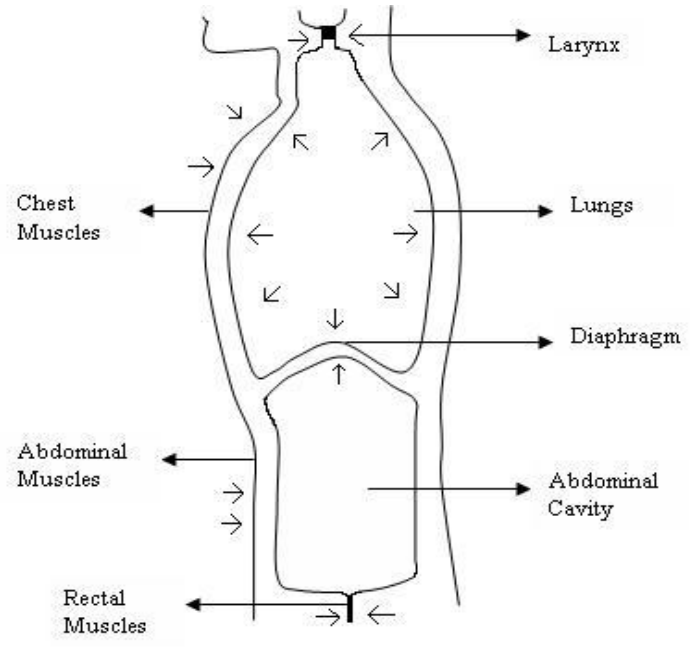

Figure 1.1 Valsalva maneuver

There are four recognized phases to VM. Figure 1.2 illustrates the four phases of the maneuver, with corresponding changes in MABP (mmHg), CBFV (cm/sec) and HR (beats per minute). Phase I is associated with the beginning of the strain (expiration with the nose and mouth closed) and a transient rise in MABP as the increase in intrathoracic pressure is transmitted to the arterial tree. During phase II_a, the atrial filling pressure falls so MABP decreases. In phase II_b there is increased sympathetic activation, causing a rise in peripheral vascular resistance, which leads to a small increase in MABP and HR. Phase III is associated with the release of the intrathoracic pressure influence (strain) on the arterial tree resulting in sudden fall in MABP. Finally, phase IV sees an immediate "overshoot" in MABP because of the persistence of increased sympathetic tone and systemic vascular resistance. A reflex bradycardia then

results due to stimulation of arterial baroreceptors, and both MABP and HR return to baseline values.

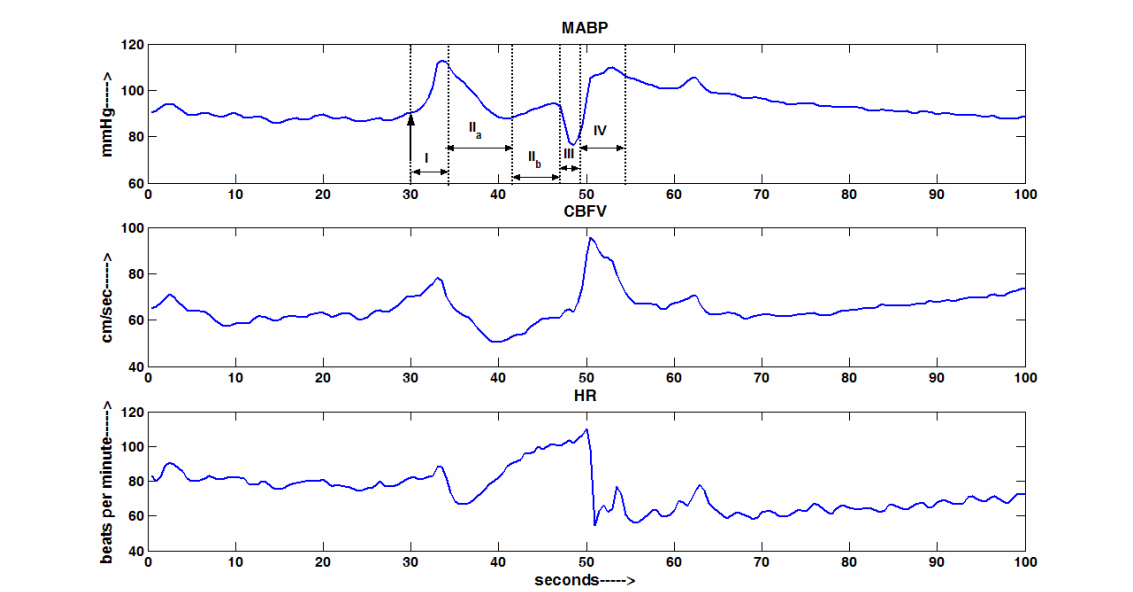

Figure 1.2 Phases (I through IV) associated with Valsalva maneuver shown in the mean arterial blood pressure (MABP) subplot. The vertical arrow indicates the onset of the maneuver. The corresponding cerebral blood flow velocity (CBFV) and heart rate (HR) changes are shown in the subsequent subplots.

VM is used as diagnostic tool to evaluate the condition of the heart and is done as a treatment to correct abnormal heart rhythms or relieve chest pain. It has been used as to test the integrity of autonomic function and may represent a dynamic challenge to the autoregulatory mechanisms of cerebral circulation. Changes in cerebral hemodynamics during the maneuver are mediated by both mechanical effects of the changes in intrathoracic pressure and the elicited autonomic neural activity. The differentiation between the mechanical effects and the autonomic effects has been done using ganglion blockade with trimethaphan, the infusion of which essentially removes the autonomic neural activity. The changes in cerebral hemodynamics during VM have

potentially significant clinical implications. If cerebral autoregulation is the process regulating CBFV during phase IV of the maneuver, then the rapid rise in MABP should be followed by a rapid rise in CBFV, which is quickly returned to baseline values by dynamic autoregulation, before MABP returns to normal (Figure 1.2). In case of patients with impaired autoregulation, the magnitude of MABP reduction during a routine VM (phases II_a and III) is substantially greater than in normal subjects. This would result in substantial reduction in CBFV which may ultimately lead to syncope. Such effects can be also be seen in studies [13, 18, and 44] introducing ganglion blockade by trimethaphan drug infusion for removal of the autonomic neural control of dynamic autoregulation.

1.3 Previous Studies Involving Human Cerebral Circulation and its Modeling

Physiological modeling and system identification is aimed towards a better understanding of the dynamics of various living systems. Modeling effort ranges from graphic depiction of physiological process to mathematical emulation of realistic living systems that unravels the mechanisms that underlie various complex physiological functions. Physiological modeling strives to create a framework that would help with the integration of experimental observations. A successful model also provides guidance to new experiments, which may modify or generalize the model in turn suggesting newer experiments.

In the context of human cerebral circulation under various pathophysiological conditions, several studies [9, 10, 11, 13, 15, 16, 18, 20, 21, 23, 24, 25, 26, and 29] have

been done to understand pressure-flow velocity relationships using non-parametric techniques such as transfer function analysis [5, 6, 12, and 44] using cross correlation techniques [4, 5]. Non-linear analysis and neural network modeling studies of dynamic cerebral autoregulation have also been conducted [7, 8]. Studies [28, 30, 41, 42, and 43] involving frequency-domain and time-domain analysis of CBFV and its correlation with MABP for assessing dynamics of autoregulation, developing indices for the degree and quality of autoregulation and deriving clinical and physiological implications for detection of autonomic dysfunction have all been well described and documented. There have also been investigations employing linear lumped parametric models such as autoregressive ARX models [11, 44] and various Windkessel models [16, 32]. These models relate MABP and CBFV data for characterizing the dynamics of cerebral blood flow regulation. It has been seen that even though treating the vasculature in this manner is a gross simplification of the system, lumped models have been shown to provide good results and have aided the understanding of physiological systems. Further more, there have been studies to test the validity and reliability of these models [35, 36, and 37].

1.4 Objectives and Overview of the Thesis

Lumped parameter models like ARX and Windkessel models are easy to solve, find their application in real time modeling where it is necessary to analyze data that include dynamic changes, and are simple enough to be implemented in a clinical setting. Windkessel models have an added advantage that they provide a model structure in terms of individual elements (resistors, capacitors, and inductors) of their

electrically analogous circuit. This makes it easier to extract the dynamic variation of each of the elements from the measured data. It may also be possible to interpret physiological changes with changes in the value of the elements.

The present study is focused on employing single input single output linear lumped parametric models (ARX and Windkessel) to the data collected from normal human subjects and computing the model parameters. The data consisted of beat-to-beat mean arterial blood pressure (MABP, mmHg) considered as input to the model, and cerebral blood flow velocity (CBFV, cm/sec) considered as output of the model. For some models and modeling methodologies, the data consisted of cerebral perfusion pressure (CPP, mmHg, estimated from MABP) and CBFV [18]. The measurement of the data from the subjects was done while the subjects were performing Valsalva maneuver with and without the use of trimethaphan for ganglion blockade, the infusion of which essentially removes the autonomic neural activity.

Referring to previous studies involving human cerebral circulation and its modeling in section 1.3, there have been no investigations in applying Windkessel models to cerebral autoregulation data in conjunction with Valsalva maneuver for ganglion blockade. Although there has been a previous study [44] involving ARX models, it was limited to second order models only. Also under the same context, one doesn't find a comprehensive comparison of the performance of various models and modeling techniques with respect to ARX models and Windkessel models. The main objective of this study was to examine the relative performance and limitations of the above mentioned linear modeling options and to demonstrate newer modeling

methodologies for them. All of these modeling methods rely on the assumption that the dynamic autoregulatory mechanism can be approximated by a linear system, ignoring all nonlinearities, like those related to fluid flow. It has been assumed that the MABP and CBFV are correlated without taking into account any phase lag between them. Another presumption is that the middle cerebral artery (MCA), where CBFV is measured, does not change its diameter, and hence the words cerebral blood flow velocity (CBFV) and cerebral blood flow (CBF) have been used interchangeably. Also, effects due to changes in venous and intracranial pressure are not specifically included in the data and the models where data was MABP and CBFV. These effects were considered while estimating CPP from MABP and modeling CPP and CBFV.

Since for linear model estimation it is required that the input be persistently exciting, another purpose of this study was to examine and establish the efficacy of beat-to-beat blood pressure time sequence in serving as an input stimulus. Furthermore, this involved investigating the possibility of using a shorter data segment of 1.5 minute duration of changes in MABP for obtaining linear model estimation of cerebral autoregulation. None of the studies in section 1.3 have involved this type of testing and validation, and only one previous investigation has examined the use of 3 minute input data [11]. Most of the previous studies have used the traditional 6 minutes duration of pressure and flow data [12, 13, and 44].

The rest of this thesis is arranged in the following way. Chapter 2 presents the experimental setup and protocol for the data collection and provides various model structures and modeling techniques applied to the data. Chapter 3 presents the results

obtained from different modeling approaches and studies. Chapter 4 deals with the discussion for the results and limitations. Finally, chapter 5 details the conclusions and directions for future work.

CHAPTER 2

METHODS

This chapter presents the experimental setup, protocol for data collection and various model structures and modeling methodologies applied to the data. All the data analysis algorithms in this study were developed, tested and evaluated in MATLAB (ver. 5.2 and ver. 6.5) and Simulink (ver. 5.0) environments, some of which are shown in Appendix A.

2.1 Experimental Setup and Data Acquisition

2.1.1 Subjects

Data for the present study was obtained from ten healthy subjects, 8 men and 2 women, aged 29±6 years in supine resting position. No subject smoked, used recreational drugs or had known medical problems. Subjects were screened carefully with regard to their medical history and a physical examination with a 12-lead Electrocardiogram (ECG). All subjects signed an informed consent form approved by the Institutional Review Boards of the University of Texas Southwestern Medical Center at Dallas and Presbyterian Hospital of Dallas.

2.1.2 Instrumentation

Heart rate (HR) was monitored continuously by ECG. The beat-to-beat mean arterial blood pressure (MABP, mmHg) was measured non-invasively with finger photoplethysmography (Finapres Ohmeda, Amsterdam, Netherlands). The cerebral blood flow velocity (CBFV, cm/sec) was recorded from the middle cerebral artery (MCA) with transcranial Doppler ultrasonography (TCD). A 2-MHz probe (Multiflow DWL, Elektronische Systeme, Sipplingen, Germany) was placed over the subject's temporal window and fixed at a constant angle with a probe holder to secure the probe position during the experiments. This technique allows non-invasive and repeatable estimates of changes in CBFV on a beat-to-beat basis.

2.1.3 Experimental Protocol

All experiments were performed in the morning at least 2 hours after a light breakfast in a quiet environmentally controlled laboratory with an ambient temperature of 25 °C. The subjects were asked to refrain from heavy exercise and caffeinated or alcoholic beverages at least 24 hours before the tests. After at least 30 minutes of supine rest, 6 minutes of baseline data were collected during spontaneous breathing. This data collection was repeated again after approximately 1 hour to test the reproducibility of MABP and CBFV. Then, the subjects performed a Valsalva maneuver (VM) with an expiratory strain of 30 mmHg for 15 seconds. The strain pressure during the VM was monitored by a sphygmomanometer (Tycos, Arden, NC, USA). Typical changes in MABP, HR and CBFV during the maneuver were observed in all subjects before ganglion blockade. After performance of the baseline VM, intravenous infusion of

trimethaphan (trimethaphan camsylate, Cambridge Laboratories, UK) was begun at a low dose of 3 mg min^{-1}. Three minutes after the infusion, a VM was performed again to evaluate the HR responses to the changes in MABP. The infusion dose was increased incrementally by 1 mg min^{-1} if the HR response during the preceding maneuver was still present. This procedure was repeated at each level of infusion until the absence of HR response was observed. The ultimate infusion dose used for ganglion blockade was 6-7 mg min^{-1} in the present study. The efficacy of ganglion blockade was demonstrated not only by the absence of HR response, but also by the absence MABP recovery during phase II or MABP overshoot during phase IV of the Valsalva maneuver, suggesting the removal of autonomic neural activity. In general, from the multiple maneuvers (3-4) performed by each subject with and without infusion, the first VM was considered practice and the last one was used for data analysis. Thus, there were four types of data recordings for each of the ten subjects, spontaneous with no infusion (SNI), spontaneous with infusion (SI), Valsalva maneuver with no infusion (VNI) and Valsalva maneuver with infusion (VI).

2.1.4 Data Pre-processing

The data recordings were interpolated and resampled[§] at 2 Hz using cubic spline interpolation. For the purpose of examining the efficacy of beat-to-beat blood pressure time sequence in serving as an input stimulus and to investigate the use of a short data segment of 1.5 minute, 6 minutes SNI data and its four non-overlapping contiguous 1.5 minute sections were examined. For the other part of the study involving modeling

[§] The MATLAB function *interp1* was used

methodologies and their comparison, first 1.5 minute section of the 6 minute SNI recording, and approximately 90 seconds (1.5 minute) of SI, VNI and VI data recordings were used. Prior to any analysis, all data sequences were first detrended* by removing their mean values, and then normalized by the range of time series (maximum value of the sequence minus minimum value of the sequence). Figure 2.1 through Figure 2.4 illustrate approximately 90 seconds recordings of MABP and CBFV for subject number 1 for all the four (SNI, SI, VNI, and VI) data conditions.

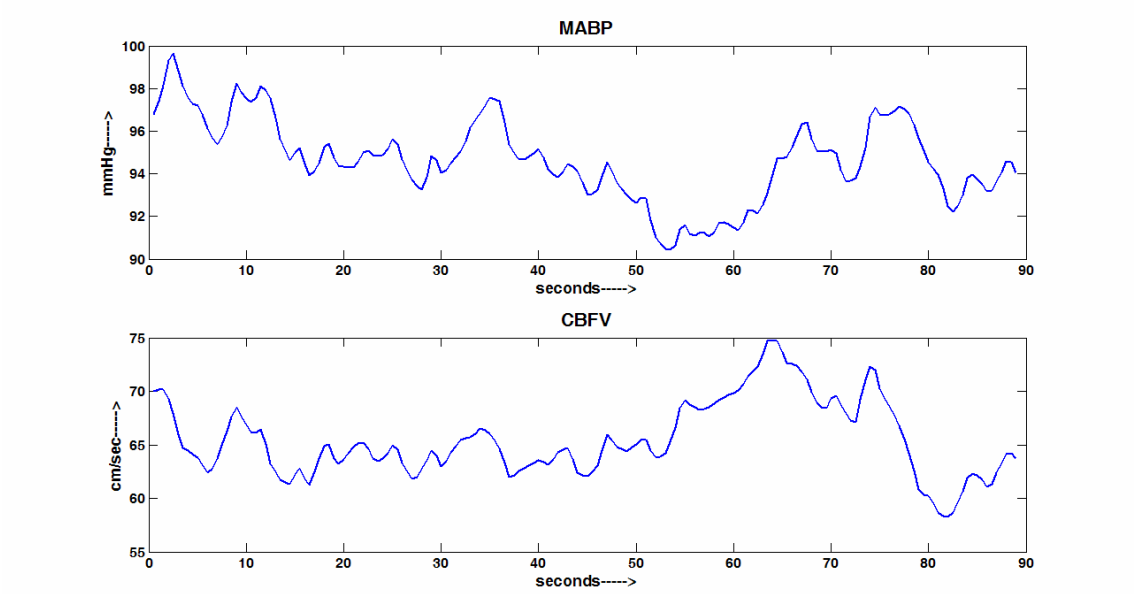

Figure 2.1 Spontaneous with no infusion (SNI) mean arterial blood pressure (MABP) and cerebral blood flow velocity (CBFV) data

* The MATLAB function *dtrend* was used

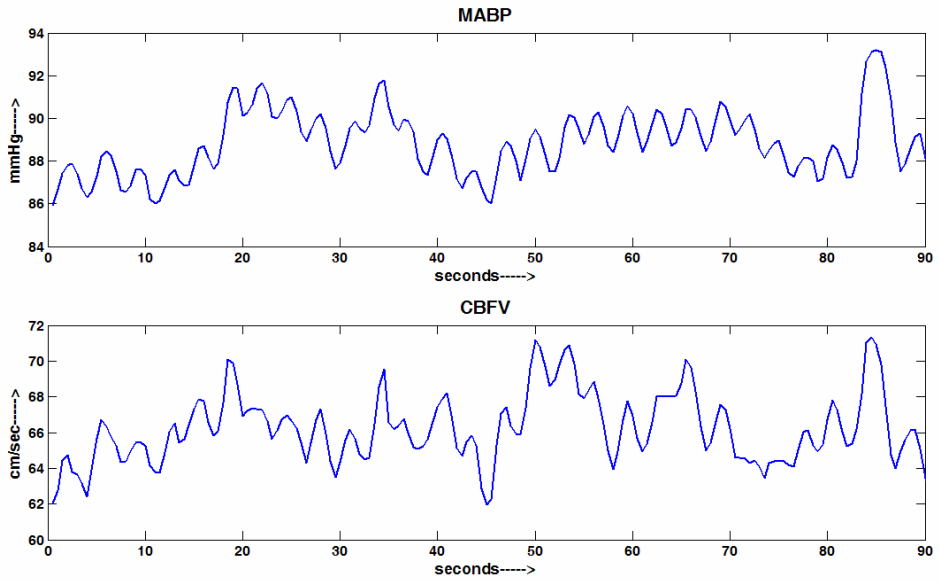

Figure 2.2 Spontaneous with infusion (SI) mean arterial blood pressure (MABP) and cerebral blood flow velocity (CBFV) data

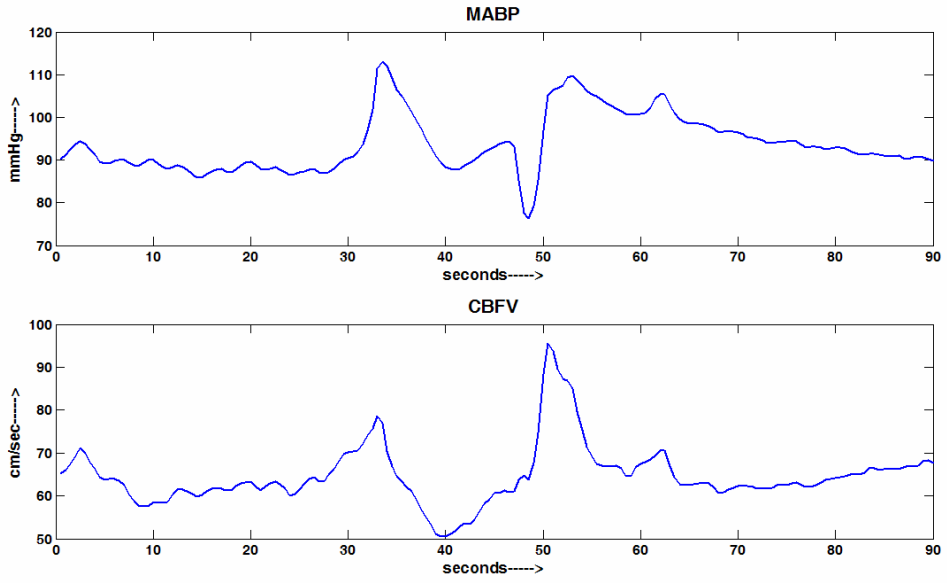

Figure 2.3 Valsalva maneuver with no infusion (VNI) mean arterial blood pressure (MABP) and cerebral blood flow velocity (CBFV) data

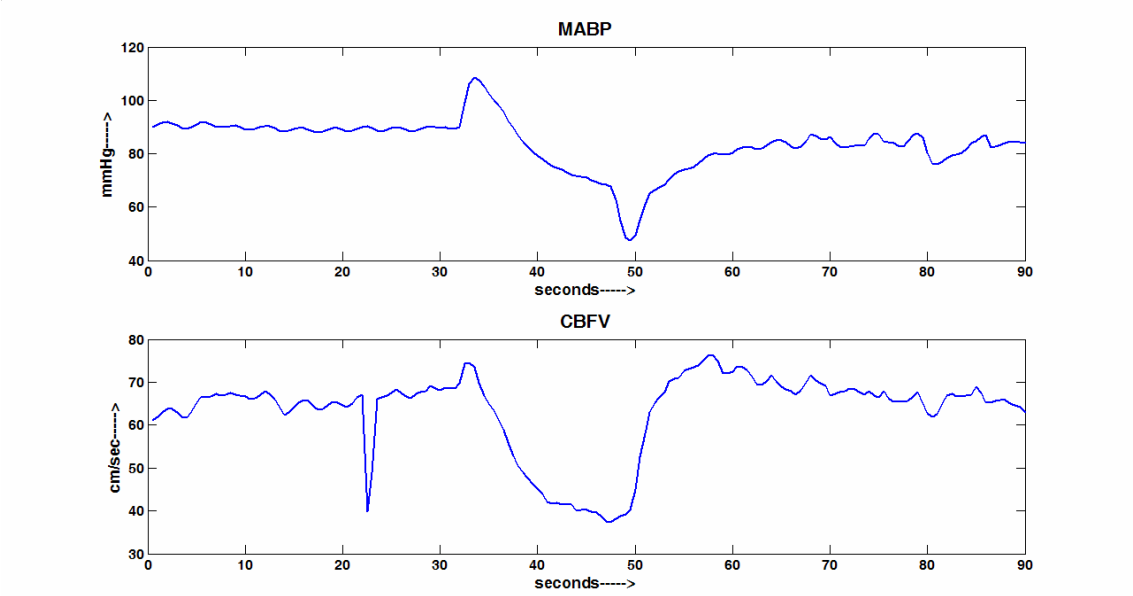

Figure 2.4 Valsalva maneuver with infusion (VI) mean arterial blood pressure (MABP) and cerebral blood flow velocity (CBFV) data

2.2 Modeling Methodologies

This section describes the two types of modeling approaches (ARX and Windkessel) employed to the data collected as mentioned in the previous section. Section 2.2.1 discusses the ARX modeling technique and modeling schemes associated with it. Section 2.2.2 details Windkessel estimation and various types of Windkessel models employed in the present study, section 2.2.3 discusses different modeling schemes associated with them.

2.2.1 ARX Model Estimation

For linear system parametric identification of an autoregressive ARX model [1, 2, 14, 27, and 44], the model describes the relationship between input signal, output signal, and disturbance signal or noise, through a set of linear difference equations

where the output at a given time t is computed as a linear combination of the current and past outputs and the current and past inputs. In general the structure for ARX identification is,

$$y(k) = G(q).u(k) + H(q).\varepsilon(k) \tag{2.1}$$

where y is the output, u is the input and ε is the noise, k is the sample number (instance) and q is the index of the domain in which the model transfer function is analyzed. G is the process model, which represents the causal relationship between the deterministic input u and output y to the model, H is the noise model.

In many cases, the effect of noise on the model output may be insignificant as compared to the input signal. Hence, it is often not necessary to include an accurate noise model in the system modeling such as in the study of cerebral autoregulation [8, 11, and 12]. Thus, for a single input, single output model the structure (excluding the noise model H) can be represented as,

$$y(k) + \sum_{i=1}^{n} a_i y(k-i) = \sum_{i=0}^{m} b_i u(k-i) \tag{2.2}$$

$$G(q) = \frac{\sum_{i=0}^{m} b_i q^{-i}}{1 + \sum_{i=1}^{n} a_i q^{-i}} \tag{2.3}$$

The transfer function in Z-domain for the above model structure G(q) would be,

$$G(z) = \frac{b_0 + b_1 z^{-1} + ... + b_m z^{-m}}{1 + a_1 z^{-1} + ... + a_n z^{-n}} \tag{2.4}$$

In ARX model estimation, the model structure is set a priori, but with unknown model order (i.e. the upper bound on m and n). The model identification is reduced to

estimating the model order and its parameters (a_i and b_i) using input and output data that give the best agreement between model's (computed or predicted) output and the measured one. There are various criteria that are used to select a model and its order, such as mean squared error (MSE), Akaike's index or final prediction error (FPE) [22]. In case of this study, the MSE value between the measured and predicted output was used.

With respect to selection and restriction of the orders m and n of the ARX model, there were two modeling schemes that have been followed in this study[§]. They will be referred to as ARX-1 and ARX-2 modeling schemes.

2.2.1.1 ARX-1 Modeling Scheme

The block diagram in Figure 2.5 illustrates the ARX-1 modeling scheme for each subject for all the four data conditions. All the possible causal ARX models with orders m and n ranging from 1 to 10 (a total of 55 models) were considered using MABP (u_1) as the input and CBFV (v_1) as the output. The mean squared error (MSE) value between the predicted output (v_2) from each of these models and v_1 was then calculated based on the following general equation,

$$MSE = \frac{\sum_{i=0}^{Ln} \left[v_x(i) - v_y(i) \right]^2}{L_n} \tag{2.5}$$

where v_x and v_y are the two data sequences for which the MSE value is to be calculated and L_n is the length of the data sequences.

[§] The MATLAB function *arx* was used

The model having the smallest MSE value was selected as the best. This way, for each of the 10 subjects, there were four best models generated, one for each of the SNI, SI, VNI, and VI conditions of the data respectively.

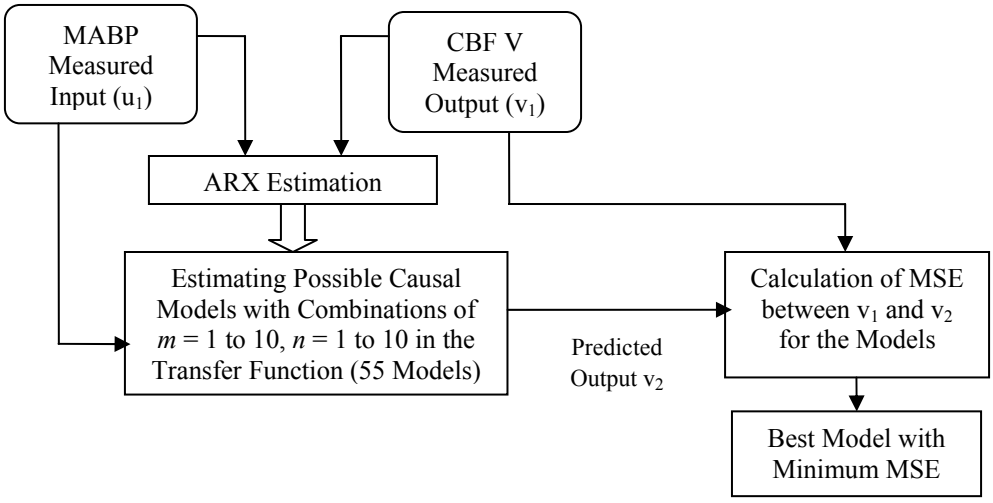

Figure 2.5 ARX-1 modeling scheme

2.2.1.2 ARX-2 Modeling Scheme

The block diagram in Figure 2.6 illustrates the ARX-2 modeling scheme for each subject for all the four data conditions. In this type of modeling scheme, ARX model orders *m* and *n* were restricted to be 1, 2, and 3, utilizing MABP (u_1) as the input and CBFV (v_1) as the output. This way, for each of the 10 subjects, for each of the SNI, SI, VNI, and VI conditions of the data, there were three models (one 1st order, one 2nd order, and one 3rd order model) generated. Hence, the total number of models for each subject was 12. The mean squared error (MSE) value between the predicted output (v_2)

from each of these models and v_1 was then calculated based on equation 2.5. The rationale behind restricting the model order was to provide a comparison between the performance of ARX and Windkessel models (Windkessel models generally are limited to 1st, 2nd and 3rd order model structures). Also, a comparison between the performances of ARX-1 and ARX-2 modeling schemes would provide an insight in reason behind fitting lower order models to physiological data and trying to select models of order as high as 10.

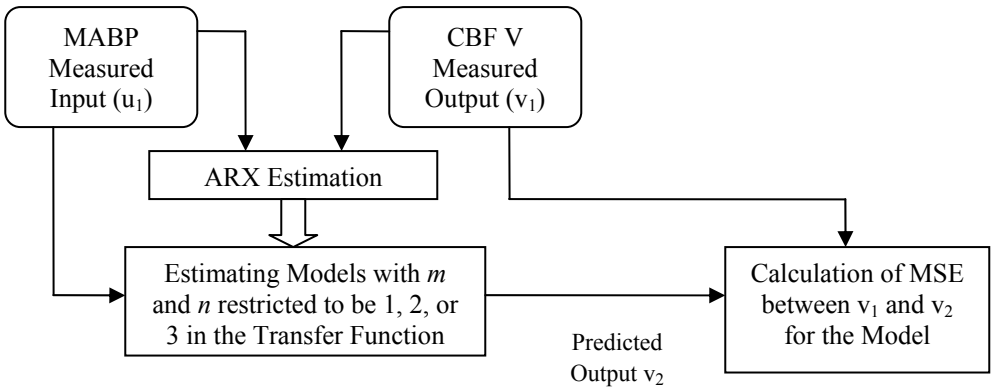

Figure 2.6 ARX-2 modeling scheme

2.2.2 Windkessel Model Estimation

Windkessel and similar lumped models are often used to represent blood flow and pressure in arterial system and to capture the dynamics of cerebral circulation [17, 31, 32, 33, 34, 35, 36, 37, 38, 39, and 40]. These lumped models can be derived from electrical circuit analogies where current (*i*) represents blood flow and voltage (*v*) represents pressure. Resistances (R) represent arterial and peripheral resistance that

occurs as a result of viscous dissipation inside vessels, capacitors (C) represent volume compliance of the vessels that allows them to store significant amounts of blood, and inductors (L) represent inertia of the blood flow in vessels.

The Windkessel model was originally put forward by Stephen Hales in 1733 and further developed by Otto Frank in 1899. Frank used Windkessel model to describe blood flow in the heart and systemic arteries, modeling the arterial system as a compliant reservoir fed by the heart (C_s), driving a simple resistive load (R_s) modeled as resistance to the outflow (Figure 2.7). The original (two-element) Windkessel model (Figure 2.8) comprised an electric circuit with one resistor and one capacitor; where the capacitor represented the compliance of the large arteries while the resistor represented the resistance of the small arteries and arterioles (so called resistance vessels). The two-element Windkessel model was later extended to the three-element Windkessel model, which had two resistors and a capacitor (Figure 2.9). The additional resistor was thought to represent the characteristic impedance of aorta and the large compliance vessels. The three-element model is and has been widely used and accepted.

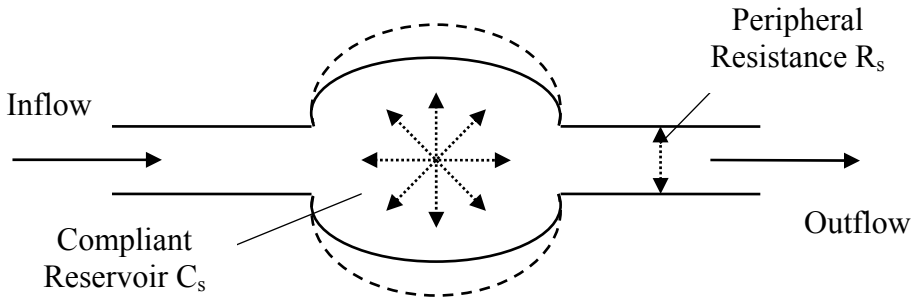

Figure 2.7 Frank's simple Windkessel model of arterial vascular system

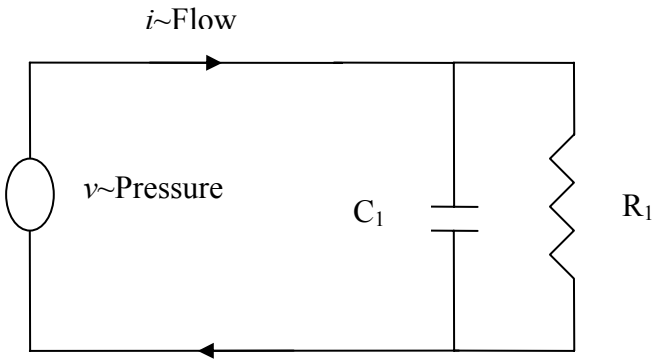

Figure 2.8 Original (two-element) Windkessel model with one resistor (R_1) and one capacitor (C_1)

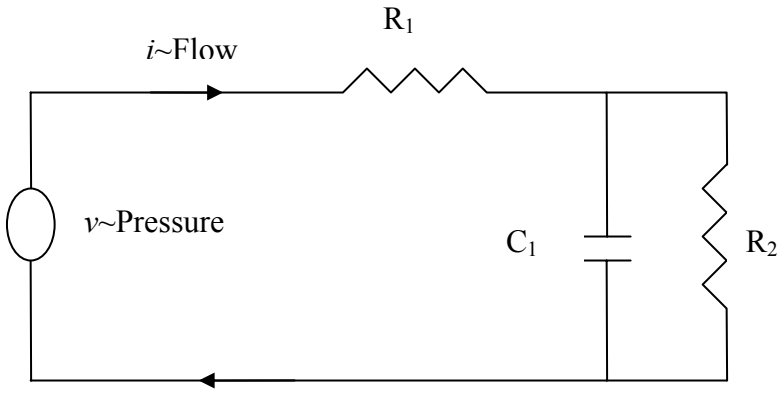

Figure 2.9 Three-element Windkessel model with two resistors (R_1 and R_2) and one capacitor (C_1)

Even though the Windkessel model was originally derived for the ventricle and aorta for cardiovascular modeling, it has been successfully employed for cerebrovascular modeling [16, 32]. Also, investigators have modified the three-element Windkessel model in several ways to produce significant improvements in fitting of the model output to the measured output [17, 31, 32, 36, 37, 38, 39, and 40]. The modifications to the original model have come in various forms, addition of

capacitances to mimic local and distal compliances, addition of resistor-capacitor combinations to expand the model to more finite levels like arterioles, capillaries and veins and addition of inductance-resistance combination to add inertial effect associated with long vessels. Although these modifications generated better results over the original Windkessel model, their physiological interpretations were not always obvious and apparent. Windkessel models are easy to understand and simple in their structure, however, these models include a number of parameters (resistors, capacitors, and inductors), and it is not obvious how to estimate the parameters from measurements of just blood flow and pressure. Generally the estimation of these parameters depends on minimization or maximization of a cost-function (a function of time or frequency) to either fit the model time-domain output to the measured time-domain output, or match the measured and model frequency responses.

The present study employs the basic three-element Windkessel model and four of its modified versions, which have shown significant improvements in fitting of the model output to the measured output in previous cardiovascular and cerebrovascular modeling studies. Their transfer functions using Laplace transform (S-domain) have been analyzed considering MABP as input to the model and CBFV as output to the model.

2.2.2.1 Model 1: Windkessel 3-Element Model [16, 21, 32, 33, 34, 35, 37, 38]

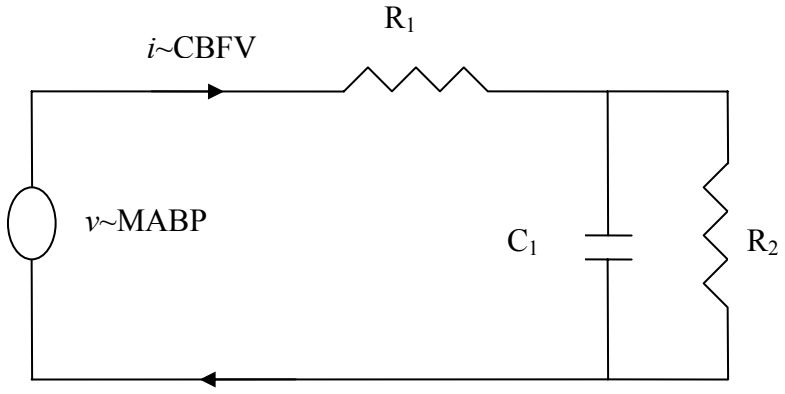

Figure 2.11 Windkessel 3-element model

Figure 2.11 illustrates the structure for the basic 3-element Windkessel model (Model 1), with input MABP analogous to voltage (v) and output CBFV analogous to current (i). The transfer function in S-domain for Model 1 in terms of its parameters R_1, R_2, and C_1, is,

$$g_1(s) = \frac{i(s)}{v(s)} = \frac{[sC_1R_2 + 1]}{[sC_1R_1R_2 + (R_1 + R_2)]} \tag{2.6}$$

2.2.2.2 Model 2: Modified Windkessel 5-Element Model [32]

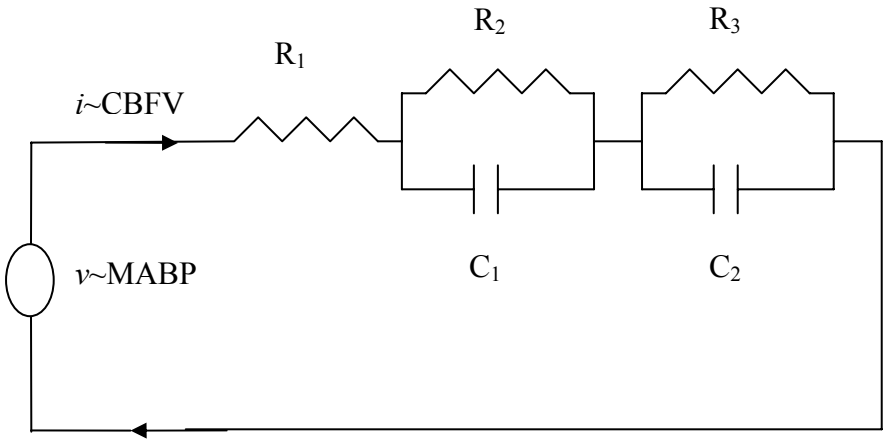

Figure 2.12 Modified Windkessel 5-element model

Figure 2.12 illustrates the structure for a 5-element modified Windkessel model (Model 2), with input MABP analogous to voltage (v) and output CBFV analogous to current (i). The transfer function in S-domain for Model 2 in terms of its parameters R_1, R_2, R_3, C_1, and C_2, is,

$$g_2(s) = \frac{i(s)}{v(s)} = \frac{\left[s^2 R_2 R_3 C_1 C_2 + s(R_3 C_2 + R_2 C_3) + 1\right]}{\left[s^2 R_1 R_2 C_1 R_3 C_2 + s(R_1 R_3 C_2 + R_1 R_2 C_1 + R_3 C_2 R_2 + R_2 C_1 R_3) + (R_1 + R_2 + R_3)\right]} \tag{2.7}$$

2.2.2.3 Model 3: Modified Windkessel 5-Element Model [31]

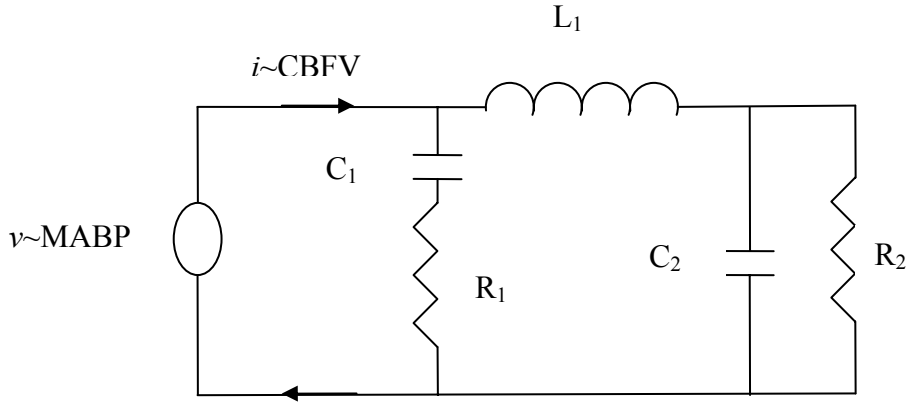

Figure 2.13 Modified Windkessel 5-element model

Figure 2.13 illustrates the structure for another 5-element modified Windkessel model (Model 3), with input MABP analogous to voltage (v) and output CBFV analogous to current (i). The transfer function in S-domain for Model 3 in terms of its parameters R_1, R_2, L_1, C_1, and C_2, is,

$$g_3(s) = \frac{i(s)}{v(s)} = \frac{\left[s^3 C_1 L_1 R_2 C_2 + s^2\left(R_1 C_1 R_2 C_2 + C_1 L_1\right) + s\left(R_1 C_1 + R_2 C_2 + C_1 R_2\right) + 1\right]}{\left[s^3 R_1 C_1 R_2 C_2 L_1 + s^2\left(R_1 C_1 L_1 + R_2 C_2 L_1\right) + s\left(R_1 C_1 R_2 + L_1\right) + R_2\right]} \quad (2.8)$$

2.2.2.4 Model 4: Modified Windkessel 5-Element Model [39]

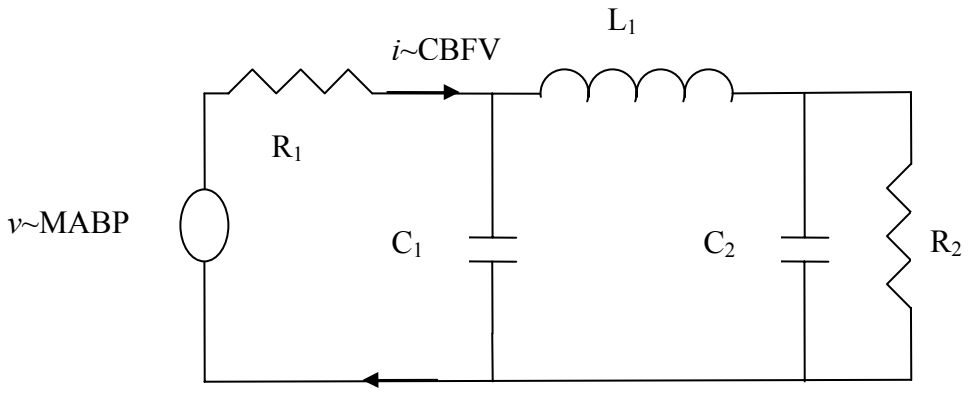

Figure 2.14 Modified Windkessel 5-element model

Figure 2.14 illustrates the structure for yet another 5-element modified Windkessel model (Model 4), with input MABP analogous to voltage (v) and output CBFV analogous to current (i). The transfer function in S-domain for Model 4 in terms of its parameters R_1, R_2, L_1, C_1, and C_2, is,

$$g_4(s) = \frac{i(s)}{v(s)} = \frac{\left[s^3 L_1 R_2 C_2 C_1 + s^2 C_1 L_1 + s(R_2 C_2 + C_1 R_2) + 1\right]}{\left[s^3 R_1 C_1 R_2 C_2 L_1 + s^2 (R_1 C_1 L_1 + R_2 C_2 L_1) + s(R_2 C_2 R_1 + R_1 C_1 R_2 + L_1) + (R_1 + R_2)\right]} \tag{2.9}$$

2.2.2.5 Model 5: Modified Windkessel 4-Element Model [17, 38]

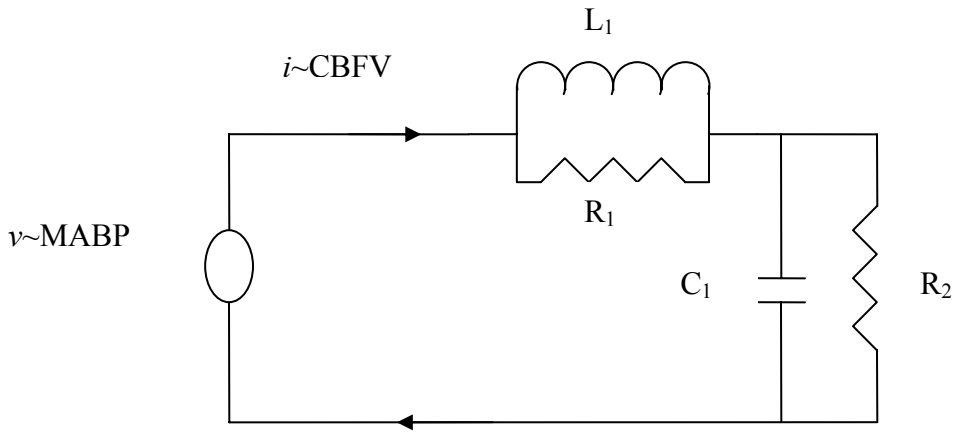

Figure 2.15 Modified Windkessel 4-element model

Figure 2.15 illustrates the structure for a 4-element modified Windkessel model (Model 5), with input MABP analogous to voltage (v) and output CBFV analogous to current (i). The transfer function in S-domain for Model 5 in terms of its parameters R_1, R_2, L_1, and C_1, is,

$$g_5(s) = \frac{i(s)}{v(s)} = \frac{\left[s^2 C_1 R_2 L_1 + s(L_1 + C_1 R_1 R_2) + R_1\right]}{\left[s^2 R_1 C_1 R_2 L_1 + s(R_1 L_1 + R_2 L_1) + (R_1 R_2)\right]} \tag{2.10}$$

2.2.3 Windkessel Modeling Schemes

From the section 2.2.2 it is relatively clear that the Windkessel models are easy to understand and simple, yet defined in their structure. However, these models include a number of parameters (R, L, and C), and the real challenge of the model identification is the estimation of these parameters from the measurements of just MABP and CBFV. In pervious investigations [16, 21, 31, 32, 34, 35, 37, and 38] the extraction of these

parameters was done by minimization or maximization of a cost-function, which may be a function of time or frequency. The present study involves parameter selection by a two-phase optimization[§] of the parameters of a Windkessel model. This optimization is done by minimization of the MSE in frequency domain for the measured and predicted impedance curves, and MSE in time domain for the measured and predicted outputs. They are referred as frequency-domain optimization phase and time-domain optimization phase respectively. The advantage of this two phase optimization process is that it converges to final values of the parameters which yield better time-domain fit of the model output and result in lower time-domain MSE value between the measured and the model output, as compared to single stage parameter extraction techniques similar to those used in previous investigations.

For frequency-domain optimization phase, first an impedance curve for the measured data (detrended and normalized MABP and CBFV) was generated. This was done by finding the cross-correlation, S_{yx}, of CBFV and MABP sequences, and the auto-correlation, S_{xx}, of MABP. Then by Welch's averaged, modified periodogram method[*], a 512 point fast Fourier transform (FFT) of S_{yx} and S_{yx} was calculated with 50 percent overlap, using a Hanning window and a sampling frequency of 2 Hz. The measured impedance curve Z_m was calculated from dividing the absolute value (modulus) of the FFT of S_{yx} by the absolute value of the FFT of S_{xx}. In the equations 2.6 through 2.10, replacing the complex variable *s* in the each of the transfer function for the five Windkessel models, by $j\omega$, where *j* is imaginary number ($\sqrt[2]{-1}$) and ω is

[§] The MATLAB function *fminimax* was used

[*] The MATLAB function *psd* was used

frequency (rad/sec), would present the transfer function as a function of ω with unknown values of parameters. Taking the absolute value (modulus) of this transfer function would yield the predicted impedance curve for the model, $Z_{p.}$ Essentially, the frequency-domain optimization is selection of the parameters of the model in order to fit Z_p to Z_m, such that the MSE value between Z_m and Z_p is minimized.

Time-domain optimization phase involves selecting those parameters, R, C and L of a Windkessel model, which minimize the MSE value between the measured time domain output (CBFV) and predicted (model) time domain output, for fitting the predicted output to the measured one. To calculate the predicted time domain output, the estimated model was subjected to the measured time domain input (MABP).

2.2.3.1 Optimization Algorithm

This section provides an overview of the optimization method used in the present study. For both frequency-domain and time-domain optimization phases, parameters of the Windkessel models were estimated using a constrained optimization technique. In this technique, a multivariable function is minimized, starting at an initial estimate. The value of the variables (parameters R, C, and L of the model) are subject to constraints, in terms of lower and upper bounds that they can attain. The lower and the upper bound values are decided keeping physiologically considerations in mind and referring pervious cerebral blood flow modeling studies. In the present study, for the part which involves analyzing the five Windkessel models for fitting them to the subject data, the lower and the upper boundary values were 0.1 and 50 for the frequency-domain optimization phase and 0.01 and 100 for the time-domain optimization phase

respectively, for every parameter. The difference in the boundary values for the two phases accounts for the situation when the frequency-domain optimization phase yields parameter estimates which are close to its boundary values, particularly to the upper boundary value. This allows the time-domain optimization phase to start with an initial estimate that is approximately at the midpoint of the range of its boundary values, and hence result in better parameter estimates. This strategy is advantageous in case where the two phases are sequential and final estimates of one phase act as initial estimates for the subsequent phase.

In constrained optimization, the general aim is to transform the problem into an easier sub-problem that can then be solved and used as the basis of an iterative process. In this way the constrained problem is solved using a sequence of parameterized unconstrained optimizations, which in the limit (of the sequence) converge to the constrained problem. This method is commonly referred to as Sequential Quadratic Programming (SQP) method, since a QP sub-problem is solved at each major iteration (also known as Iterative Quadratic Programming, Recursive Quadratic Programming, and Constrained Variable Metric methods) [2].

Constrained methods use the solution of a sub-problem to yield a search direction in which the solution is estimated to lie. The minimum along the path formed from this search direction is generally approximated using a search procedure. In the present study, this search procedure was a cubic polynomial method, where a function evaluation is made at every iteration. At each iteration an update is performed when a new point is found that results in a lower value of the multivariable function being

minimized. Value of each function parameter is also updated by a step at every iteration. If this step does not result into a lower function value, then further reduction in the step is done to form a new step, Usual method for this reduction is to use bisection, i.e., to continually halve the step length until a reduction is achieved in the function output. The values of the optional parameters like the step size, maximum number of iterations, maximum number of function evaluations, and termination tolerance on the constraint violation can be provided before the start of the optimization to improve the efficiency and accuracy of the process. More details about the optimization algorithm can be found in [2].

While SQP method has been implemented and tested over a large number of test problems, it has certain limitations. For instance, the function to be minimized must be continuous and the optimization may result in only the local solutions. Also, the method is very sensitive to the initial estimates. Based on the number of parameters optimized and the sequence of performing the frequency-domain and time-domain optimization phases, three types of Windkessel modeling schemes were obtained. They will be referred to as Windkessel-1, Windkessel-2 and Windkessel-3 modeling schemes.

2.2.3.2 Windkessel-1 Modeling Scheme

The Windkessel-1 relies on the approximation that the resistance parameter R_1 for the each of the five Windkessel models can be extracted from the highest frequency point of the measured impedance curve Z_m. As discussed in section 2.2.3, in the equations 2.6 through 2.10, replacing the complex variable *s* in the each of the transfer function for the five Windkessel models, by $j\omega$, where *j* is imaginary number ($\sqrt[2]{-1}$)

and ω is frequency (rad/sec), would present the transfer function as a function of ω with unknown values of parameters, taking the absolute value (modulus) of this transfer function would yield the predicted impedance Z_p. For instance, the transfer function $g_1(s)$ in equation 2.6 would take the form,

$$g_1(\omega) = \frac{[j\omega C_1 R_2 + 1]}{[j\omega C_1 R_1 R_2 + (R_1 + R_2)]} \tag{2.11}$$

Dividing the numerator and the denominator in equation 2.11 by $j\omega$ would give,

$$g_1(\omega) = \frac{[C_1 R_2 + 1/j\omega]}{[C_1 R_1 R_2 + (R_1/j\omega + R_2/j\omega)]} \tag{2.12}$$

Applying the limit of ω tending to infinity, to modulus of $g_1(\omega)$ in equation 2.12 would give,

$$\lim_{\omega\to\infty}|g_1(\omega)| = \lim_{\omega\to\infty} Z_p = 1/R_1 \tag{2.13}$$

Hence in order to fit Z_p to Z_m, the value of the resistance parameter R_1 is taken from the highest frequency point of the measured impedance curve Z_m, this value will be referred to as V_{R1}. By applying this approximation technique to the transfer functions of rest of the models (equations 2.7-2.10), V_{R1} in each of the models can be extracted in a similar way.

The block diagram in Figure 2.16 illustrates the methodology used for Windkessel-1 modeling scheme. First, using the input (u_1, MABP) and output (v_1, CBFV) a measured impedance curve Z_m is generated. Value of parameter R_1 is extracted from the highest present frequency value of Z_m. The frequency-domain optimization phase optimizes all the parameters, except R_1, of the Windkessel model

being analyzed, for least square fitting of Z_p to Z_m (minimizing the MSE between the two). For the 3-element Windkessel model (Model 1), the initial estimates (Initial Estimates 1) of the parameters being optimized for frequency-domain optimization were taken from the results of a pervious cerebral blood flow modeling study [16]. For the rest of the four Windkessel models, the initial estimate for every parameter was the middle point value of the range of the boundary condition (constraint) for the optimization of that parameter (section 2.2.3.1). Thus, at the end of the optimization, V_{R1} and value of every frequency-domain optimized parameter of the Windkessel model (Estimate 1) is given.

The time-domain optimization phase is the process of least square fitting of the model output to the measured output, by optimizing the parameters, except R_1, starting from the Estimate 1 values (Initial Estimates 2 = Estimate 1). At the end of the optimization, V_{R1}, and of every time-domain optimized parameter of the Windkessel model (Estimate 2) is given. The Estimate 2 along with V_{R1}, are taken as the final values of the model parameters. Based on equation 2.5, MSE is calculated between v_1 and the predicted output v_2 of model with these final values. The Windkessel-1 modeling scheme utilizes the value of parameter R_1 (V_{R1}, extracted from Z_m) in both the frequency-domain and time domain optimizations, but R_1 is essentially never optimized. This modeling scheme was applied to all the 10 subjects' data, to all the four data conditions (SNI, SI, VNI, and VI) for each subject, and for all the five Windkessel models.

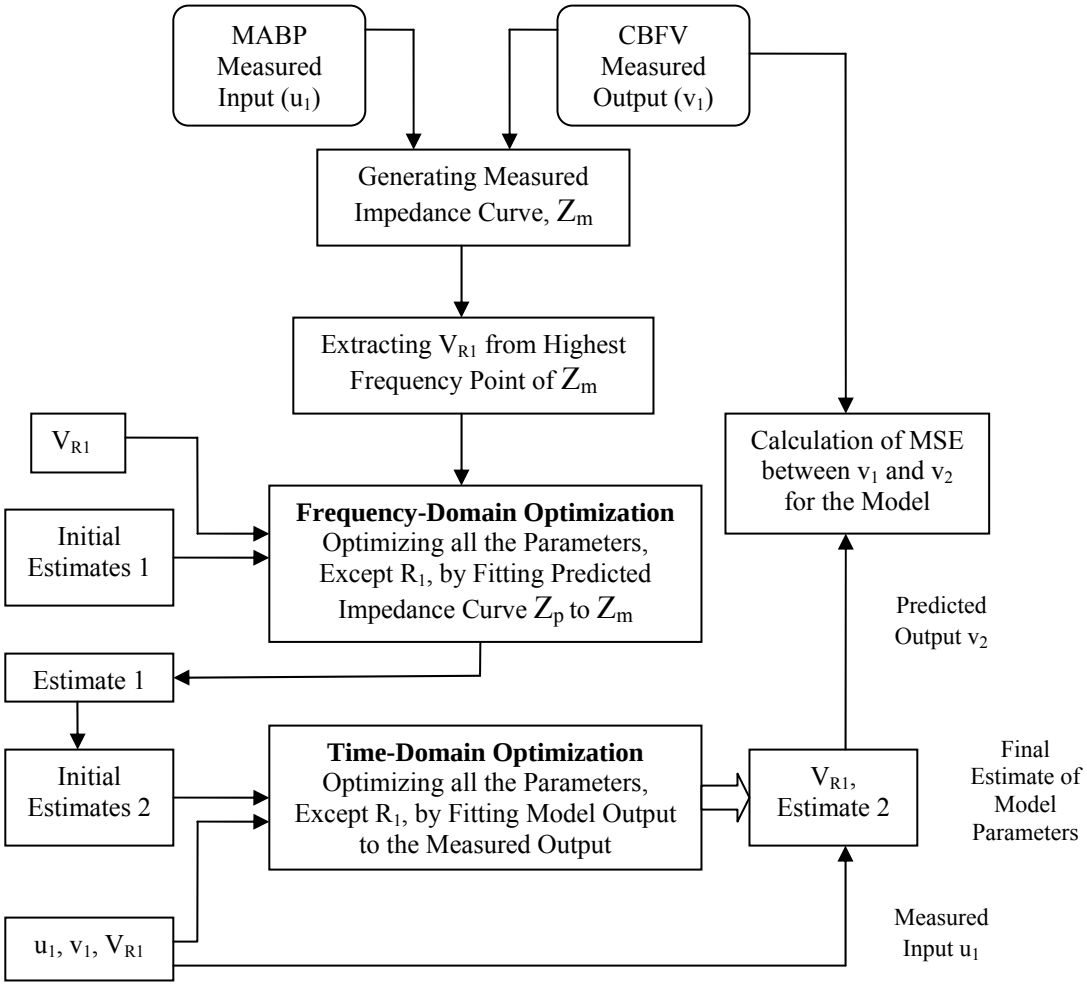

Figure 2.16 Windkessel-1 modeling scheme

2.2.3.3 Windkessel-2 Modeling Scheme

The block diagram in Figure 2.17 illustrates the methodology used for Windkessel-2 modeling scheme. First, using the input (u_1, MABP) and output (v_1, CBFV) a measured impedance curve Z_m was generated. Value of parameter R_1 is extracted from the highest present frequency value of Z_m, as discussed in section 2.2.3.2. The frequency-domain optimization phase optimizes all the parameters, except

R_1, of the Windkessel model being analyzed, for least square fitting of Z_p to Z_m (minimizing the MSE between the two). For the 3-element Windkessel model (Model 1), the initial estimates (Initial Estimates 1) of the parameters being optimized for frequency-domain optimization were taken from the results of a pervious cerebral blood flow modeling study [16]. For the rest of the four Windkessel models, the initial estimate for every parameter was the middle point value of the range of the boundary condition (constraint) for the optimization of that parameter (section 2.2.3.1). Thus at the end of the optimization, V_{R1} and value of every frequency-domain optimized parameter of the Windkessel model (Estimate 1) is given.

The time-domain optimization phase in this scheme optimizes all the parameters, including R_1, starting from V_{R1}, and Estimate 1 values (Initial Estimates 2 = [V_{R1}, Estimate 1]) for least square fitting of the model output to the measured output. At the end of the optimization, the numerical value of every time-domain optimized parameter of the Windkessel model (Estimate 2) is given, which is taken as the final value of that model parameter. Based on equation 2.5, MSE is calculated between v_1 and the predicted output v_2 of model with these final values. The Windkessel-2 modeling scheme utilizes the value of parameter R_1 (V_{R1}, extracted from Z_m) in the frequency-domain optimization, and as initial estimate for the time domain optimization. This modeling scheme was applied to all the 10 subjects' data, to all the four data conditions for each subject, and for all the five Windkessel models.

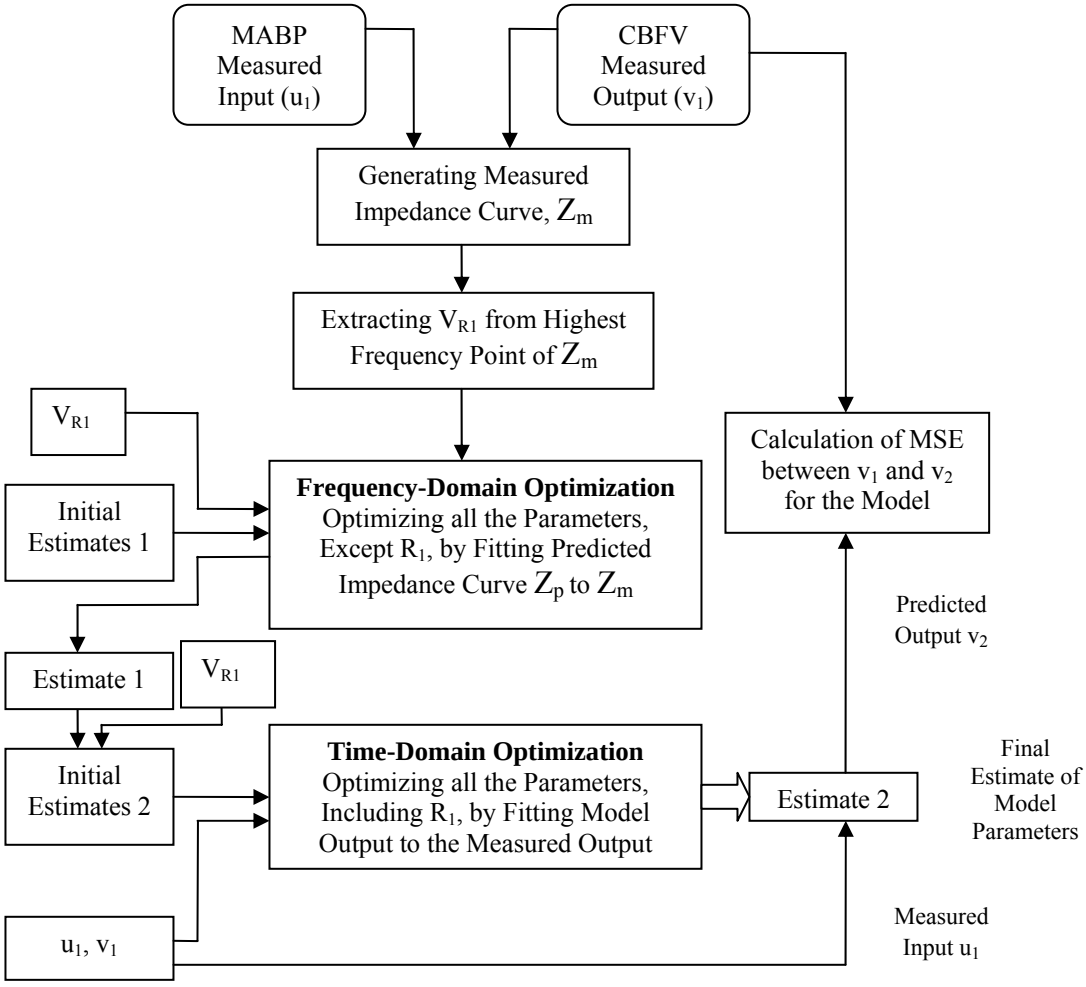

Figure 2.17 Windkessel-2 modeling scheme

2.2.3.4 Windkessel-3 Modeling Scheme

In Windkessl-3 scheme, simultaneous frequency-domain and time-domain optimization is performed, in contrast to sequential processes of Windkessel-1 and Windkessel-2 schemes where first optimization in frequency-domain and then in time-domain is performed. Hence in this type of modeling scheme, simultaneous

minimization of the MSE in frequency domain for the measured and predicted impedance curves, and MSE in time domain for the measured and predicted outputs, is done[§]. For this purpose, frequency and time domain MSE values are weighed by certain weighting coefficients for the optimization, such that the sum of the two weighting coefficients (one for frequency-domain MSE, W_f, another for time-domain MSE, W_t) is 1. Hence W_t is varied from 0.1 to 0.9 in steps of 0.1, whereas $W_f = 1 - W_t$. From all of these 9 combinations of W_t and W_f (including one where $W_t = W_f = 0.5$), selection of the model parameters is done for the combination which produces the minimum time-domain MSE value.

The block diagram in Figure 2.18 illustrates the methodology used for Windkessel-3 modeling scheme. Using the input (u_1, MABP) and output (v_1, CBFV) a measured impedance curve Z_m was generated. The frequency-domain MSE between Z_p and Z_m is calculated. The time-domain MSE between the predicted (model) output and the measured output is also calculated. The optimization process minimizes the weighted frequency and time domain MSE values simultaneously, and for the 9 combination of W_t and W_f, generates 9 sets of optimized parameters for the Windkessel model under analysis. Then for each of these 9 sets of model parameters, based on equation 2.5, time-domain MSE value is calculated between v_1 and the predicted output v_2 of model. The set of parameters yielding minimum MSE value is taken as the final estimate. This modeling scheme was applied to all the 10 subjects' data, to all the four data conditions for each subject, and for only the 3-element Windkessel model (Model

[§] The MATLAB function *fgoalattain* was used

1). The initial estimates of the parameters being optimized were taken from the results of a pervious cerebral blood flow modeling study involving Model 1 [16] and the lower and the upper boundary values were respectively 0.01 and 100 for the optimizations.

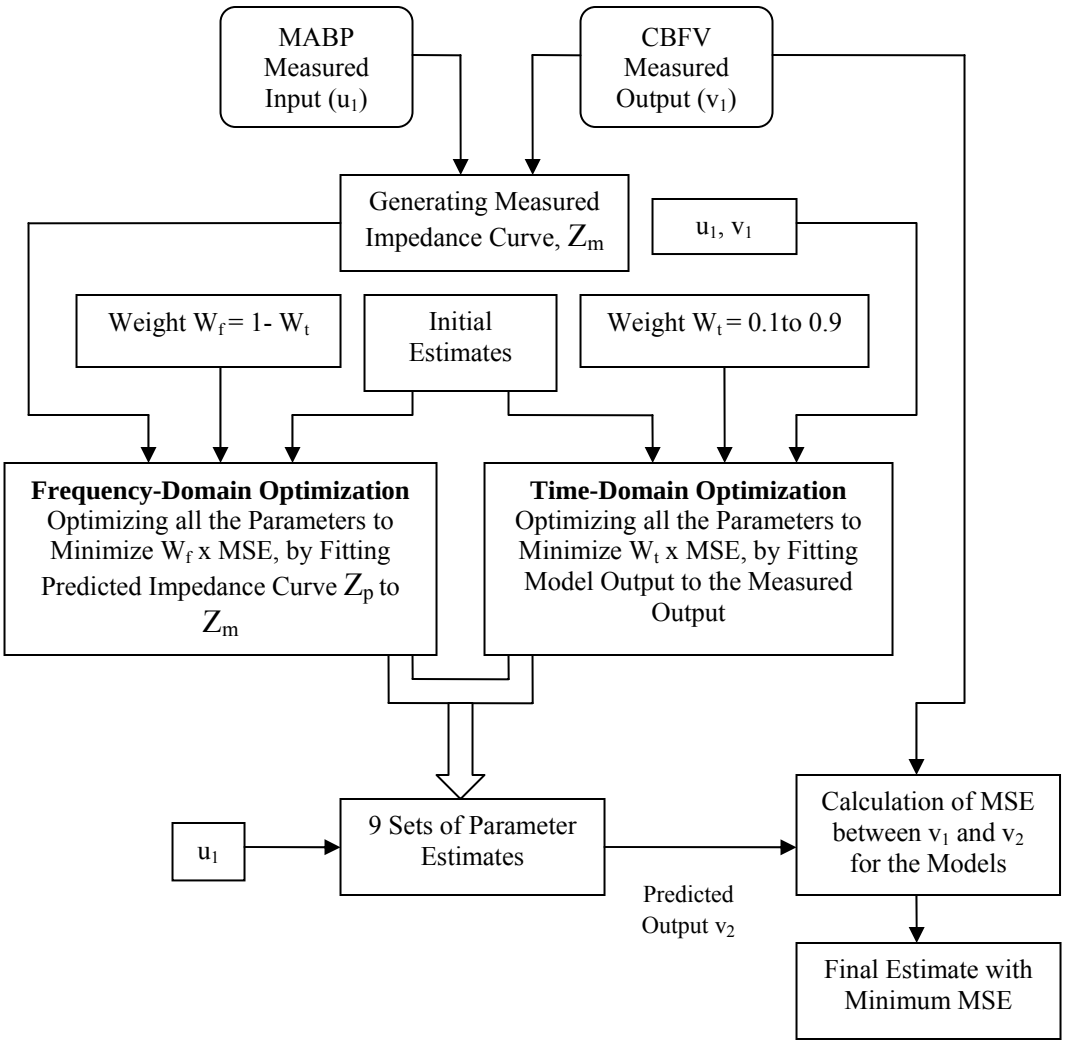

Figure 2.18 Windkessel-3 modeling scheme

2.3 Establishing the Adequacy and Efficacy of 1.5 Minute MABP as Input Stimulus

For a linear model estimation it is required that the input be persistently exciting. This section focuses on that part of study which is aimed to establish if the MABP is adequately persistently exciting to properly estimate a linear model. In addition the possibility of using a short data segment of 1.5 minute of changes in MABP for linear model identification was examined. This is of relevance because various linear modeling investigations involve use of a pathophysiological condition, like Valsalva maneuver with and without ganglion blockade in the present study, which last approximately 1.5 minute long.

The data used for this part of the study was spontaneous no infusion (SNI) data. The aim was to prove that beat-to-beat MABP sequence is as effective as pseudo random binary sequence (PRBS). This is of importance, because PRBS is a very wide bandwidth signal and is considered persistently exciting. The study was based on parametric identification of autoregressive ARX and Windkessel models. In case of Windkessel models, the study was done by performing Monte-Carlo simulations (random-walk method) for 1000 trials.

2.3.1 ARX Models

This study was based on ARX-1 modeling scheme. The block diagrams in Figure 2.19 and Figure 2.20 illustrate the steps for the applied methodology for analysis of the ARX models for each of the 10 subjects. All the possible causal ARX models with numerator and denominator order (*m* and *n*) ranging from 1 to 10 (a total of 55 models) were considered using measured MABP (u_1) as input and CBFV (v_1) data as output

sequences. Based on equation 2.5, the MSE values between the predicted output (v_2) from these models and v_1 were then calculated and the model having smallest MSE value was selected as the best. This model will be referred to as M_a.

For the next two steps, M_a was treated as an unknown system. In step 2 of investigation, model M_a was subjected to PRBS signal (u_2) with minimum value of -1, maximum value of +1, initial seed equal to zero and sample time equal to 0.5 seconds to obtain the computed output (v_3). All the possible causal ARX models with *m* and *n* ranging from 1 to 10 (a total of 55 models) were fitted to u_2 and v_3. Based on equation 2.5, the MSE values between the predicted output (v_4) of the estimated models and v_3 (used to estimate the model parameters) were then calculated and the model with the smallest MSE value was selected as the best, M_{e1}. The third step involved subjecting M_a to measured MABP (u_1) instead of PRBS. Again, all the 55 possible valid ARX models with *m* and *n* ranging from 1 to 10 were fitted to u_1 and resulting Ma output (v_5). From equation 2.5, MSE between the predicted output (v_6) from these models and computed output (v_5) was then calculated and the model having smallest MSE value was selected as the best, M_{e2}.

In order to compare all three models, M_a, M_{e1} and M_{e2}, in the fourth and final step of the study, M_{e1} and M_{e2} were excited with the measured MABP as input (u_1) and MSE values for the predicted outputs (v_2 for M_a , v_7 for M_{e1}, and v_8 for M_{e2}) and measured CBFV (v_1) were calculated based on equation 2.5. This four-step study was carried out for all 10 subjects, first with 6 minutes SNI data, and then with all the four non-overlapping contiguous 1.5 min sections of the measured 6 minute SNI data.

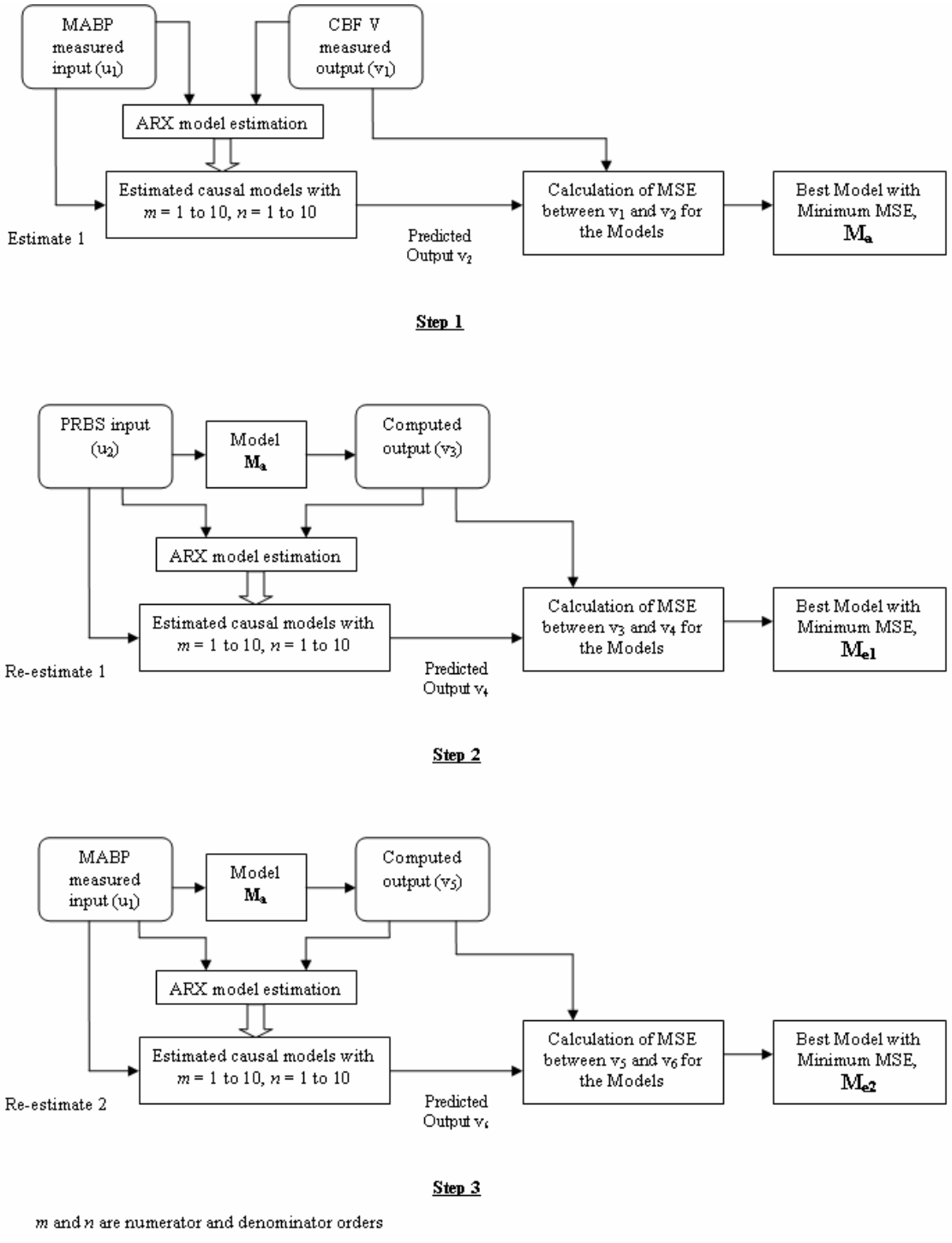

Figure 2.19 Steps 1 to 3 for the ARX modeling methodology for establishing the adequacy and efficacy of 1.5 minute MABP as input stimulus

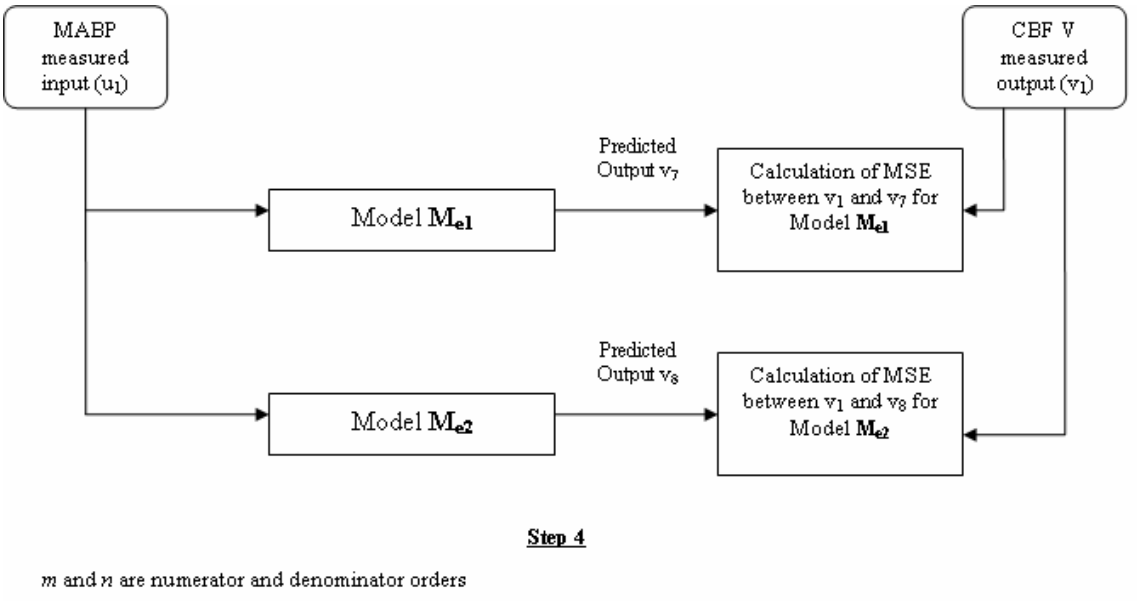

Figure 2.20 Step 4 for the ARX modeling methodology for establishing the adequacy and efficacy of 1.5 minute MABP as input stimulus

2.3.2 Monte-Carlo Simulations for Windkessel Modeling Schemes

This study was based on performing 1000 trials Monte-Carlo simulation for Windkessel-1 and Windkessel-2 modeling schemes. The block diagram in Figure 2.21 illustrates the applied methodology. First a simulated Windkessel model (M_a) was created with its parameters (R, C, and L), referred as true-parameters, being taken from a set of randomly generated numbers in a specific range. The range for these random numbers was defined and different for each of the true-parameters of M_a. M_a was subjected to input (u_1) and the computed output (v_1) was measured. Then with u_1 and v_1, a Windkessel estimation of M_a was carried out using one of the modeling schemes, the estimated model being called as M_e (estimated-parameters). M_e was subjected to u_1 and MSE value between v_1 and the predicted output (v_2) was calculated from equation 2.5. The same process was repeated for a total of 1000 trials, with the true-parameters being

different for each trial. The initial estimates of the optimization process for each of the two modeling schemes were also taken from another set of random numbers, which also were different for each trial. Essentially, the range for generating a random initial estimate of a parameter was the range in which its true-parameter was generated. For both frequency-domain and time-domain optimization, the lower and the upper boundary values (constraints) of a parameter were the lower and the upper limits of the range in which the random values for its true-parameter and initial estimate were generated.

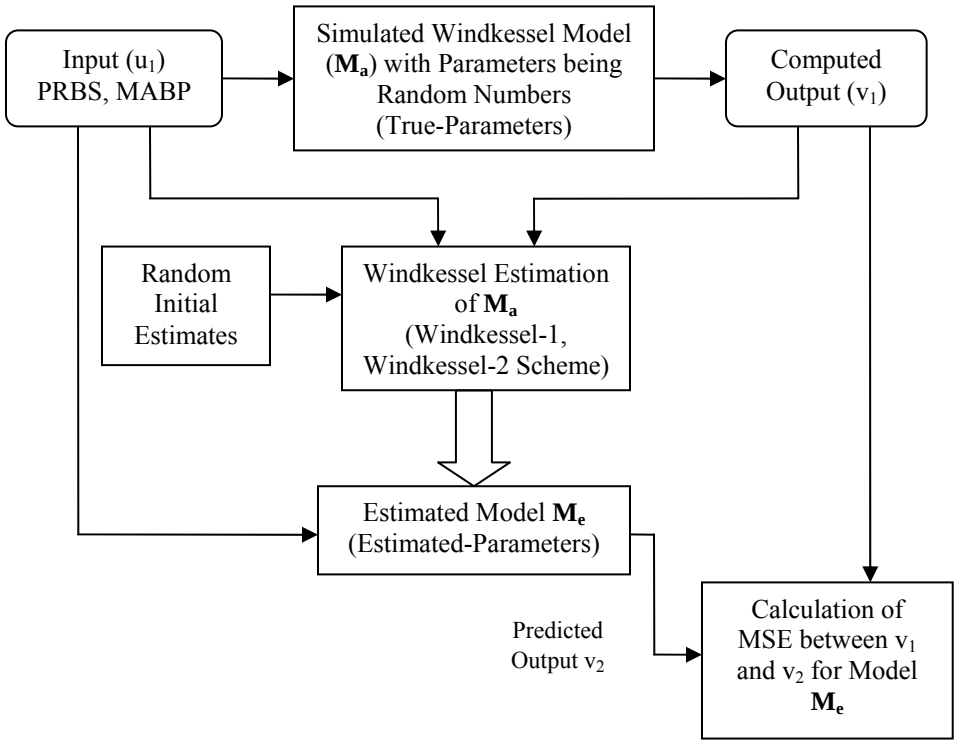

Figure 2.21 Methodology for Monte-Carlo simulations of Windkessel modeling schemes, for establishing the adequacy and efficacy of 1.5 minute MABP as input stimulus

The Monte-Carlo simulation study was first carried out with u_1 as a 1.5 minute duration PRBS signal (minimum value of -1, maximum value of +1, initial seed equal to zero, and sample time equal to 0.5 seconds), and then with all 10 subjects' SNI MABP data, where u_1 was the first 1.5 min section of the measured 6 minute data. In case of the u_1 being MABP data, the subject data was selected randomly for each trial from the group of 10 subjects' data. This entire investigation was done first with the Windkessel estimation in the block diagram (Figure 2.21) as Windkessel-1 modeling scheme and then as Windkessel-2 modeling scheme, for M_a being each of the five Windkessel models (section 2.2.2). Thus, there were four sets of Monte-Carlo simulation results generated for each of the five Windkessel models, (1) with PRBS input and Widnkessel-1 modeling scheme; (2) with PRBS input and Widnkessel-2 modeling scheme; (3) with MABP input and Widnkessel-1 modeling scheme; and (4) with MABP input and Widnkessel-2 modeling scheme. Along with the aim of testing the efficacy of using 1.5 minute MABP for linear modeling, this part of the study involving the Monte-Carlo simulations was an exhaustive test for the algorithms designed for Windkessel-1 and Windkessel-2 modeling schemes.

2.4 Estimating Cerebral Perfusion Pressure from MABP [18]

It has been believed that autoregulation is the mechanism which maintains constant cerebral blood flow (CBF) within a wide range of changing cerebral perfusion pressure (CPP), and not just the mean arterial blood pressure (MABP), because of the fact that intracranial pressure (ICP) and cerebral venous pressure (CVP) do not remain

constant at all times, especially during straining conditions like those during a VM (phase I, II_a, and II_b). Thus it is suggested that changes in CPP is the actual physiological trigger for autoregulation and not MABP, and while modeling of cerebral autoregulation, CPP and CBFV should be examined.

Hence in the present study, for the purpose of estimating CPP (mmHg) from MABP (mmHg) in case of the VNI and VI data for the 10 subjects, the value of the expiratory pressure (which approximates changes in intrathoracic pressure and thus CVP and ICP) during the VM (30 mmHg) was subtracted from phase II_a, and II_b. It was assumed that ICP and CVP are low and remain relatively constant under phase IV where there is no straining. Due to the difficulty in estimating transient changes in CPP during rapid phase I and phase III of the VM, the pressure values for these phases were obtained by cubic spline interpolation[§] of the VNI and VI pressure data from which 30 mmHg has been subtracted for phase II_a, and II_b. The CBFV data remained unchanged. The 3-element Windkessel model (Model 1) with Windkessel-1 modeling scheme was applied to the CPP and CBFV data taken as the measured input and output respectively, for VNI and VI conditions for all 10 subjects. Figure 2.22 illustrates the MABP and corresponding CPP for VNI condition of subject number 1.

[§] The MATLAB function *interp1* was used

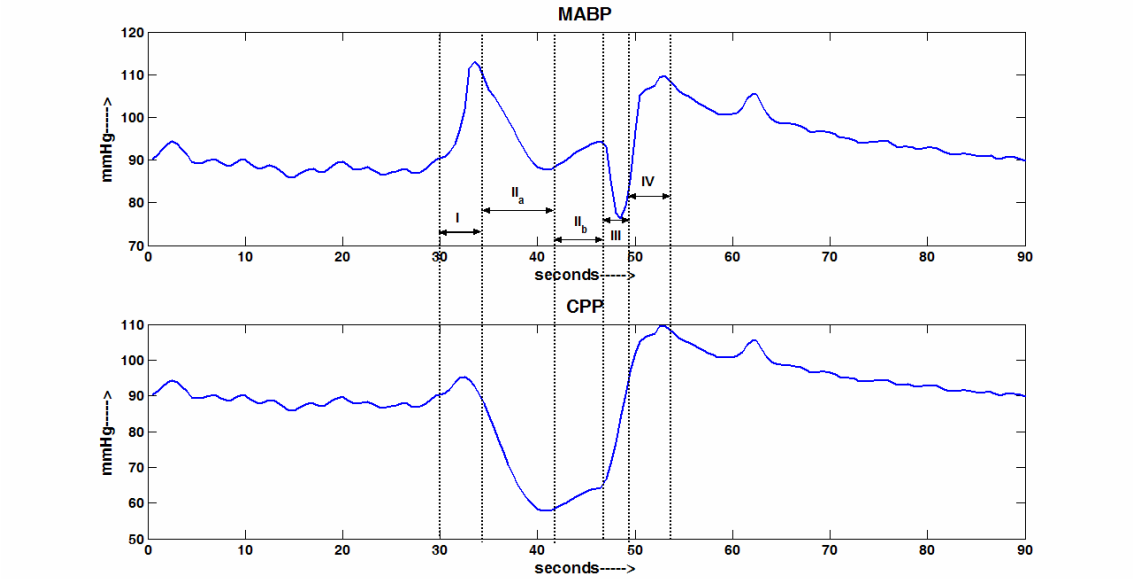

Figure 2.22 Valsalva maneuver with no infusion (VNI) mean arterial blood pressure (MABP) and cerebral perfusion pressure (CPP) data

CHAPTER 3

RESULTS

3.1 Results for Establishing the Adequacy and Efficacy of 1.5 Minute MABP as Input Stimulus

This section presents the results for analysis of the MABP (SNI) and comparison of those with the PRBS results, to test if MABP is adequately persistently exciting for estimating to yield a linear model. The section includes the results for the tests using ARX models (based on ARX-1 modeling scheme) and for Monte-Carlo simulations (1000 trials) of Windkessel models (based on Windkessel-1 and Windkessel-2 modeling schemes).

3.1.1 Results for ARX Models

From the present study, one MSE value for each of the three models, M_a, M_{e1} and M_{e2}, was generated per subject, for each of the 5 data sequences used (one 6 minutes and four 1.5 minutes) of the MABP (SNI) data. For each of the 10 subjects, MSE values for M_a, M_{e1} and M_{e2} models were equal for the 6 minutes study. Also, for each of the four 1.5 minute studies, the MSE values for M_a, M_{e1} and M_{e2} models were equal for a given single subject. Table 3.1 shows the MSE values of 10 subjects for all the three models, for each type of data set used. Table 3.2 shows the t-test results (P_{val}) for the MSE values of 10 subjects between the 6 minutes study and four 1.5 minute

studies. Table 3.3 shows the t-test results (P_{val}) for the MSE values of 10 subjects between the four 1.5 minute studies. The statistical level of significance for the t-tests was 0.05. Table 3.4 shows the average orders of numerator (*m*) and denominator (*n*) of the three models for each type of data set used.

Table 3.1 MSE values of 10 subjects for M_a, M_{e1} and M_{e2}

Subject No.	6 min MSE	1st 1.5 min MSE	2nd 1.5 min MSE	3rd 1.5 min MSE	4th 1.5 min MSE
1	0.0131	0.0125	0.0244	0.0205	0.0149
2	0.0165	0.0404	0.0231	0.0351	0.0195
3	0.0160	0.0190	0.0119	0.0111	0.0366
4	0.0350	0.0237	0.0314	0.0617	0.0441
5	0.0237	0.0280	0.0431	0.0213	0.0122
6	0.0166	0.0217	0.0464	0.0190	0.0461
7	0.0229	0.0251	0.0125	0.0507	0.0236
8	0.0159	0.0214	0.0287	0.0212	0.0094
9	0.0235	0.0155	0.0084	0.0255	0.0235
10	0.0107	0.0208	0.0190	0.0166	0.0135
Average	0.0194	0.0228	0.0249	0.0283	0.0243
STD	0.0070	0.0076	0.0128	0.0162	0.0134

Table 3.2 Comparison (t-test) of MSE values between 6 minute and 1.5 minute data sets of 10 subjects

	6 min and 1st 1.5 min	6 min and 2nd 1.5 min	6 min and 3rd 1.5 min	6 min and 4th 1.5 min
P_{val}	0.311465	0.254741	0.136559	0.319139

Table 3.3 Comparison (t-test) of MSE values between four 1.5 minute data sets of 10 subjects

	1st and 2nd 1.5 min	1st and 3rd 1.5 min	1st and 4th 1.5 min	2nd and 3rd 1.5 min	2nd and 4th 1.5 min	3rd and 4th 1.5 min
P_{val}	0.666059	0.351873	0.758237	0.611198	0.926369	0.561499

Table 3.4 Average numerator (*m*) and denominator (*n*) model orders of 10 subjects

	Model M_a		Model M_{e1}		Model M_{e2}	
	m	n	m	n	m	n
6 min	7.1	7.1	9.8	9.8	9.8	9.8
1st 1.5 min	8.5	8.5	10	10	9.9	9.9
2nd 1.5 min	7.4	7.4	9.2	9.2	9.6	9.6
3rd 1.5 min	9.7	9.7	10	10	10	10
4th 1.5 min	9	9	10	10	9.8	9.8

3.1.2 Results of Monte-Carlo Simulations for Windkessel Modeling Schemes

3.1.2.1 Results for Windkessel-1 Modeling Scheme with PRBS Input

This section presents the average MSE values (Table 3.10), true-parameters (M_a) and estimated-parameters (M_e) (Table 3.5 through Table 3.9) of 1000 trials Monte-Carlo simulation for Windkessel-1 modeling scheme with PRBS as the input, for each of the five Windkessel models. Histograms (Figure 3.1 through Figure 3.10) for true-

parameter values and estimated-parameter values for the resistance parameter R_1 of each of the five Windkessel models have also been shown.

Table 3.5 Average values of true-parameters (M_a) and estimated parameters (M_e) of Model 1 for Windkessel-1 modeling scheme with PRBS as the input

	R_1	R_2	C_1
Average M_a	10.4230	5.5639	3.0562
STD M_a	2.0503	1.4206	1.1531
Average M_e	10.3370	5.2361	3.0919
STD M_e	2.0514	1.3909	1.1203

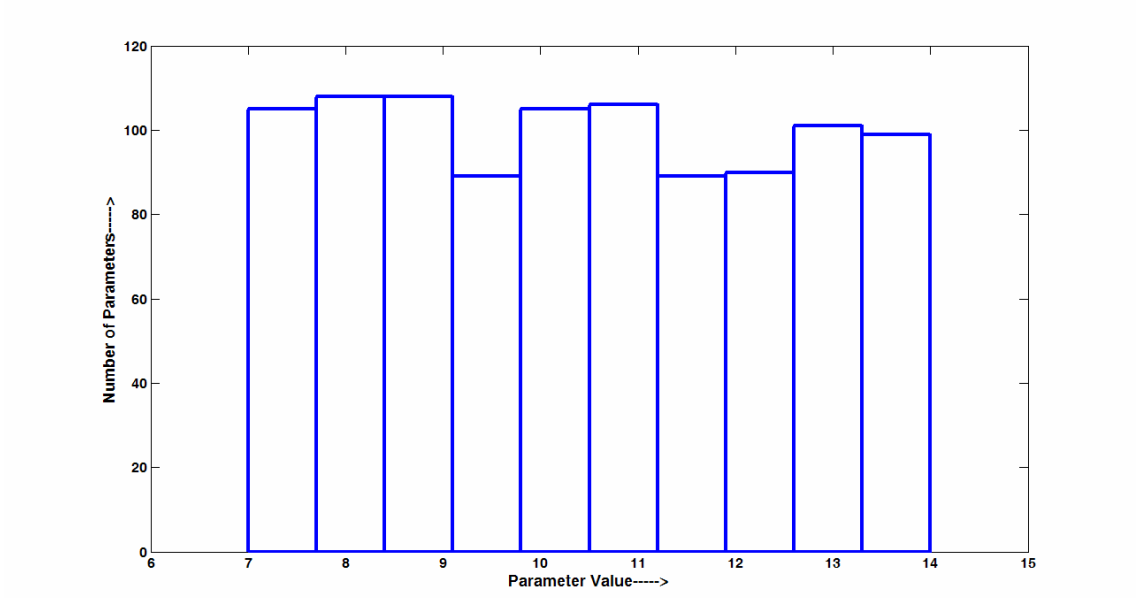

Figure 3.1 Histogram of true-parameter value for resistance parameter R_1 of Model 1 for Windkessel-1 modeling scheme with PRBS as the input

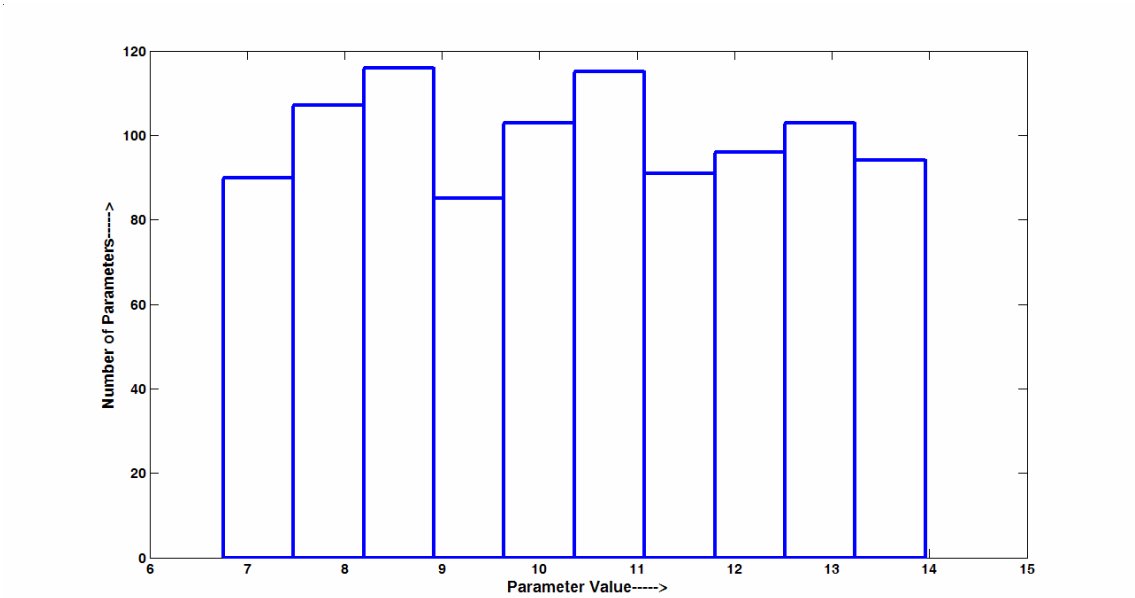

Figure 3.2 Histogram of estimated -parameter value for resistance parameter R_1 of Model 1 for Windkessel-1 modeling scheme with PRBS as the input

Table 3.6 Average values of true-parameters (M_a) and estimated parameters (M_e) of Model 2 for Windkessel-1 modeling scheme with PRBS as the input

	R_1	R_2	C_1	R_3	C_2
Average M_a	10.4340	5.5388	3.0050	6.9854	4.5769
STD M_a	2.0706	1.4263	1.1534	1.7559	1.4880
Average M_e	10.2900	4.6537	2.7770	9.5013	4.8921
STD M_e	2.0746	1.1163	0.98681	1.3305	0.93773

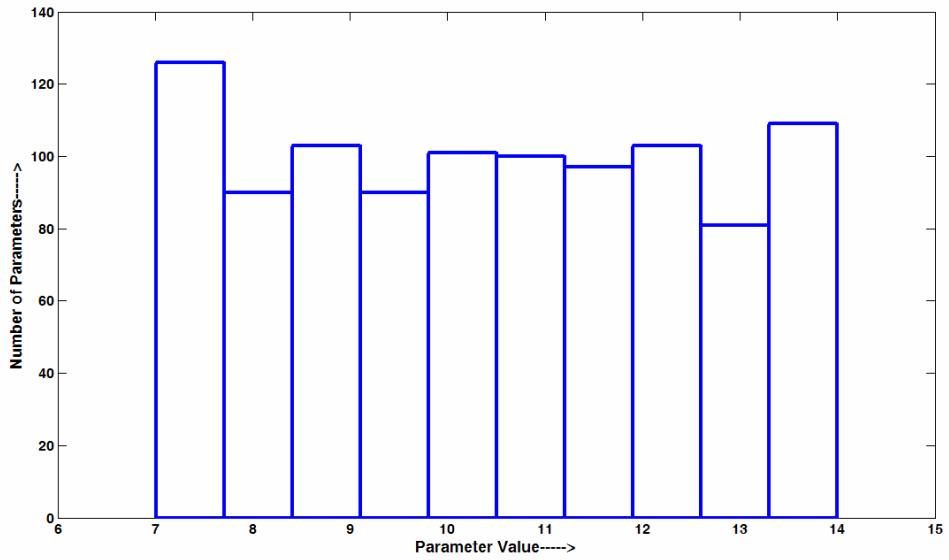

Figure 3.3 Histogram of true-parameter value for resistance parameter R_1 of Model 2 for Windkessel-1 modeling scheme with PRBS as the input

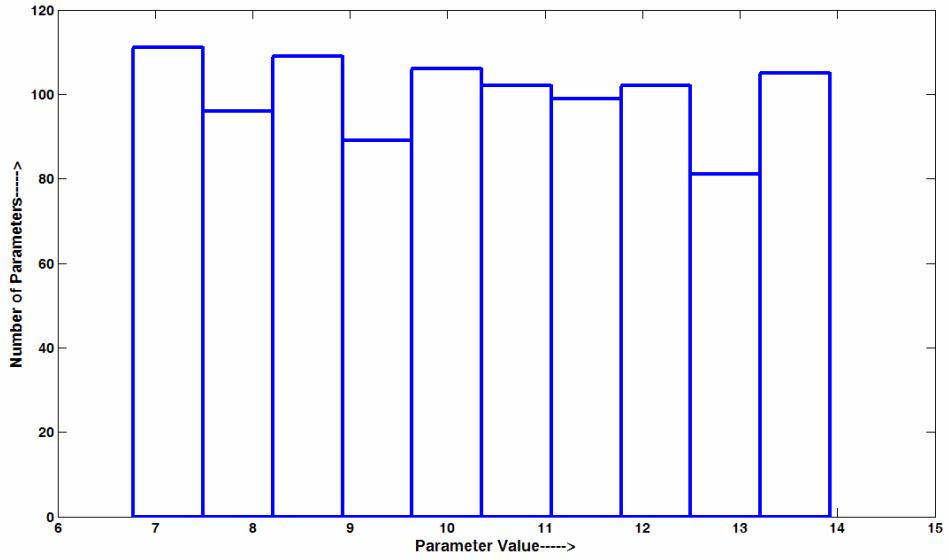

Figure 3.4 Histogram of estimated -parameter value for resistance parameter R_1 of Model 2 for Windkessel-1 modeling scheme with PRBS as the input

Table 3.7 Average values of true-parameters (M_a) and estimated parameters (M_e) of Model 3 for Windkessel-1 modeling scheme with PRBS as the input

	R_1	R_2	C_1	C_2	L_1
Average M_a	10.4340	5.5388	3.0050	6.9854	4.5769
STD M_a	2.0706	1.4263	1.1534	1.7559	1.4880
Average M_e	31.4310	5.6463	1.6536	6.7841	4.8131
STD M_e	46.4680	1.5108	1.1092	1.7332	1.5285

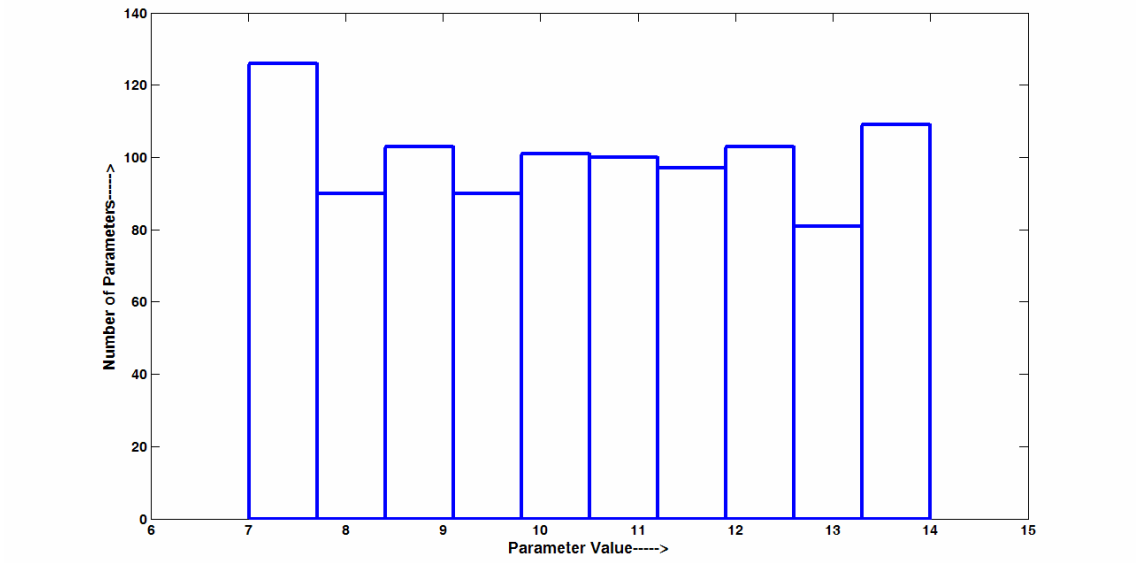

Figure 3.5 Histogram of true-parameter value for resistance parameter R_1 of Model 3 for Windkessel-1 modeling scheme with PRBS as the input

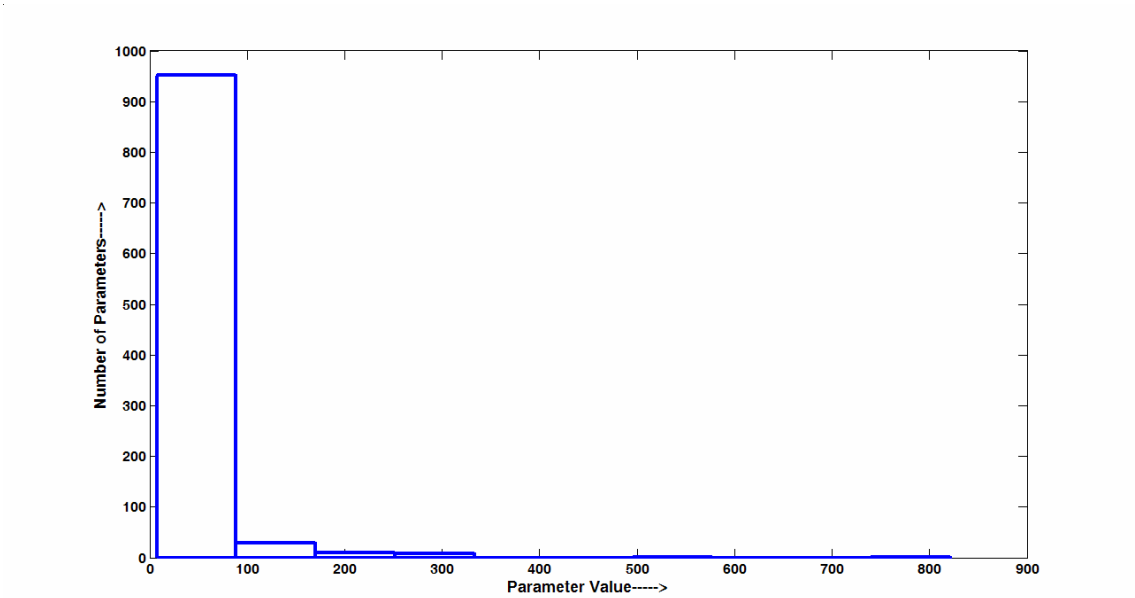

Figure 3.6 Histogram of estimated -parameter value for resistance parameter R_1 of Model 3 for Windkessel-1 modeling scheme with PRBS as the input

Table 3.8 Average values of true-parameters (M_a) and estimated parameters (M_e) of Model 4 for Windkessel-1 modeling scheme with PRBS as the input

	R_1	R_2	C_1	C_2	L_1
Average M_a	10.4340	5.5388	3.0050	6.9854	4.5769
STD M_a	2.0706	1.4263	1.1534	1.7559	1.4880
Average M_e	10.3180	4.0332	3.2317	6.7029	4.6186
STD M_e	2.0715	0.78857	1.1464	1.7269	1.3515

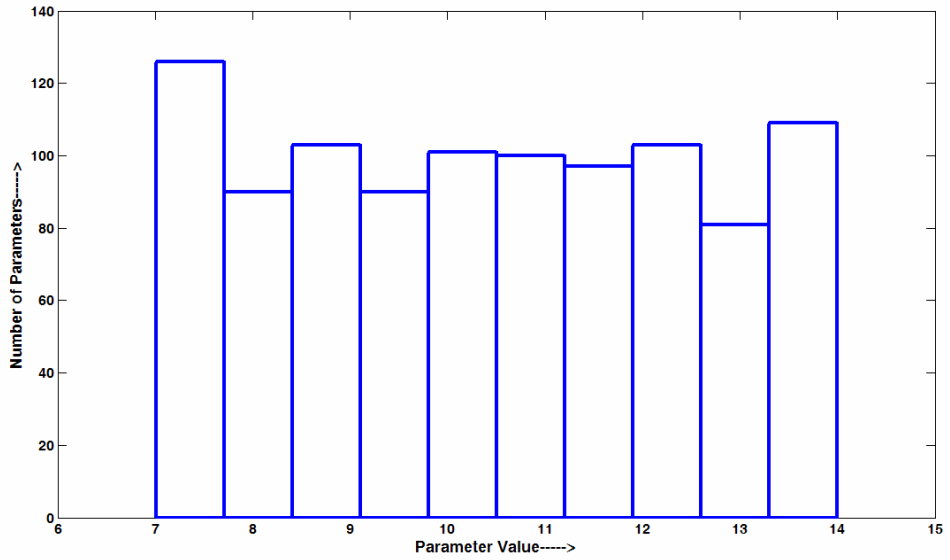

Figure 3.7 Histogram of true-parameter value for resistance parameter R_1 of Model 4 for Windkessel-1 modeling scheme with PRBS as the input

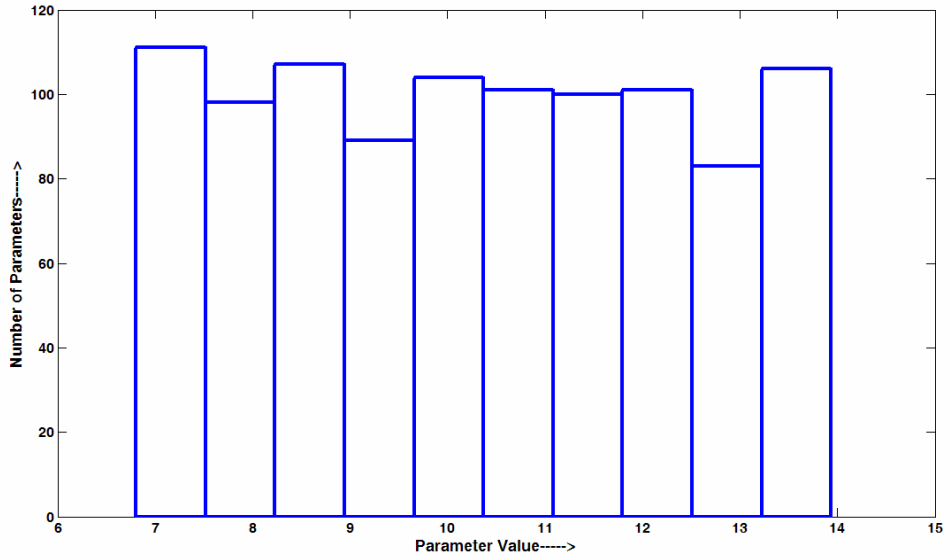

Figure 3.8 Histogram of estimated -parameter value for resistance parameter R_1 of Model 4 for Windkessel-1 modeling scheme with PRBS as the input

Table 3.9 Average values of true-parameters (M_a) and estimated parameters (M_e) of Model 5 for Windkessel-1 modeling scheme with PRBS as the input

	R_1	R_2	C_1	L1
Average M_a	10.4930	5.5396	3.0018	4.5158
STD M_a	2.0558	1.4338	1.1624	1.4556
Average M_e	54.4250	5.3154	2.6686	4.8947
STD M_e	81.6580	1.2342	1.0848	1.5661

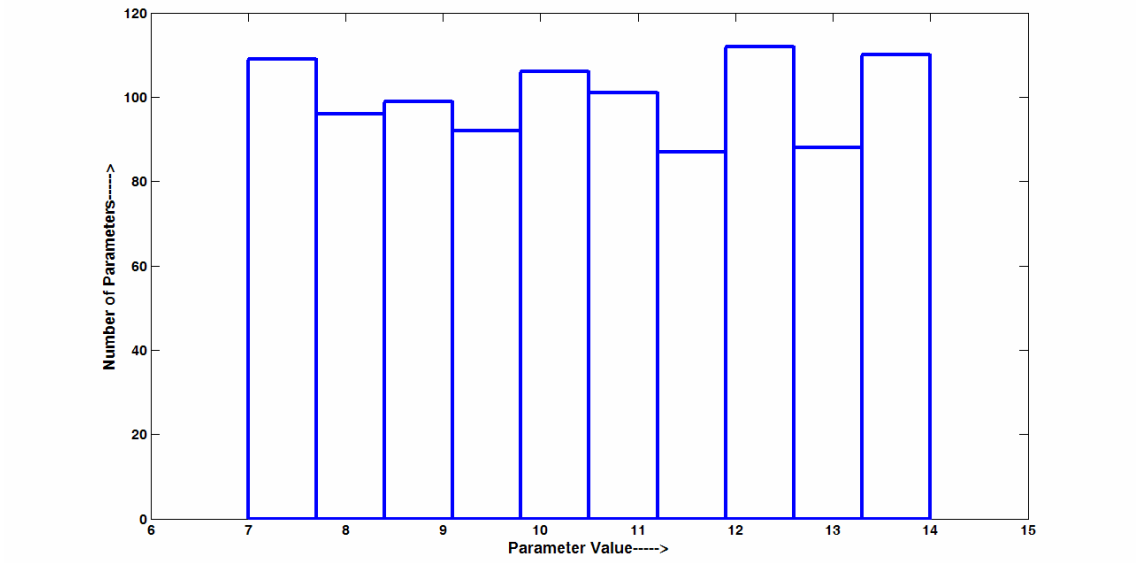

Figure 3.9 Histogram of true-parameter value for resistance parameter R_1 of Model 5 for Windkessel-1 modeling scheme with PRBS as the input

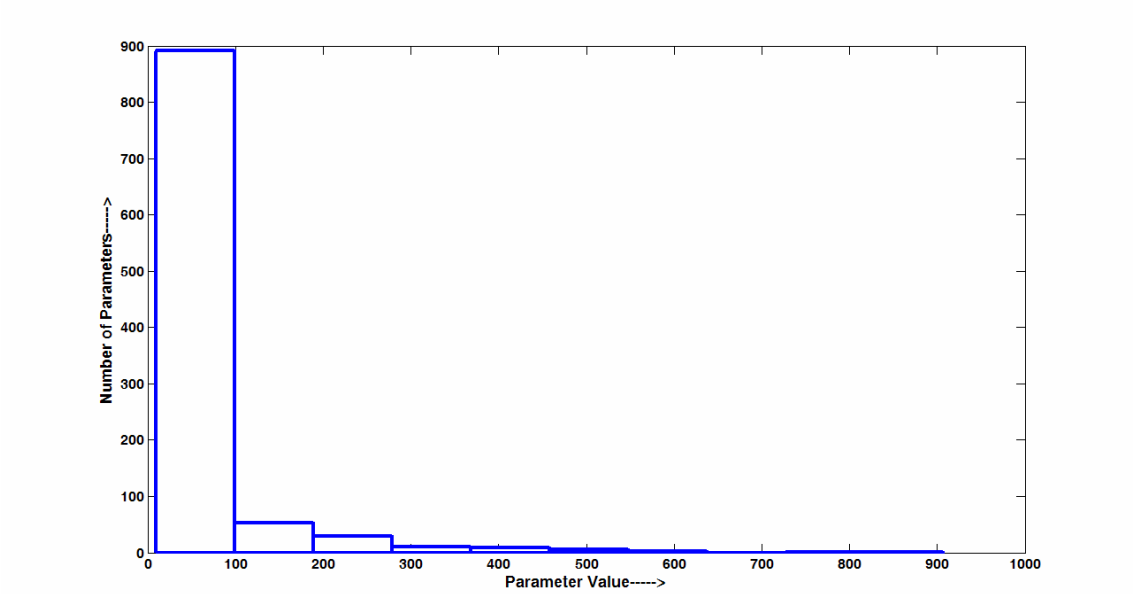

Figure 3.10 Histogram of estimated -parameter value for resistance parameter R_1 of Model 5 for Windkessel-1 modeling scheme with PRBS as the input

Table 3.10 Average MSE values for five Windkessel models for Windkessel-1 modeling scheme with PRBS input

	Model 1	Model 2	Model 3	Model 4	Model 5
Average MSE	4.5558E-07	1.1422E-06	5.5E-03	3.2178E-006	1.7E-03
STD	8.3469E-07	1.6167E-06	2.91E-02	1.3678E-005	1.5E-03

3.1.2.2 Results for Windkessel-1 Modeling Scheme with MABP Input

This section presents the average MSE values (Table 3.16), true-parameters (M_a) and estimated-parameters (M_e) (Table 3.11 through Table 3.15) of 1000 trials Monte-Carlo simulation for Windkessel-1 modeling scheme with first 1.5 minute section of the 6 minute MABP (SNI) as the input, for each of the five Windkessel models. Histograms (Figure 3.11 through Figure 3.20) for true-parameter values and estimated-parameter

values for the resistance parameter R_1 of each of the five Windkessel models have also been shown.

Table 3.11 Average values of true-parameters (M_a) and estimated parameters (M_e) of Model 1 for Windkessel-1 modeling scheme with MABP as the input

	R_1	R_2	C_1
Average M_a	10.5070	5.5285	2.9799
STD M_a	2.0503	1.4220	1.1811
Average M_e	10.8330	5.8900	3.2253
STD M_e	2.2065	1.8608	1.2817

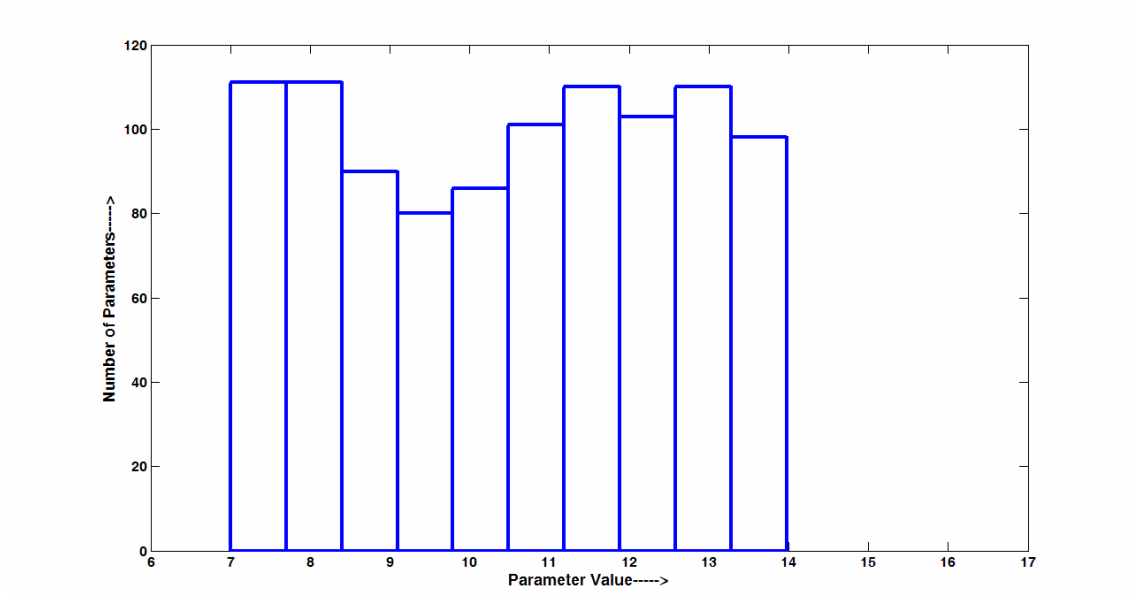

Figure 3.11 Histogram of true-parameter value for resistance parameter R_1 of Model 1 for Windkessel-1 modeling scheme with MABP as the input

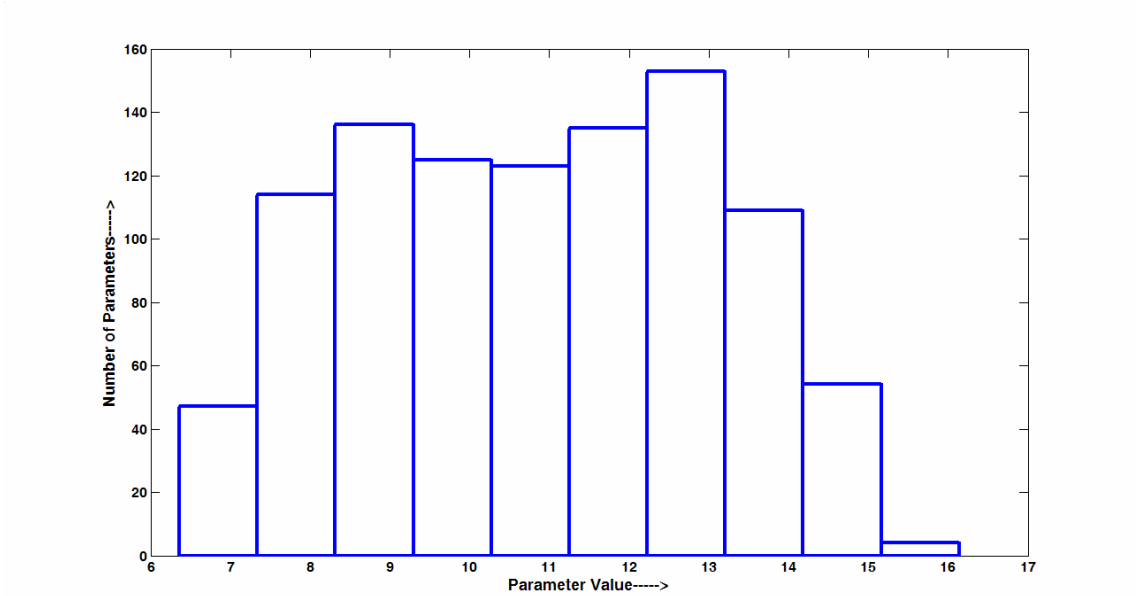

Figure 3.12 Histogram of estimated -parameter value for resistance parameter R_1 of Model 1 for Windkessel-1 modeling scheme with MABP as the input

Table 3.12 Average values of true-parameters (M_a) and estimated parameters (M_e) of Model 2 for Windkessel-1 modeling scheme with MABP as the input

	R_1	R_2	C_1	R_3	C_2
Average M_a	10.4960	5.5047	3.0135	7.0022	4.4622
STD M_a	1.9900	1.4459	1.1878	1.7104	1.4511
Average M_e	10.8810	5.7555	3.0349	9.3987	4.7755
STD M_e	2.3345	1.9705	1.4158	1.5097	1.3901

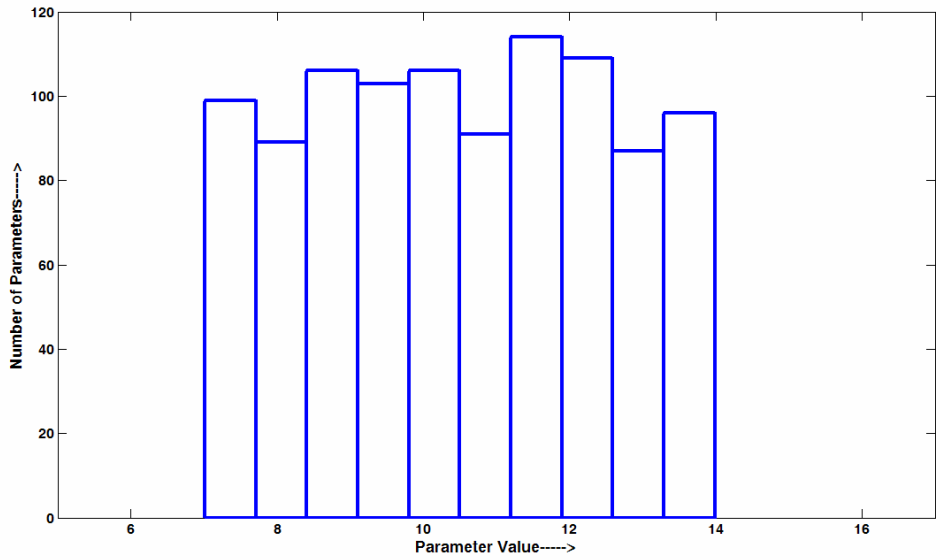

Figure 3.13 Histogram of true-parameter value for resistance parameter R_1 of Model 2 for Windkessel-1 modeling scheme with MABP as the input

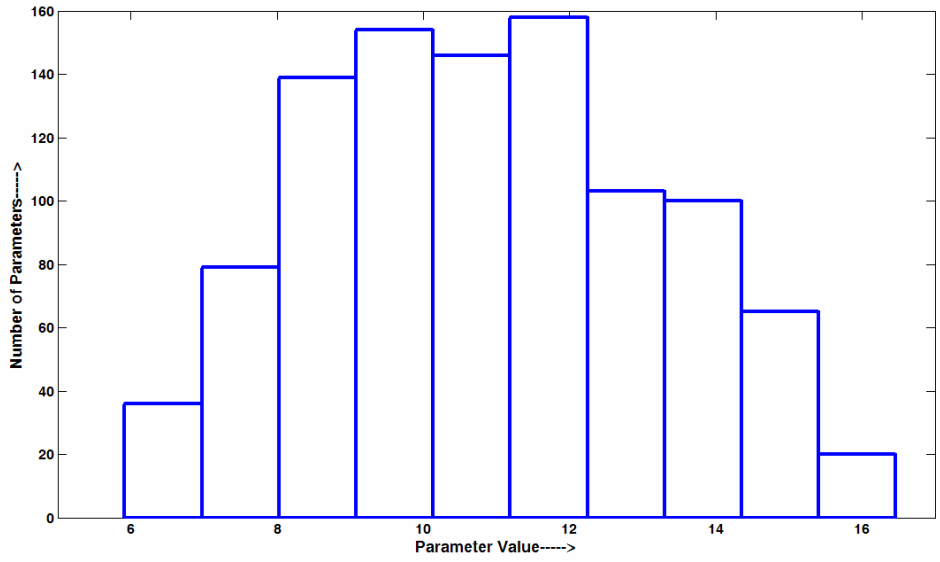

Figure 3.14 Histogram of estimated -parameter value for resistance parameter R_1 of Model 2 for Windkessel-1 modeling scheme with MABP as the input

Table 3.13 Average values of true-parameters (M_a) and estimated parameters (M_e) of Model 3 for Windkessel-1 modeling scheme with MABP as the input

	R_1	R_2	C_1	C_2	L_1
Average M_a	10.4960	5.5047	3.0135	7.0022	4.4622
STD M_a	1.9900	1.4459	1.1878	1.7104	1.4511
Average M_e	3.8924	4.1657	1.2789	7.7019	4.0221
STD M_e	11.7690	1.3747	0.9050	1.8541	1.2931

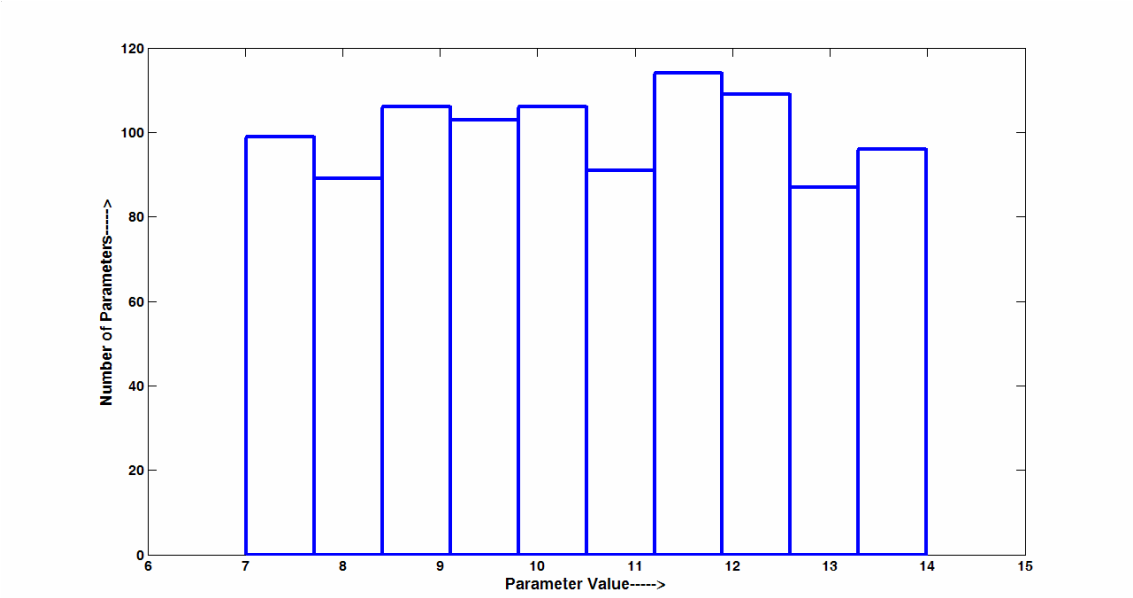

Figure 3.15 Histogram of true-parameter value for resistance parameter R_1 of Model 3 for Windkessel-1 modeling scheme with MABP as the input

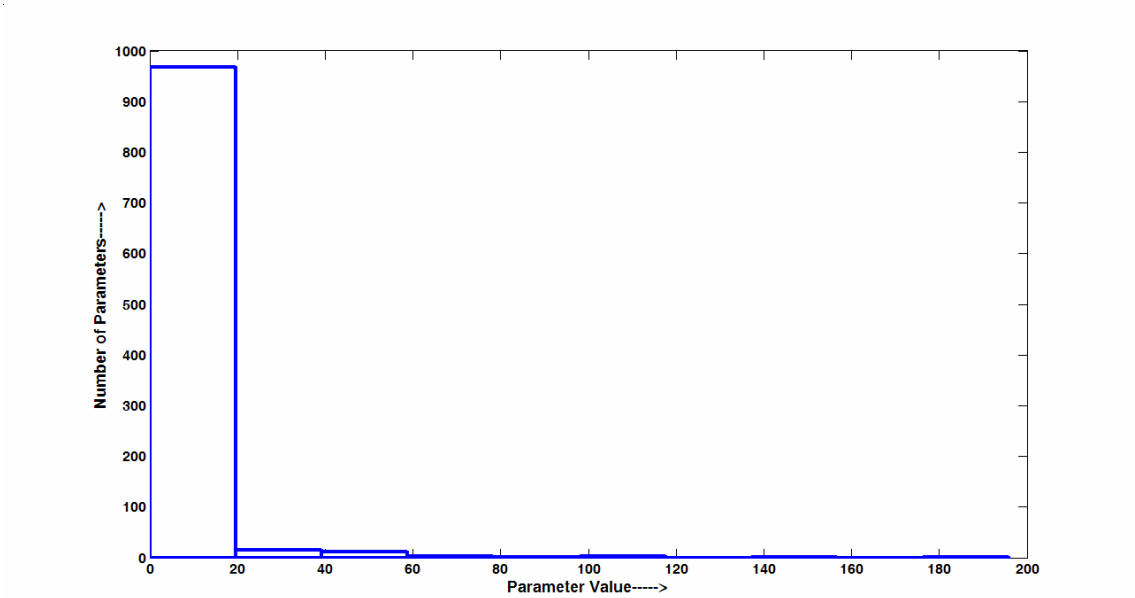

Figure 3.16 Histogram of estimated -parameter value for resistance parameter R_1 of Model 3 for Windkessel-1 modeling scheme with MABP as the input

Table 3.14 Average values of true-parameters (M_a) and estimated parameters (M_e) of Model 4 for Windkessel-1 modeling scheme with MABP as the input

	R_1	R_2	C_1	C_2	L_1
Average M_a	10.4960	5.5047	3.0135	7.0022	4.4622
STD M_a	1.9900	1.4459	1.1878	1.7104	1.4511
Average M_e	10.7200	4.8132	3.5650	5.9863	3.8964
STD M_e	2.3150	2.0204	1.3925	2.1684	1.7830

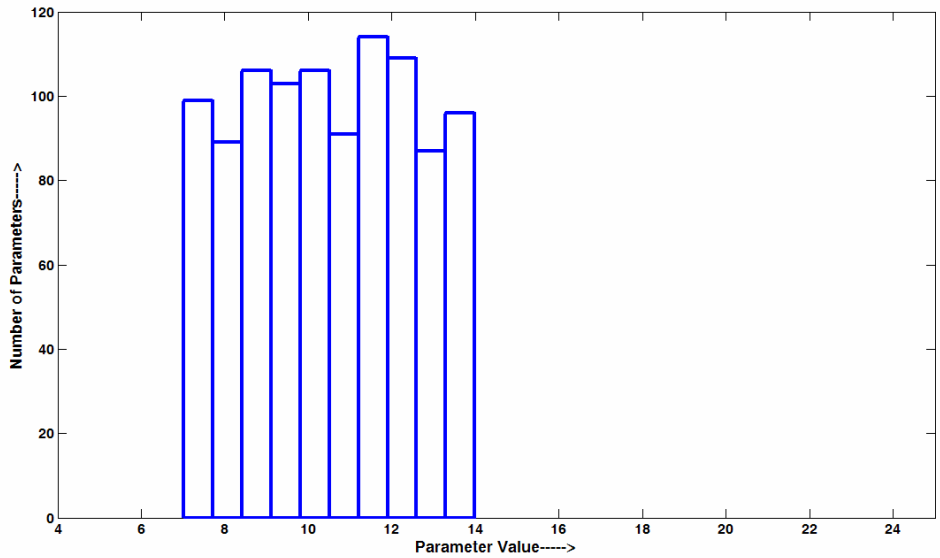

Figure 3.17 Histogram of true-parameter value for resistance parameter R_1 of Model 4 for Windkessel-1 modeling scheme with MABP as the input

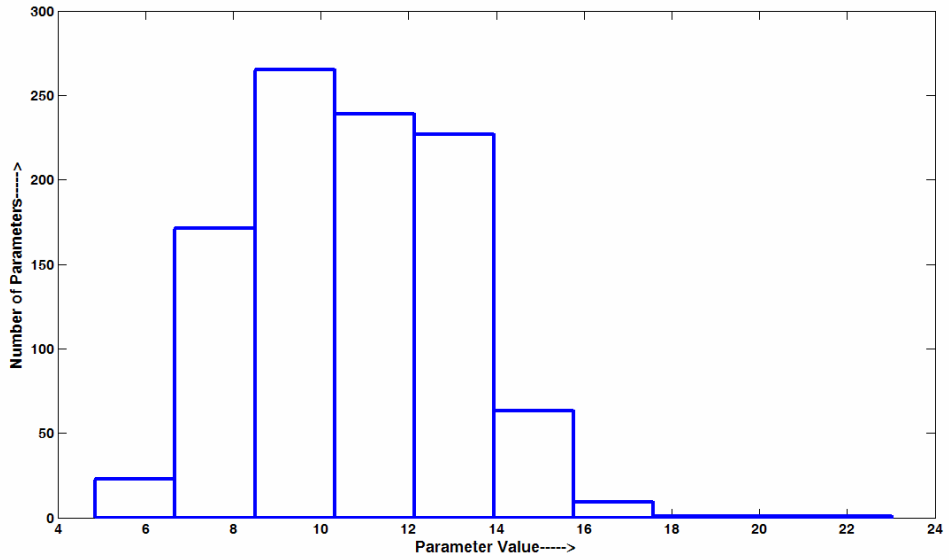

Figure 3.18 Histogram of estimated -parameter value for resistance parameter R_1 of Model 4 for Windkessel-1 modeling scheme with MABP as the input

Table 3.15 Average values of true-parameters (M_a) and estimated parameters (M_e) of Model 5 for Windkessel-1 modeling scheme with MABP as the input

	R_1	R_2	C_1	L1
Average M_a	10.5870	5.5659	3.0049	4.4477
STD M_a	2.0381	1.4436	1.1774	1.4262
Average M_e	6.1941	5.0987	2.9331	4.1528
STD M_e	13.1390	1.9568	1.5060	1.5386

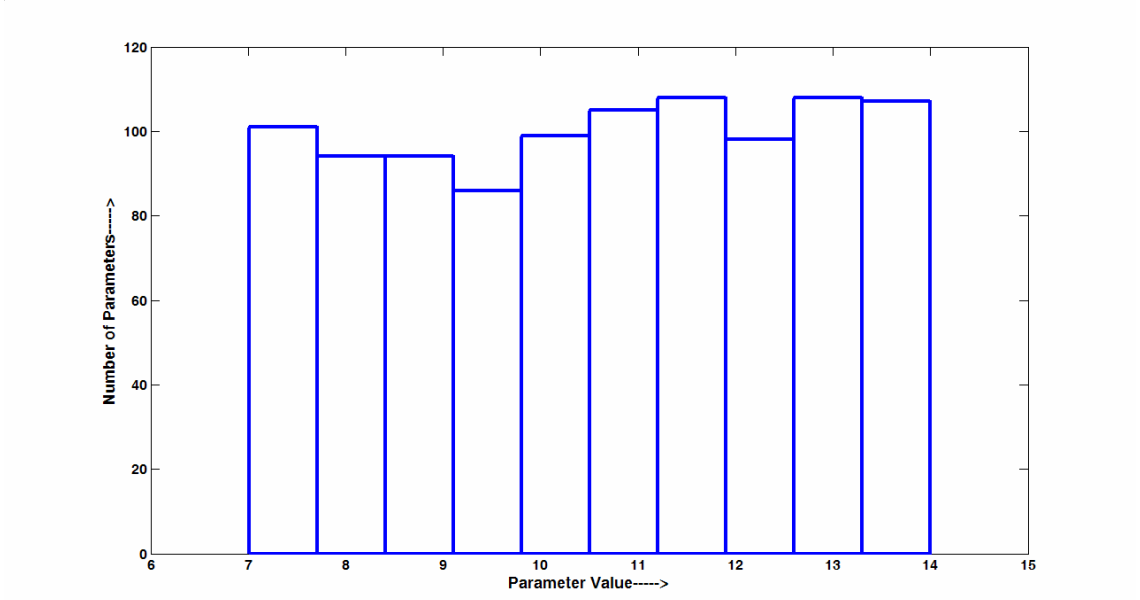

Figure 3.19 Histogram of true-parameter value for resistance parameter R_1 of Model 5 for Windkessel-1 modeling scheme with MABP as the input

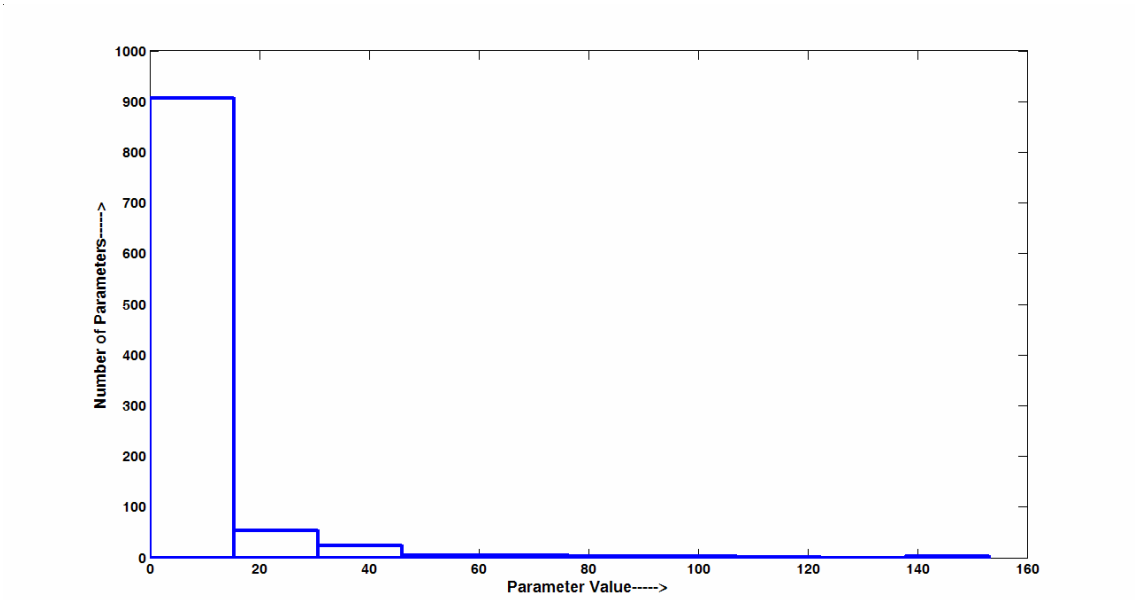

Figure 3.20 Histogram of estimated -parameter value for resistance parameter R_1 of Model 5 for Windkessel-1 modeling scheme with MABP as the input

Table 3.16 Average MSE values for five Windkessel models for Windkessel-1 modeling scheme with MABP input

	Model 1	Model 2	Model 3	Model 4	Model 5
Average MSE	1.6983E-06	2.4799E-06	6.03E-02	9.1161E-06	3.95E-02
STD	2.9331E-06	3.5338E-06	2.494E-01	2.2350E-05	1.137E-01

3.1.2.3 Results for Windkessel-2 Modeling Scheme with PRBS Input

This section presents the average MSE values (Table 3.22), true-parameters (M_a) and estimated-parameters (M_e) (Table 3.17 through Table 3.21) of 1000 trials Monte-Carlo simulation for Windkessel-2 modeling scheme with PRBS as the input, for each of the five Windkessel models. Histograms (Figure 3.21 through Figure 3.30) for true-parameter values and estimated-parameter values for the resistance parameter R_1 of each of the five Windkessel models have also been shown.

Table 3.17 Average values of true-parameters (M_a) and estimated parameters (M_e) of Model 1 for Windkessel-2 modeling scheme with PRBS as the input

	R_1	R_2	C_1
Average M_a	10.4230	5.5639	3.0562
STD M_a	2.0503	1.4206	1.1531
Average M_e	10.4230	5.2845	3.0761
STD M_e	2.0497	1.5010	1.1707

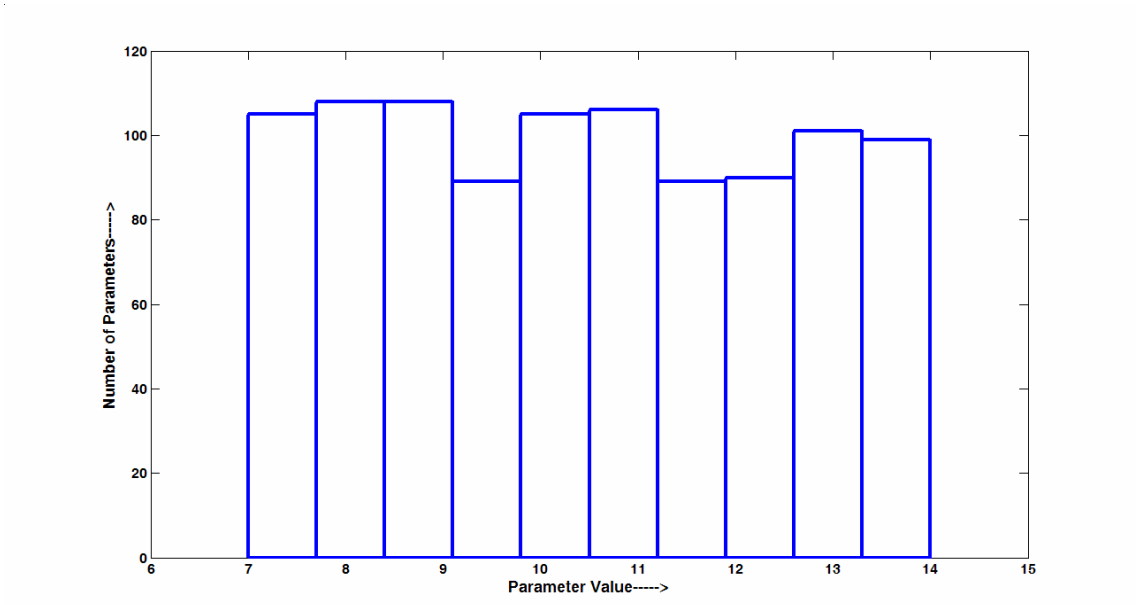

Figure 3.21 Histogram of true-parameter value for resistance parameter R_1 of Model 1 for Windkessel-2 modeling scheme with PRBS as the input

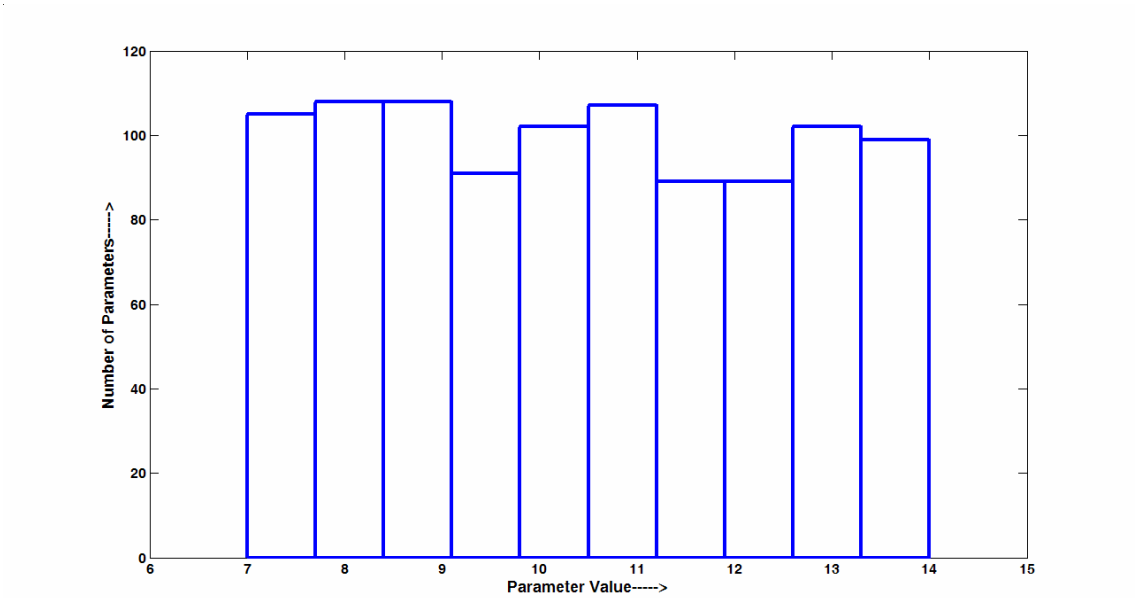

Figure 3.22 Histogram of estimated -parameter value for resistance parameter R_1 of Model 1 for Windkessel-2 modeling scheme with PRBS as the input

Table 3.18 Average values of true-parameters (M_a) and estimated parameters (M_e) of Model 2 for Windkessel-2 modeling scheme with PRBS as the input

	R_1	R_2	C_1	R_3	C_2
Average M_a	10.4340	5.5388	3.0050	6.9854	4.5769
STD M_a	2.0706	1.4263	1.1534	1.7559	1.4880
Average M_e	10.4340	4.8745	2.6755	9.6261	4.8651
STD M_e	2.0702	1.1828	1.0138	1.2782	0.9148

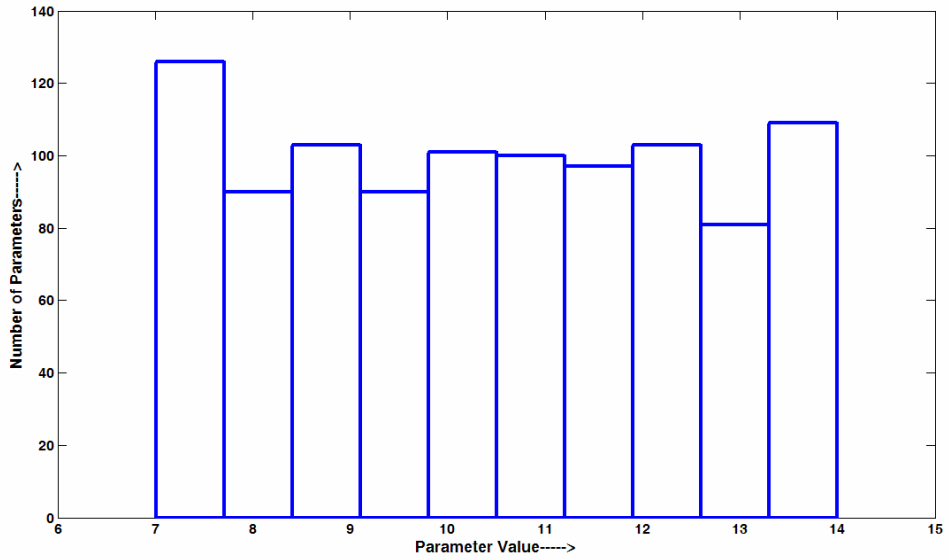

Figure 3.23 Histogram of true-parameter value for resistance parameter R_1 of Model 2 for Windkessel-2 modeling scheme with PRBS as the input

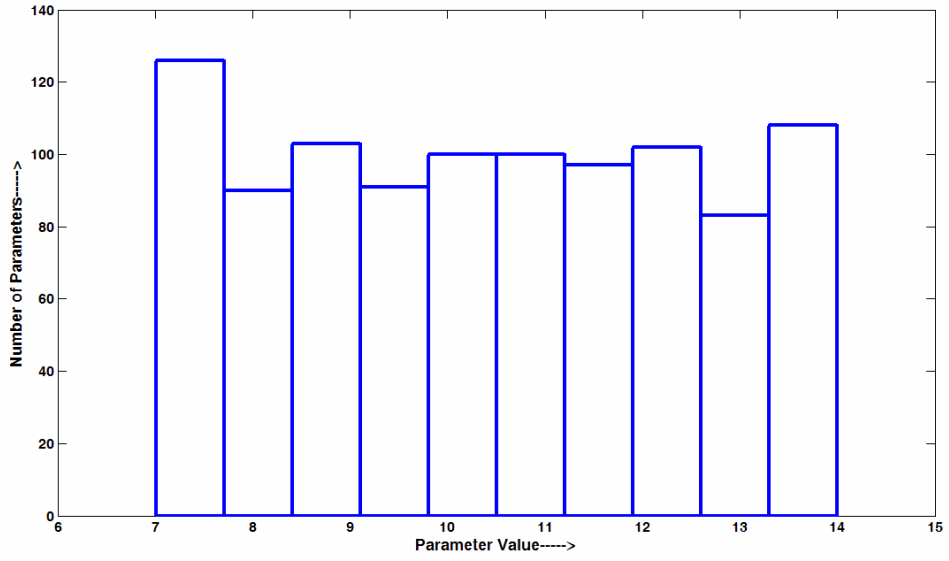

Figure 3.24 Histogram of estimated -parameter value for resistance parameter R_1 of Model 2 for Windkessel-2 modeling scheme with PRBS as the input

Table 3.19 Average values of true-parameters (M_a) and estimated parameters (M_e) of Model 3 for Windkessel-2 modeling scheme with PRBS as the input

	R_1	R_2	C_1	C_2	L_1
Average M_a	10.4340	5.5388	3.0050	6.9854	4.5769
STD M_a	2.0706	1.4263	1.1534	1.7559	1.4880
Average M_e	10.4940	5.4479	3.0371	6.9683	4.6976
STD M_e	2.1013	1.4639	1.2332	1.7779	1.4910

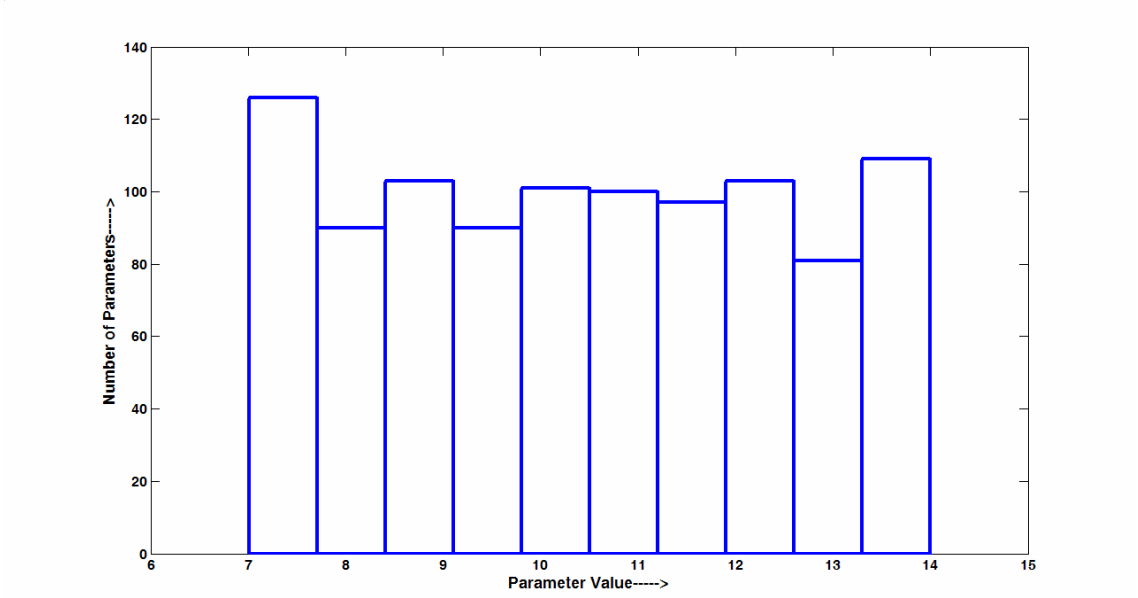

Figure 3.25 Histogram of true-parameter value for resistance parameter R_1 of Model 3 for Windkessel-2 modeling scheme with PRBS as the input

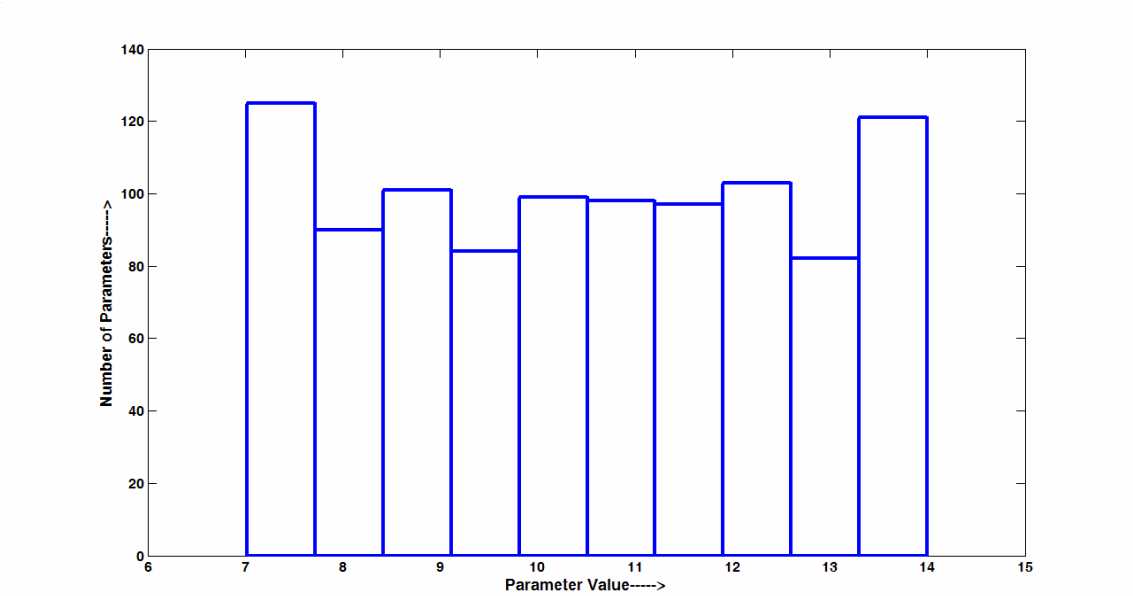

Figure 3.26 Histogram of estimated -parameter value for resistance parameter R_1 of Model 3 for Windkessel-2 modeling scheme with PRBS as the input

Table 3.20 Average values of true-parameters (M_a) and estimated parameters (M_e) of Model 4 for Windkessel-2 modeling scheme with PRBS as the input

	R_1	R_2	C_1	C_2	L_1
Average M_a	10.4340	5.5388	3.0050	6.9854	4.5769
STD M_a	2.0706	1.4263	1.1534	1.7559	1.4880
Average M_e	10.4450	7.6277	3.3873	7.1113	4.0696
STD M_e	2.0720	0.75853	1.2572	1.8975	1.4601

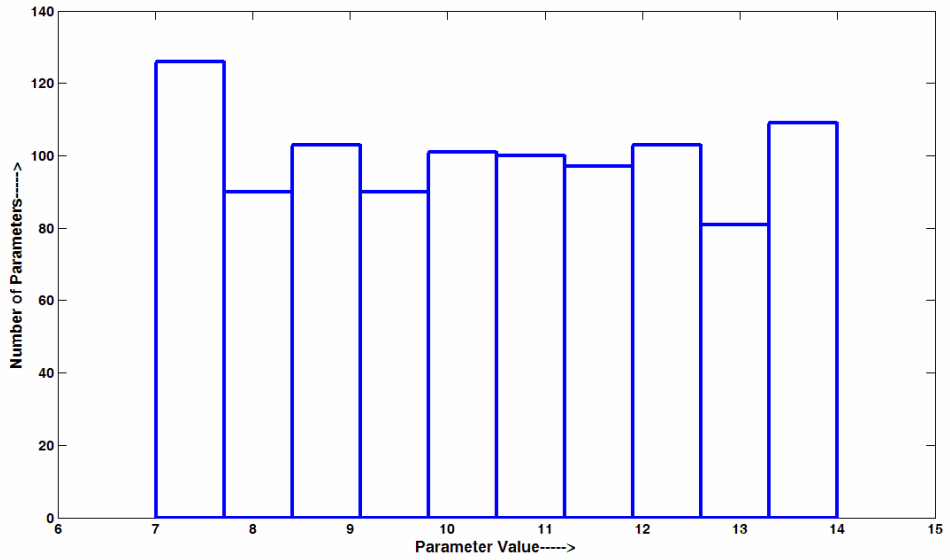

Figure 3.27 Histogram of true-parameter value for resistance parameter R_1 of Model 4 for Windkessel-2 modeling scheme with PRBS as the input

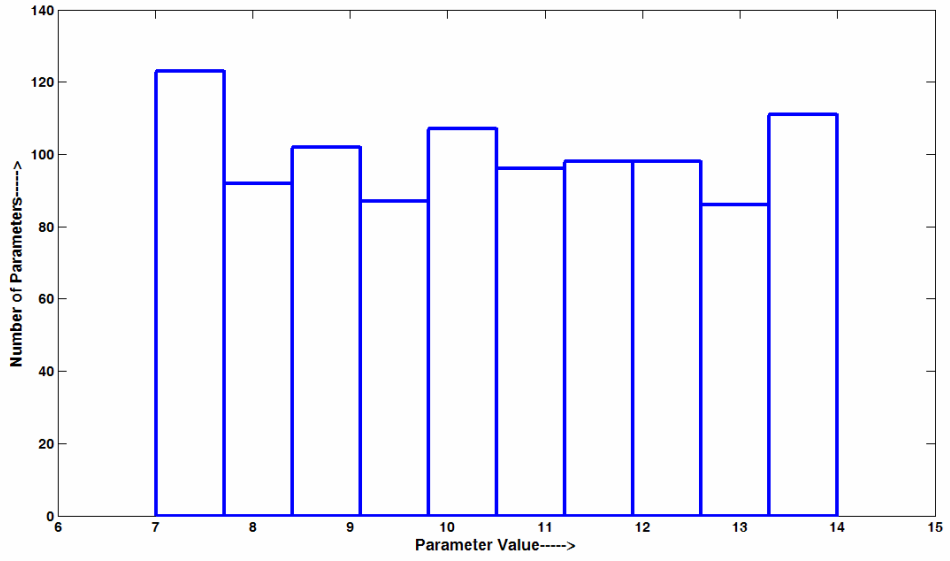

Figure 3.28 Histogram of estimated -parameter value for resistance parameter R_1 of Model 4 for Windkessel-2 modeling scheme with PRBS as the input

Table 3.21 Average values of true-parameters (M_a) and estimated parameters (M_e) of Model 5 for Windkessel-2 modeling scheme with PRBS as the input

	R_1	R_2	C_1	L1
Average M_a	10.4930	5.5396	3.0018	4.5158
STD M_a	2.0558	1.4338	1.1624	1.4556
Average M_e	10.4930	5.5396	3.0018	4.5158
STD M_e	2.0559	1.4338	1.1624	1.4556

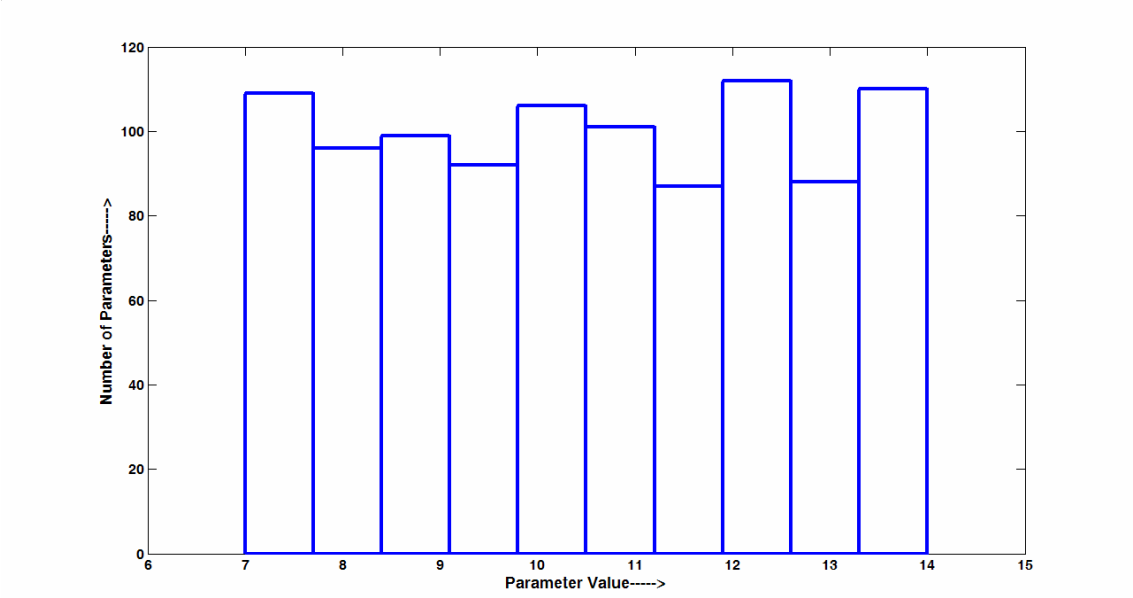

Figure 3.29 Histogram of true-parameter value for resistance parameter R_1 of Model 5 for Windkessel-2 modeling scheme with PRBS as the input

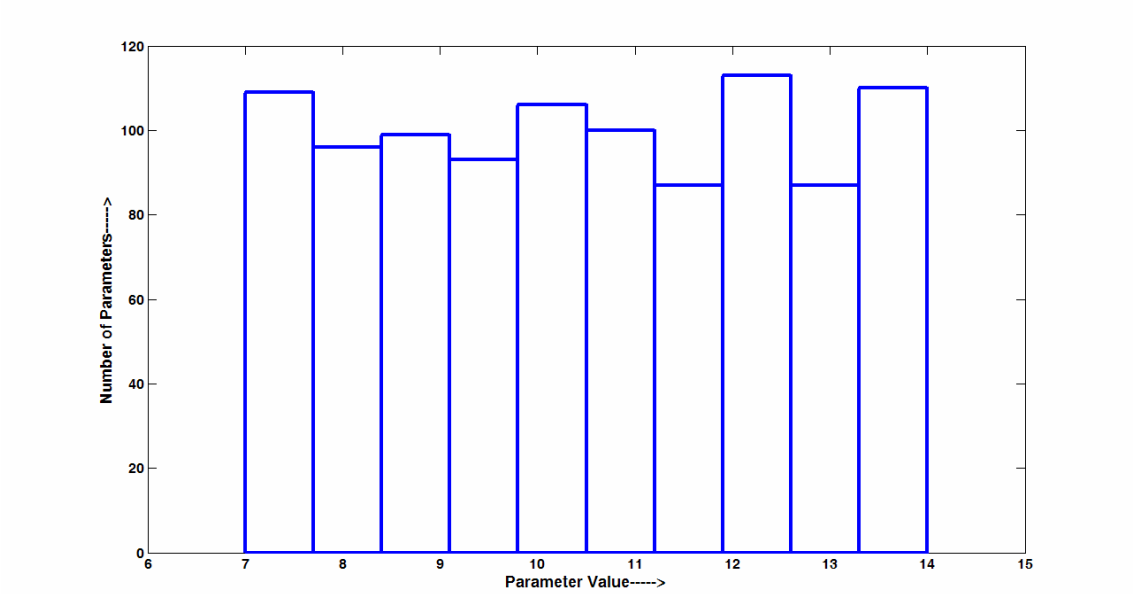

Figure 3.30 Histogram of estimated -parameter value for resistance parameter R_1 of Model 5 for Windkessel-2 modeling scheme with PRBS as the input

Table 3.22 Average MSE values for five Windkessel models for Windkessel-2 modeling scheme with PRBS input

	Model 1	Model 2	Model 3	Model 4	Model 5
Average MSE	2.1995E-08	3.1807E-08	4.6E-03	4.6159E-06	7.0492E-11
STD	1.0012E-07	1.7981E-07	2.92E-02	1.4494E-05	5.9846E-10

3.1.2.4 Results for Windkessel-2 Modeling Scheme with MABP Input

This section presents the average MSE values (Table 3.28), true-parameters (M_a) and estimated-parameters (M_e) (Table 3.23 through Table 3.27) of 1000 trials Monte-Carlo simulation for Windkessel-2 modeling scheme with first 1.5 minute section of the 6 minute MABP (SNI) as the input, for each of the five Windkessel models. Histograms (Figure 3.31 through Figure 3.40) for true-parameter values and estimated-parameter

values for the resistance parameter R_1 of each of the five Windkessel models have also been shown.

Table 3.23 Average values of true-parameters (M_a) and estimated parameters (M_e) of Model 1 for Windkessel-2 modeling scheme with MABP as the input

	R_1	R_2	C_1
Average M_a	10.5070	5.5285	2.9799
STD M_a	2.0503	1.4220	1.1811
Average M_e	10.5160	5.5097	3.0334
STD M_e	2.0557	1.6138	1.2273

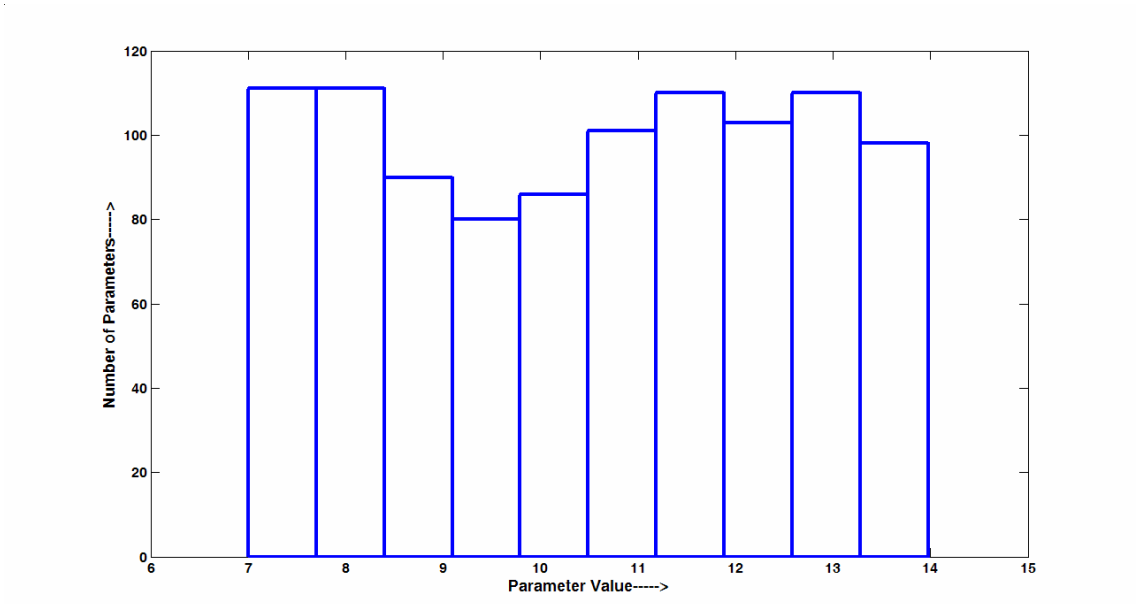

Figure 3.31 Histogram of true-parameter value for resistance parameter R_1 of Model 1 for Windkessel-2 modeling scheme with MABP as the input

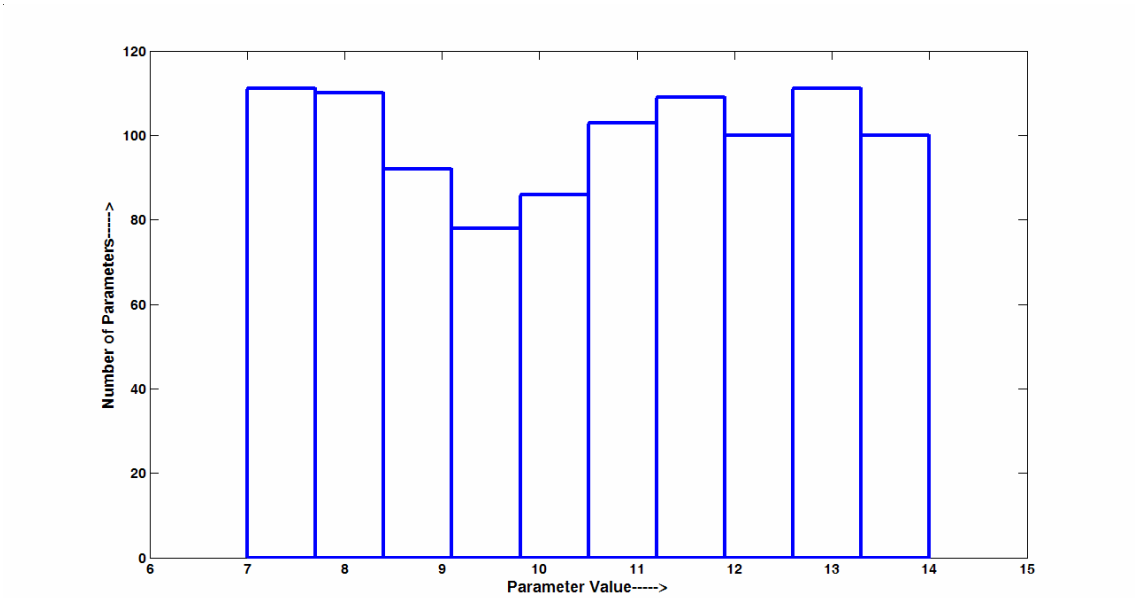

Figure 3.32 Histogram of estimated -parameter value for resistance parameter R_1 of Model 1 for Windkessel-2 modeling scheme with MABP as the input

Table 3.24 Average values of true-parameters (M_a) and estimated parameters (M_e) of Model 2 for Windkessel-2 modeling scheme with MABP as the input

	R_1	R_2	C_1	R_3	C_2
Average M_a	10.4960	5.5047	3.0135	7.0022	4.4622
STD M_a	1.9900	1.4459	1.1878	1.7104	1.4511
Average M_e	10.4990	5.4583	2.6018	9.2680	5.1708
STD M_e	1.9917	1.4876	1.0598	1.6538	0.97631

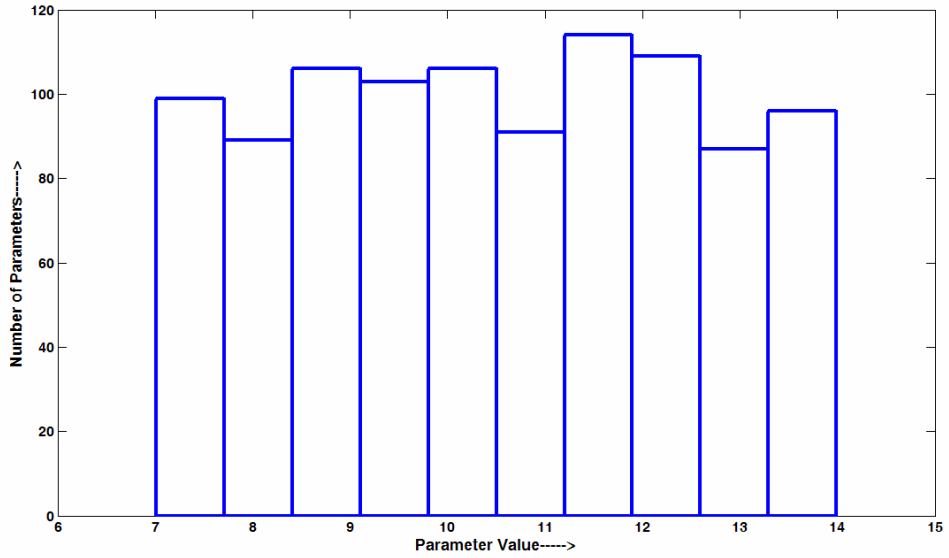

Figure 3.33 Histogram of true-parameter value for resistance parameter R_1 of Model 2 for Windkessel-2 modeling scheme with MABP as the input

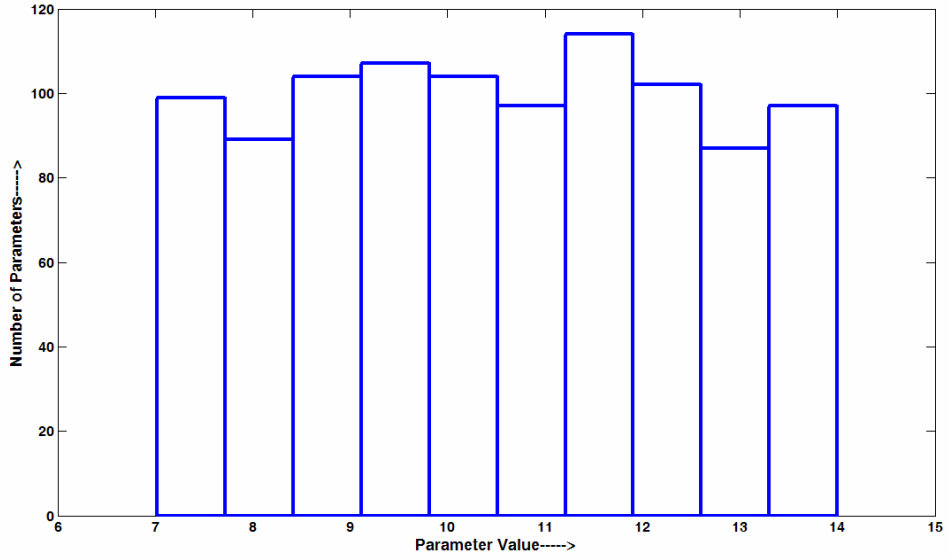

Figure 3.34 Histogram of estimated -parameter value for resistance parameter R_1 of Model 2 for Windkessel-2 modeling scheme with MABP as the input

Table 3.25 Average values of true-parameters (M_a) and estimated parameters (M_e) of Model 3 for Windkessel-2 modeling scheme with MABP as the input

	R_1	R_2	C_1	C_2	L_1
Average M_a	10.4960	5.5047	3.0135	7.0022	4.4622
STD M_a	1.9900	1.4459	1.1878	1.7104	1.4511
Average M_e	10.4850	5.4978	3.1251	6.9983	4.4787
STD M_e	1.9953	1.4545	1.2542	1.7113	1.4524

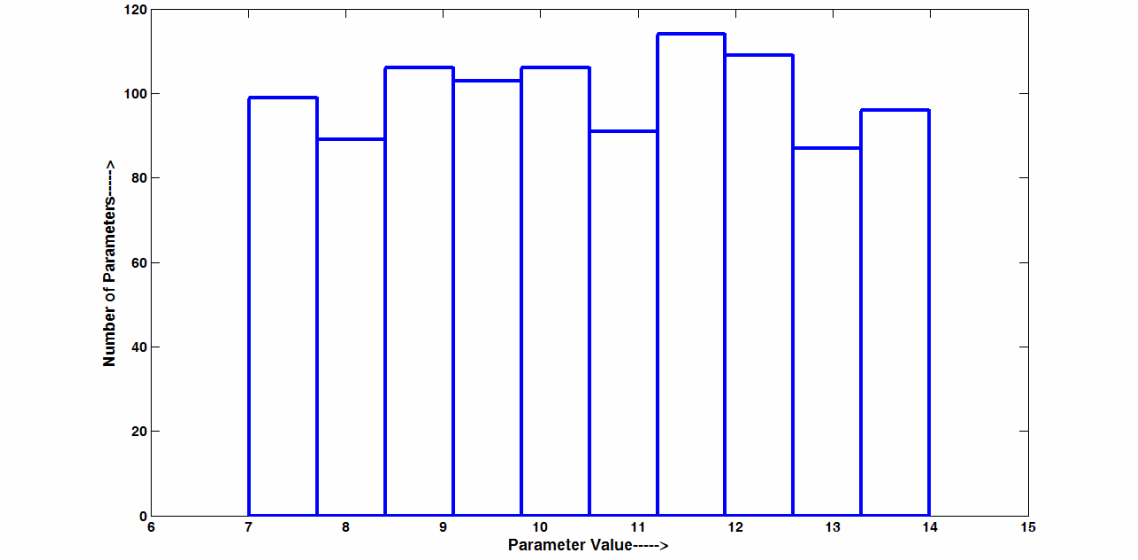

Figure 3.35 Histogram of true-parameter value for resistance parameter R_1 of Model 3 for Windkessel-2 modeling scheme with MABP as the input

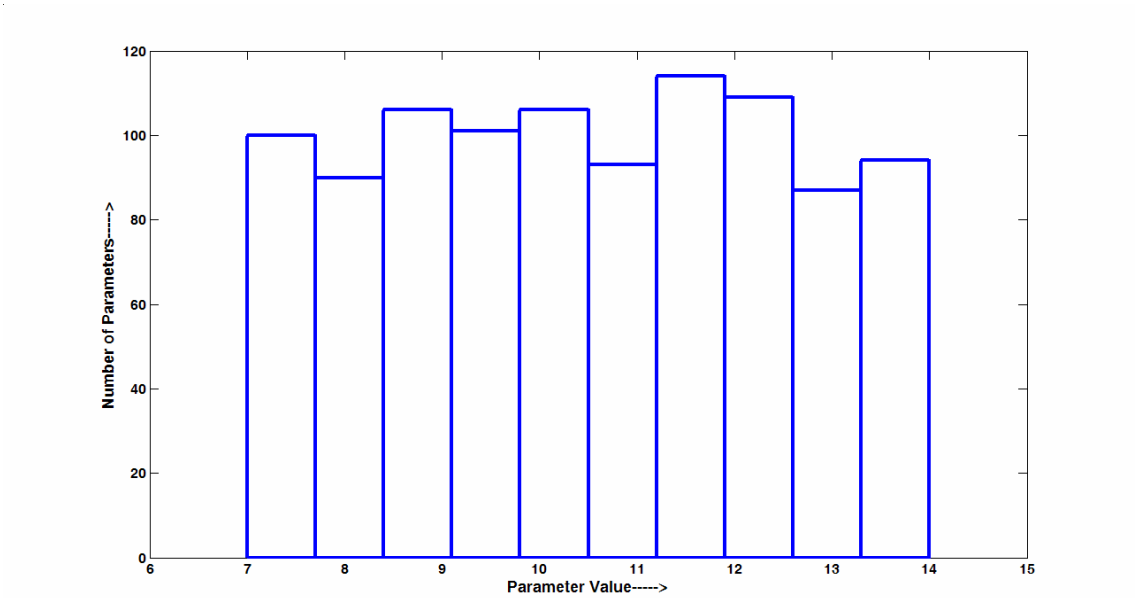

Figure 3.36 Histogram of estimated -parameter value for resistance parameter R_1 of Model 3 for Windkessel-2 modeling scheme with MABP as the input

Table 3.26 Average values of true-parameters (M_a) and estimated parameters (M_e) of Model 4 for Windkessel-2 modeling scheme with MABP as the input

	R_1	R_2	C_1	C_2	L_1
Average M_a	10.4960	5.5047	3.0135	7.0022	4.4622
STD M_a	1.9900	1.4459	1.1878	1.7104	1.4511
Average M_e	10.7350	7.4248	3.7271	7.4639	4.1468
STD M_e	2.0262	1.1877	1.2832	2.0851	1.6313

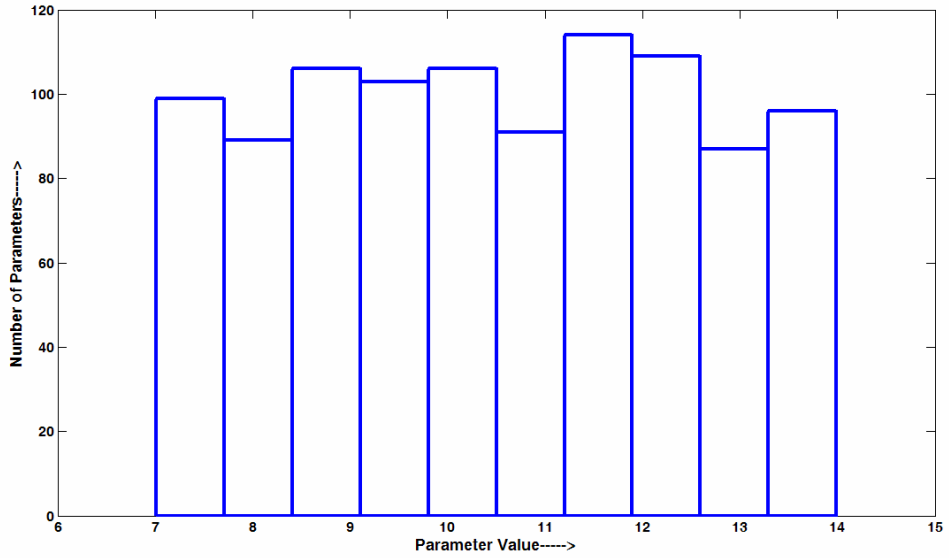

Figure 3.37 Histogram of true-parameter value for resistance parameter R_1 of Model 4 for Windkessel-2 modeling scheme with MABP as the input

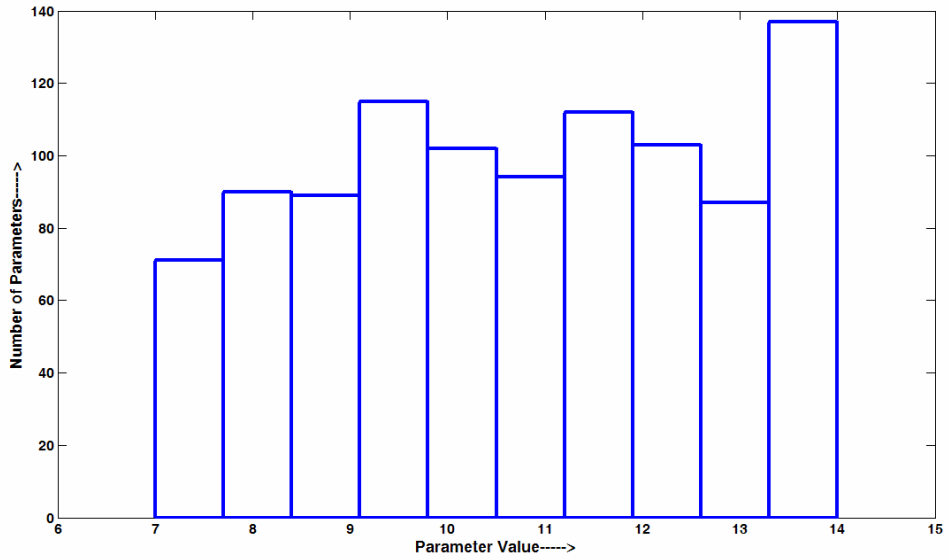

Figure 3.38 Histogram of estimated -parameter value for resistance parameter R_1 of Model 4 for Windkessel-2 modeling scheme with MABP as the input

Table 3.27 Average values of true-parameters (M_a) and estimated parameters (M_e) of Model 5 for Windkessel-2 modeling scheme with MABP as the input

	R_1	R_2	C_1	L1
Average M_a	10.5870	5.5659	3.0049	4.4477
STD M_a	2.0381	1.4436	1.1774	1.4262
Average M_e	10.5870	5.5659	3.0049	4.4477
STD M_e	2.0387	1.4437	1.1774	1.4262

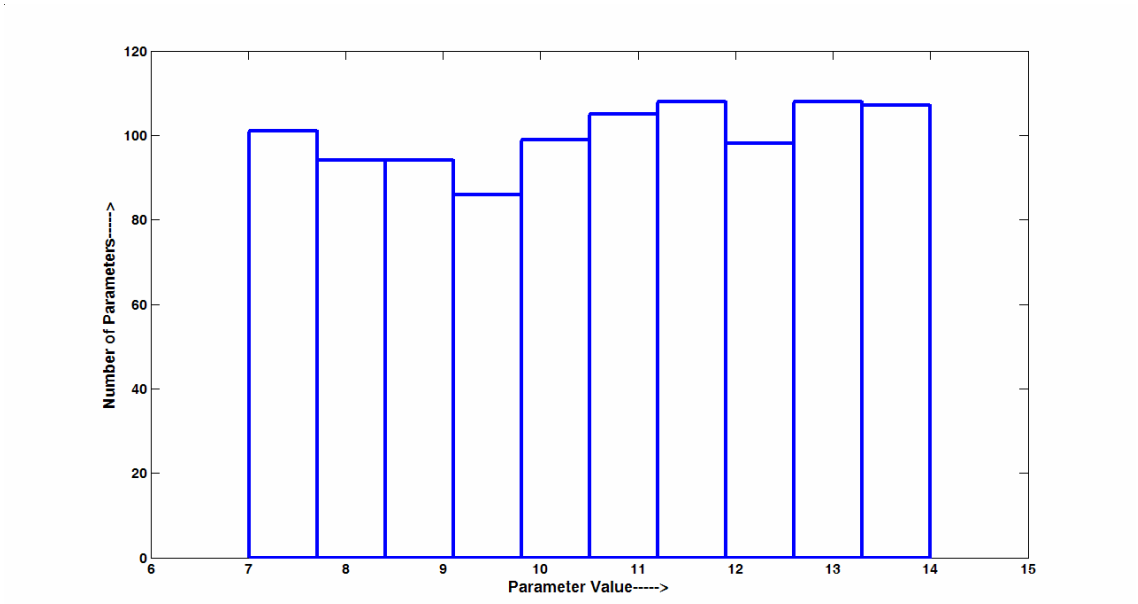

Figure 3.39 Histogram of true-parameter value for resistance parameter R_1 of Model 5 for Windkessel-2 modeling scheme with MABP as the input

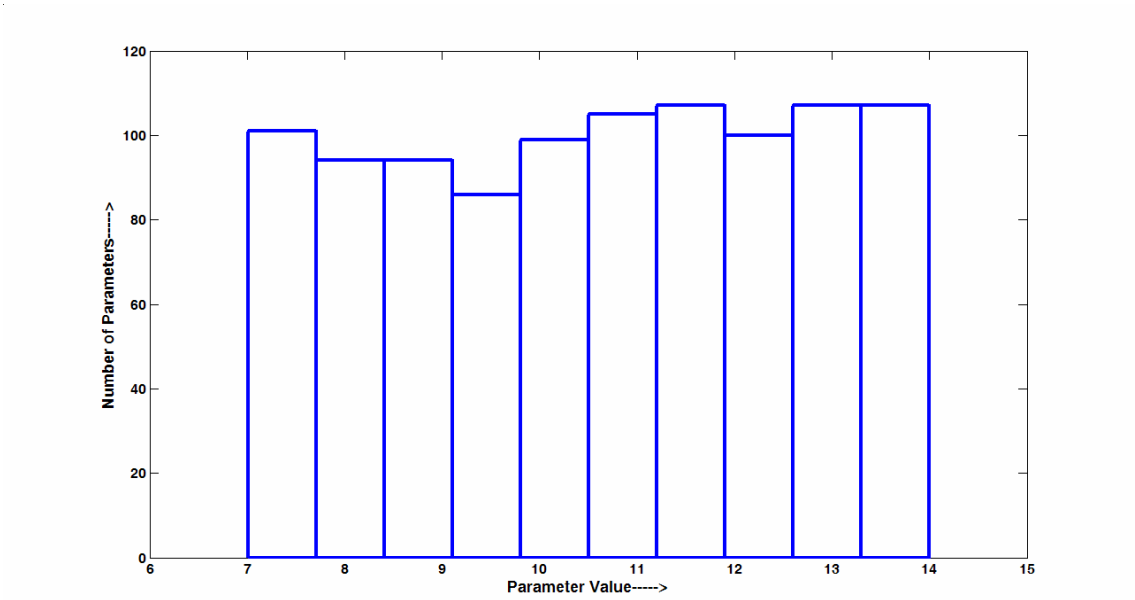

Figure 3.40 Histogram of estimated-parameter value for resistance parameter R_1 of Model 5 for Windkessel-2 modeling scheme with MABP as the input

Table 3.28 Average MSE values for five Windkessel models for Windkessel-2 modeling scheme with MABP input

	Model 1	Model 2	Model 3	Model 4	Model 5
Average MSE	1.2628E-08	2.6668E-08	8.2433E-04	6.5998E-06	2.5043E-10
STD	3.8493E-08	6.7055E-08	1.33E-02	1.6543E-05	5.1541E-09

3.2 Modeling Results for MABP and CBFV Data

This section presents the results of applying various linear, lumped parameter models and modeling methodologies, discussed in section 2.2, to MABP and CBFV data of all the 10 subjects for the four types of data conditions (SNI, SI, VNI, and VI).

3.2.1 MSE and Parameter Value Results

This section presents MSE values and average parameter values for 10 subjects using the ARX models (ARX-1 and ARX-2 modeling schemes described in section 2.2.1) and the five Windkessel models (Windkessel-1, Windkessel-2, and Windkessel-3 modeling schemes described in section 2.2.3).

Appendix B presents the results for the comparisons based on t-tests (P_{val}) for the MSE values of 10 subjects for four data conditions, between ARX-2, Windkessel-1, Windkessel-2 and Windkessel-3 modeling schemes. The statistical level of significance for the t-tests was selected to be 0.05. For Windkessel modeling schemes, the comparison was done between MSE value results with different schemes for a given model. These comparisons were done for all the five Windkessel models. For comparing ARX-2 with Windkessel-1 and Windkessel-2 modeling schemes, models with the similar order were considered.

3.2.1.1 Results for ARX Models

Table 3.29 shows the MSE values of 10 subjects for four conditions of data with ARX-1 modeling scheme. Table 3.30 shows the average numerator (m) and denominator (n) model orders for the same. Table 3.31, Table 3.33 and Table 3.35 show the MSE values of 10 subjects for four conditions of data with ARX-2 modeling scheme, for the 1^{st}, 2^{nd}, and 3^{rd} order models respectively. The average model parameters (as per the model structure in Equation 1.4) for each of the four data

conditions are shown in the Table 3.32, Table 3.34 and Table 3.36, for the 1st, 2nd, and 3rd order models respectively with ARX-2 modeling scheme.

Table 3.29 MSE values for four data conditions of 10 subjects with ARX-1 modeling scheme

Subject No.	SNI	SI	VNI	VI
1	0.0125	0.0232	0.0140	0.0277
2	0.0404	0.0331	0.0248	0.0121
3	0.0190	0.0399	0.0093	0.0462
4	0.0237	0.0290	0.0131	0.0386
5	0.0280	0.0482	0.0287	0.1145
6	0.0217	0.0397	0.0502	0.0297
7	0.0251	0.0245	0.0184	0.0436
8	0.0214	0.0506	0.0126	0.0190
9	0.0155	0.0264	0.0176	2.8671
10	0.0208	0.0266	0.0146	0.0143
Average	0.0228	0.0341	0.0203	0.3213
STD	0.0076	0.0099	0.0120	0.8950

Table 3.30 Numerator (*m*) and denominator (*n*) model orders for four data conditions of 10 subjects with ARX-1 modeling scheme

	SNI		SI		VNI		VI	
Subject No.	m	n	m	m	n	n	m	n
1	4	4	10	10	2	2	1	1
2	8	8	10	10	7	7	10	10
3	8	8	10	10	9	9	9	9
4	9	9	1	1	10	10	2	2
5	10	10	2	2	2	2	6	6

Table 3.30 *Continued.*

6	10	10	4	4	2	2	6	6
7	8	8	10	10	10	10	2	2
8	9	9	6	6	9	9	2	2
9	10	10	10	10	2	2	1	1
10	9	9	3	3	6	6	3	3
Average	8.5	8.5	6.6	6.6	5.9	5.9	4.2	4.2
STD	1.8	1.8	3.8	3.8	3.6	3.6	3.3	3.3

Table 3.31 MSE values for four data conditions of 10 subjects with ARX-2 modeling scheme for 1st order model (m=n=1)

Subject No.	SNI	SI	VNI	VI
1	0.0139	0.0262	0.0294	0.0277
2	0.0503	0.0535	0.0295	0.0237
3	0.0295	0.0476	0.0123	0.7397
4	0.0541	0.0290	0.0215	0.0464
5	0.0536	0.0554	0.0832	0.8201
6	0.0246	0.0504	0.0610	0.0507
7	0.0501	0.0274	0.0244	0.0488
8	0.0401	0.0522	0.0416	0.0215
9	0.0311	0.0376	0.0206	2.8671
10	0.0362	0.0332	0.0200	0.0149
Average	0.0383	0.0412	0.0344	0.4661
STD	0.0137	0.0117	0.0220	0.8992

Table 3.32 Average parameter values for four data conditions of 10 subjects with ARX-2 modeling scheme for 1st order model (m=n=1)

	a_1	b_0	b_1
SNI Average	-0.9424	0.6228	-0.6809
SNI STD	0.0408	0.2926	0.2845
SI Average	-0.9504	0.41563	-0.4430
SI STD	0.0195	0.3341	0.3087
VNI Average	-0.9405	0.5385	-0.5804
VNI STD	0.0393	0.0841	0.0768
VI Average	-0.9665	0.2961	-0.3676
VI STD	0.0484	0.2605	0.2666

Table 3.33 MSE values for four data conditions of 10 subjects with ARX-2 modeling scheme for 2nd order model (m=n=2)

Subject No.	SNI	SI	VNI	VI
1	0.0162	0.0251	0.0140	0.0277
2	0.0426	0.0394	0.0251	0.0169
3	0.0211	0.0489	0.0111	0.0526
4	0.0292	0.0298	0.0164	0.0390
5	0.0283	0.0482	0.0287	0.1535
6	0.0257	0.0398	0.0502	0.0463
7	0.0324	0.0261	0.0253	0.0448
8	0.0255	0.0548	0.0173	0.0209
9	0.0267	0.0290	0.0176	95.3820
10	0.0259	0.0285	0.0149	0.0143
Average	0.0274	0.0370	0.0221	9.5798
STD	0.0069	0.0108	0.0114	30.1478

Table 3.34 Average parameter values for four data conditions of 10 subjects with ARX-2 modeling scheme for 2nd order model (m=n=2)

	a_1	a_2	b_0	b_1	b_2
SNI Average	-1.6204	0.6743	0.6679	-1.1657	-1.6204
SNI STD	0.1045	0.0907	0.2595	0.4542	0.2126
SI Average	-1.4478	0.5283	0.3976	-0.5908	-1.4478
SI STD	0.1050	0.1154	0.3417	0.5411	0.2324
VNI Average	-1.4289	0.4990	0.5183	-0.7849	-1.4289
VNI STD	0.1992	0.1678	0.1237	0.2339	0.1667
VI Average	-1.2411	0.2845	0.1340	-0.0397	-1.2411
VI STD	0.3203	0.3273	0.3606	0.7340	0.4220

Table 3.35 MSE values for four data conditions of 10 subjects with ARX-2 modeling scheme for 3rd order model (m=n=3)

Subject No.	SNI	SI	VNI	VI
1	0.0154	0.0256	0.0245	0.0326
2	0.0436	0.0469	0.0253	0.0150
3	0.0210	0.0470	0.0099	0.0593
4	0.0282	0.0304	0.0178	0.0483
5	0.0285	0.0496	0.0481	0.2245
6	0.0238	0.0420	0.0564	0.0407
7	0.0332	0.0281	0.0199	0.0553
8	0.0299	0.0522	0.0169	0.0228
9	0.0397	0.0331	0.0217	1579.4000
10	0.0259	0.0266	0.0176	0.0143
Average	0.0289	0.0381	0.0258	157.9913
STD	0.0084	0.0104	0.0147	499.4321

Table 3.36 Average parameter values for four data conditions of 10 subjects with ARX-2 modeling scheme for 3rd order model (m=n=3)

	a_1	a_2	a_3	b_0	b_1	b_2	b_3
SNI Average	-1.8112	1.1465	-0.2958	0.6415	-1.8112	1.1465	-0.2958
SNI STD	0.1585	0.2370	0.1418	0.2442	0.4435	0.2939	0.1385
SI Average	-1.6178	0.9869	-0.3184	0.3920	-1.6178	0.9869	-0.3184
SI STD	0.1846	0.2721	0.0930	0.3443	0.5639	0.3918	0.1578
VNI Average	-1.5874	0.9454	-0.3102	0.4928	-1.5874	0.9454	-0.3102
VNI STD	0.2636	0.2983	0.1357	0.1341	0.3080	0.3088	0.1835
VI Average	-1.2797	0.5084	-0.2000	0.1660	-1.2797	0.5084	-0.2000
VI STD	0.3885	0.4004	0.1735	0.3165	0.7003	0.4959	0.1032

3.2.1.2 Results for Windkessel Models

Table 3.37 through Table 3.46 show the MSE values and average model parameters of 10 subjects for four conditions of data with Windkessel-1 modeling scheme, considering each of the five Windkessel models (section 2.2.2) consecutively. Table 3.47 through Table 3.56 show the MSE values and average model parameters of 10 subjects for four conditions of data with Windkessel-2 modeling scheme, considering each of the five Windkessel models one by one. Table 3.57 and Table 3.58 show respectively the MSE values and average model parameters of 10 subjects for four conditions of data, with Windkessel-3 modeling scheme for Model 1. Table 3.59 presents the average weights W_t and W_f for the four data conditions, corresponding to Windkessel-3 modeling scheme for Model 1.

Table 3.37 MSE values for four data conditions of 10 subjects with Windkessel-1 modeling scheme for Model 1

Subject No.	SNI	SI	VNI	VI
1	0.0260	0.0277	0.0191	0.0238
2	0.0587	0.0546	0.0270	0.1504
3	0.0368	0.0498	0.0179	0.0201
4	0.0298	0.0351	0.0254	0.0485
5	0.0771	0.0530	0.0199	0.0363
6	0.0382	0.0372	0.0735	0.0169
7	0.0290	0.0321	0.0428	0.0287
8	0.0533	0.0819	0.0250	0.0341
9	0.0242	0.0263	0.0227	0.0385
10	0.0288	0.0279	0.0129	0.0381
Average	0.0402	0.0426	0.0286	0.0435
STD	0.0174	0.0175	0.0177	0.0387

Table 3.38 Average parameter values for four data conditions of 10 subjects with Windkessel-1 modeling scheme for Model 1

	R_1	R_2	C_1
SNI Average	1.5329	8.8824	28.3617
SNI STD	0.7145	6.6301	23.2065
SI Average	1.9924	9.7894	32.5481
SI STD	1.4844	6.2837	23.4758
VNI Average	2.3760	8.1754	16.2462
VNI STD	2.0864	5.7005	18.0469
VI Average	1.3973	9.6666	13.1472
VI STD	1.9086	8.7017	15.0612

Table 3.39 MSE values for four data conditions of 10 subjects with Windkessel-1 modeling scheme for Model 2

Subject No.	SNI	SI	VNI	VI
1	0.0244	0.0273	0.0189	0.0228
2	0.0593	0.0531	0.0269	0.1510
3	0.0362	0.0477	0.0161	0.0147
4	0.0289	0.0355	0.0269	0.0433
5	0.0761	0.0576	0.0254	0.0336
6	0.0376	0.0370	0.0731	0.0165
7	0.0300	0.0318	0.0463	0.0278
8	0.0520	0.0957	0.0268	0.0338
9	0.0261	0.0261	0.0224	0.0725
10	0.0378	0.0266	0.0198	0.0303
Average	0.0408	0.0438	0.0303	0.0446
STD	0.0167	0.0214	0.0172	0.0408

Table 3.40 Average parameter values for four data conditions of 10 subjects with Windkessel-1 modeling scheme for Model 2

	R_1	R_2	C_1	R_3	C_2
SNI Average	1.5329	26.2551	35.7744	26.2550	35.7744
SNI STD	0.7145	2.7918	22.9332	2.7919	22.9332
SI Average	1.9924	26.2119	27.7462	26.2115	27.7461
SI STD	1.4844	4.1990	21.5947	4.1991	21.5948
VNI Average	2.3760	25.0278	17.4914	25.0278	17.4914
VNI STD	2.0864	0.3238	15.3908	0.3238	15.3908
VI Average	1.3973	27.4183	19.9709	27.4183	19.9773
VI STD	1.9086	4.8475	15.9619	4.8475	15.9551

Table 3.41 MSE values for four data conditions of 10 subjects with Windkessel-1 modeling scheme for Model 3

Subject No.	SNI	SI	VNI	VI
1	0.0684	0.0264	0.0176	0.0306
2	0.0492	0.0515	0.0279	0.1388
3	0.0388	0.0507	0.0189	0.0176
4	0.0272	0.0301	0.0269	0.0508
5	0.0791	0.0640	0.0261	0.0284
6	0.0423	0.0376	0.1761	0.0173
7	0.0289	0.0371	0.0451	0.0307
8	0.0509	0.0899	0.0243	0.0273
9	0.0234	0.0253	0.0248	0.0477
10	0.0266	0.0289	0.0191	0.0662
Average	0.0435	0.0442	0.0407	0.0455
STD	0.0188	0.0205	0.0482	0.0362

Table 3.42 Average parameter values for four data conditions of 10 subjects with Windkessel-1 modeling scheme for Model 3

	R_1	R_2	C_1	C_2	L_1
SNI Average	1.5329	20.3869	29.7503	4.7524	19.6246
SNI STD	0.7145	13.6190	17.6996	10.9252	33.8786
SI Average	1.9924	16.4572	27.1882	18.4241	30.8701
SI STD	1.4844	16.4845	19.8806	38.4956	47.5156
VNI Average	2.3760	25.9372	20.1745	10.0448	12.4469
VNI STD	2.0864	19.4526	15.8554	31.6071	31.1373
VI Average	1.3973	19.3522	20.4882	17.6723	24.5257
VI STD	1.9086	13.3254	14.9148	35.9070	39.0916

Table 3.43 MSE values for four data conditions of 10 subjects with Windkessel-1 modeling scheme for Model 4

Subject No.	SNI	SI	VNI	VI
1	0.0646	0.0281	0.0188	0.0337
2	0.0601	0.0488	0.0267	0.1560
3	0.0368	0.0497	0.0116	0.0144
4	0.0251	0.0352	0.0268	0.0486
5	0.0769	0.0651	0.0187	0.0307
6	0.0371	0.0371	0.0788	0.0166
7	0.0297	0.0317	0.0485	0.0407
8	0.0535	0.0991	0.0262	0.0343
9	0.0246	0.0265	0.0231	0.0766
10	0.0574	0.0273	0.0185	0.0397
Average	0.0466	0.0449	0.0298	0.0491
STD	0.0183	0.0227	0.0198	0.0414

Table 3.44 Average parameter values for four data conditions of 10 subjects with Windkessel-1 modeling scheme for Model 4

	R_1	R_2	C_1	C_2	L_1
SNI Average	1.5329	25.3912	33.1921	26.1667	24.0506
SNI STD	0.7145	2.3732	18.6805	8.3929	16.7926
SI Average	1.9924	26.9083	27.5887	30.5677	24.1092
SI STD	1.4844	3.3342	16.9141	10.3460	6.7627
VNI Average	2.3760	21.5490	14.9707	35.7082	30.8593
VNI STD	2.0864	4.7502	11.8517	15.4627	13.9224
VI Average	1.3973	22.8528	19.5813	23.0911	32.8060
VI STD	1.9086	8.9954	18.7893	14.2796	25.4029

Table 3.45 MSE values for four data conditions of 10 subjects with Windkessel-1 modeling scheme for Model 5

Subject No.	SNI	SI	VNI	VI
1	0.0251	0.0267	0.0219	0.0230
2	0.0587	0.0536	0.0314	0.1503
3	0.0283	0.0508	0.0096	0.0146
4	0.0268	0.0346	0.0252	0.0341
5	0.0354	0.0632	0.0218	0.0356
6	0.0290	0.0384	0.0782	0.0166
7	0.0285	0.0264	0.0458	0.0281
8	0.0282	0.0818	0.0146	0.0322
9	0.0170	0.0290	0.0218	0.0712
10	0.0371	0.0242	0.0213	0.0315
Average	0.0314	0.0429	0.0292	0.0437
STD	0.0110	0.0191	0.0198	0.0406

Table 3.46 Average parameter values for four data conditions of 10 subjects with Windkessel-1 modeling scheme for Model 5

	R_1	R_2	C_1	L1
SNI Average	1.5329	23.6617	8.8275	44.7052
SNI STD	0.7145	0.9367	15.7902	18.2145
SI Average	1.9924	21.5743	12.3457	36.0597
SI STD	1.4844	7.5678	16.7438	15.5624
VNI Average	2.3760	23.3314	7.7868	48.1243
VNI STD	2.0864	2.7300	8.2423	14.4253
VI Average	1.3973	23.6883	6.6599	65.1797
VI STD	1.9086	1.1810	6.4392	27.4140

Table 3.47 MSE values for four data conditions of 10 subjects with Windkessel-2 modeling scheme for Model 1

Subject No.	SNI	SI	VNI	VI
1	0.0449	0.0242	0.0185	0.0340
2	0.0591	0.0495	0.0270	0.0234
3	0.0359	0.0473	0.0177	0.0199
4	0.0268	0.0312	0.0298	0.0464
5	0.0422	0.0477	0.0175	0.0347
6	0.0370	0.0368	0.0830	0.0352
7	0.0290	0.0282	0.0330	0.0572
8	0.0460	0.0578	0.0226	0.0310
9	0.0193	0.0252	0.0222	0.0773
10	0.0349	0.0274	0.0129	0.0426
Average	0.0375	0.0375	0.0284	0.0402
STD	0.0113	0.0121	0.0202	0.0169

Table 3.48 Average parameter values for four data conditions of 10 subjects with Windkessel-2 modeling scheme for Model 1

	R_1	R_2	C_1
SNI Average	8.0161	8.2612	33.0462
SNI STD	10.2749	6.3452	22.3281
SI Average	8.6681	9.7120	32.7543
SI STD	15.4876	6.2425	23.5232
VNI Average	9.1973	8.2614	22.6639
VNI STD	12.0709	6.3383	20.0251
VI Average	22.9406	10.3099	23.5276
VI STD	38.3065	8.2813	23.2020

Table 3.49 MSE values for four data conditions of 10 subjects with Windkessel-2 modeling scheme for Model 2

Subject No.	SNI	SI	VNI	VI
1	0.0448	0.0233	0.0176	0.0241
2	0.0591	0.0495	0.0269	0.0234
3	0.0356	0.0467	0.0166	0.0168
4	0.0248	0.0332	0.0220	0.0450
5	0.0422	0.0481	0.0250	0.0223
6	0.0367	0.0362	0.0839	0.0216
7	0.0298	0.0282	0.0331	0.0270
8	0.0455	0.0578	0.0265	0.0187
9	0.0245	0.0250	0.0211	0.0773
10	0.0365	0.0264	0.0145	0.0433
Average	0.0380	0.0374	0.0287	0.0319
STD	0.0105	0.0122	0.0202	0.0186

Table 3.50 Average parameter values for four data conditions of 10 subjects with Windkessel-2 modeling scheme for Model 2

	R_1	R_2	C_1	R_3	C_2
SNI Average	7.8713	26.3359	42.9820	26.3359	42.9820
SNI STD	9.3628	2.7450	15.4970	2.7450	15.4970
SI Average	12.7735	26.4834	33.5911	26.4833	33.5912
SI STD	22.6516	4.0237	19.1495	4.0237	19.1495
VNI Average	7.2064	25.0671	25.4152	25.0671	25.4152
VNI STD	10.6611	0.3183	15.2766	0.3183	15.2767
VI Average	20.8110	27.7915	32.7508	27.7915	32.7508
VI STD	40.1255	4.6252	19.1772	4.6252	19.1772

Table 3.51 MSE values for four data conditions of 10 subjects with Windkessel-2 modeling scheme for Model 3

Subject No.	SNI	SI	VNI	VI
1	0.0401	0.0260	0.0173	0.0480
2	0.0540	0.0489	0.0273	0.0226
3	0.0361	0.0477	0.0181	0.0167
4	0.0273	0.0301	0.0206	0.0454
5	0.0481	0.0473	0.0262	0.0340
6	0.0365	0.0375	0.0991	0.0204
7	0.0288	0.0281	0.0291	0.0399
8	0.0335	0.0567	0.0236	0.0272
9	0.0214	0.0257	0.0247	0.0513
10	0.0350	0.0411	0.0133	0.0474
Average	0.0361	0.0389	0.0299	0.0353
STD	0.0097	0.0111	0.0248	0.0128

Table 3.52 Average parameter values for four data conditions of 10 subjects with Windkessel-2 modeling scheme for Model 3

	R_1	R_2	C_1	C_2	L_1
SNI Average	15.8771	20.1355	31.2447	4.1391	21.8415
SNI STD	28.6559	13.9423	15.8133	10.5438	32.7747
SI Average	21.3474	16.5538	29.1594	20.9048	31.1317
SI STD	30.9661	16.4512	16.3215	38.0726	47.5442
VNI Average	8.5425	22.2618	21.0075	11.7651	18.8416
VNI STD	10.2881	14.0492	14.7906	31.4168	34.5104
VI Average	14.0066	18.1953	19.4946	14.2211	19.9405
VI STD	30.3783	12.6804	15.9043	31.8751	31.9251

Table 3.53 MSE values for four data conditions of 10 subjects with Windkessel-2 modeling scheme for Model 4

Subject No.	SNI	SI	VNI	VI
1	0.0449	0.0250	0.0175	0.0335
2	0.0587	0.0497	0.0267	0.0234
3	0.0358	0.0474	0.0177	0.0152
4	0.0229	0.0317	0.0200	0.0468
5	0.0422	0.0481	0.0160	0.0333
6	0.0367	0.0366	0.0836	0.0385
7	0.0296	0.0281	0.0330	0.0587
8	0.0449	0.0578	0.0251	0.0341
9	0.0210	0.0256	0.0231	0.0773
10	0.0367	0.0269	0.0137	0.0413
Average	0.0373	0.0377	0.0277	0.0402
STD	0.0112	0.0120	0.0205	0.0177

Table 3.54 Average parameter values for four data conditions of 10 subjects with Windkessel-2 modeling scheme for Model 4

	R_1	R_2	C_1	C_2	L_1
SNI Average	7.9718	25.2762	35.0544	26.3504	25.2036
SNI STD	9.6189	2.3398	16.9732	8.2224	15.6754
SI Average	12.6025	26.6225	30.0333	30.2972	23.7685
SI STD	21.7436	3.3404	14.1941	10.4237	7.2445
VNI Average	7.3461	24.2064	24.0120	26.3904	25.4370
VNI STD	10.8016	2.9012	17.1942	12.9344	8.4018
VI Average	38.1045	22.9304	26.8146	22.0406	23.2772
VI STD	43.7974	7.5044	21.7643	8.7158	15.4406

Table 3.55 MSE values for four data conditions of 10 subjects with Windkessel-2 modeling scheme for Model 5

Subject No.	SNI	SI	VNI	VI
1	0.0688	0.0241	0.0246	0.0165
2	0.0588	0.0483	0.0367	0.0195
3	0.0219	0.0547	0.0071	0.0299
4	0.0292	0.0344	0.0207	0.0292
5	0.0443	0.0471	0.0197	0.0163
6	0.0458	0.0395	0.0852	0.0518
7	0.0282	0.0300	0.0311	0.0273
8	0.0487	0.0580	0.0156	0.0129
9	0.0204	0.0334	0.0149	0.0555
10	0.0363	0.0308	0.0198	0.0471
Average	0.0403	0.0400	0.0275	0.0306
STD	0.0159	0.0114	0.0219	0.0156

Table 3.56 Average parameter values for four data conditions of 10 subjects with Windkessel-2 modeling scheme for Model 5

	R_1	R_2	C_1	L1
SNI Average	7.2792	23.8807	15.6092	33.5468
SNI STD	10.6041	0.9630	9.1328	9.0880
SI Average	11.7018	21.4158	17.0747	28.9838
SI STD	16.4643	7.6545	16.2064	13.7019
VNI Average	8.1035	23.3604	12.4817	46.5449
VNI STD	11.8645	1.4264	14.6355	20.7988
VI Average	21.0600	24.2553	17.6818	46.2396
VI STD	34.3533	1.0850	17.4619	22.3397

Table 3.57 MSE values for four data conditions of 10 subjects with Windkessel-3 modeling scheme for Model 1

Subject No.	SNI	SI	VNI	VI
1	0.0365	0.0239	0.0207	0.0273
2	0.0944	0.0902	0.0526	0.0538
3	0.0521	0.0503	0.0171	0.0211
4	0.0279	0.0302	0.0359	0.0531
5	0.0975	0.0503	0.0282	0.0211
6	0.0526	0.0419	0.0952	0.0416
7	0.0291	0.0298	0.0390	0.0580
8	0.0301	0.0563	0.0231	0.0301
9	0.0222	0.0391	0.0241	0.0720
10	0.0446	0.0270	0.0140	0.0579
Average	0.0487	0.0439	0.0350	0.0436
STD	0.0269	0.0197	0.0241	0.0179

Table 3.58 Average parameter values for four data conditions of 10 subjects with Windkessel-3 modeling scheme for Model 1

	R_1	R_2	C_1
SNI Average	1.1567	3.8006	44.2428
SNI STD	0.3219	4.8674	39.8917
SI Average	1.2516	7.9053	52.1906
SI STD	0.6362	11.2822	36.0690
VNI Average	1.1649	10.4179	46.2739
VNI STD	0.3734	14.5268	39.3100
VI Average	0.8747	15.6321	42.9288
VI STD	0.4751	29.9415	36.7434

Table 3.59 Average weights (W_t and W_f) for four data conditions of 10 subjects with Windkessel-3 modeling scheme for Model 1

	W_t	W_f
SNI Average	0.3000	0.7000
SNI STD	0.2981	0.2981
SI Average	0.2500	0.7500
SI STD	0.2014	0.2014
VNI Average	0.2400	0.7600
VNI STD	0.1350	0.1350
VI Average	0.3800	0.6200
VI STD	0.2741	0.2741

3.2.2 Graphical Validation Results

This section presents the plots of measured data and model outputs for CBFV as a function of MABP under various modeling methodologies, discussed in section 2.2. The frequency responses of the models have also been shown. For comparing Windkessel-1 and Windkessel-2 methodologies, the corresponding model output plots and frequency response plots have been shown for the same subject, along with the measured input (MABP) and output (CBFV) data. Similarly the corresponding ARX-1 and ARX-2 model output plots and frequency response plots have been shown for the same subject, along with the measured data. For Windkessel modeling schemes, the comparison was done based on results for the same given model, and models with the similar order were considered for generating the corresponding ARX-2 plots. The plots for Windkessel-3 modeling scheme have been shown separately.

Since the results of these studies are numerous (a total of 240 plots), in the interest of space, only a few samples of the entire results have been shown. The samples were selected to represent good and poor results among the 10 subjects, for each of the model type (5 Windkessel models) and for each type of the data condition. The good and the poor results among the subjects were selected with the MSE value of the Windkessel-1 methodology as the basis in each model and type of data condition. Figure 3.41 through Figure 3.64 present the plots for the good results, while Figure 3.65 through Figure 3.96 present the plots for the poor results. Figure 3.93 through Figure 3.96 show the plots forWindkessel-3 scheme.

3.2.2.1 Plots for the Good Results

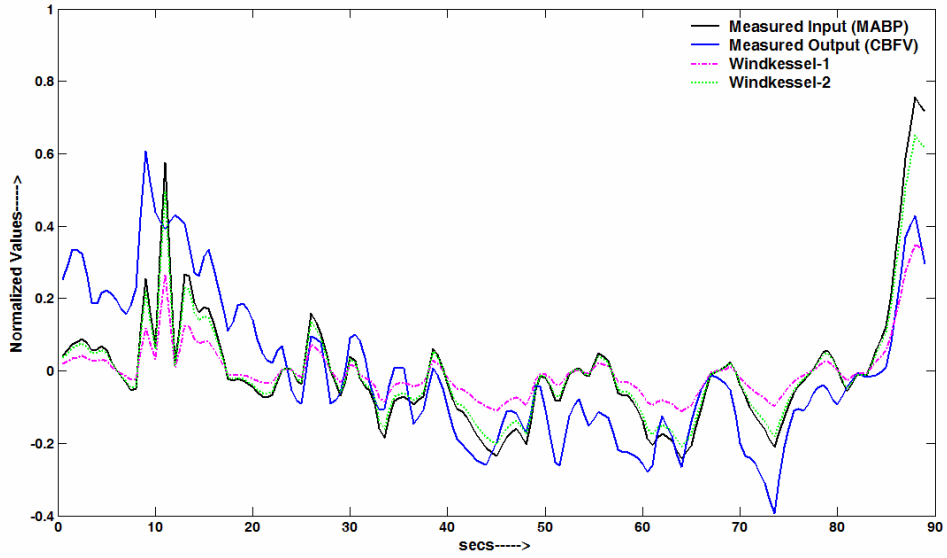

Figure 3.41 Plot of the outputs for Model 1 with Windkessel-1 and Windkessel-2 modeling schemes for SNI data of subject no. 9

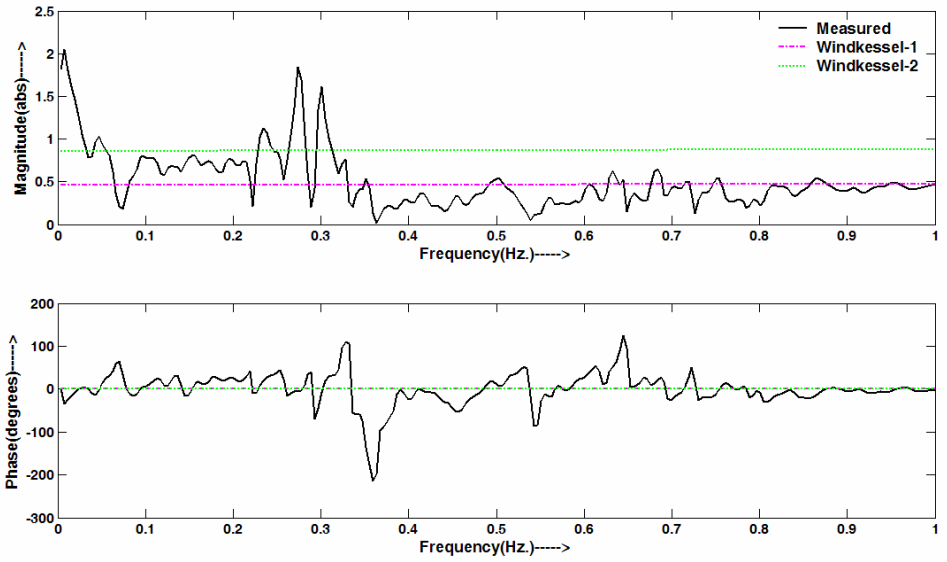

Figure 3.42 Plot of the frequency responses for Model 1 with Windkessel-1 and Windkessel-2 modeling schemes for SNI data of subject no. 9

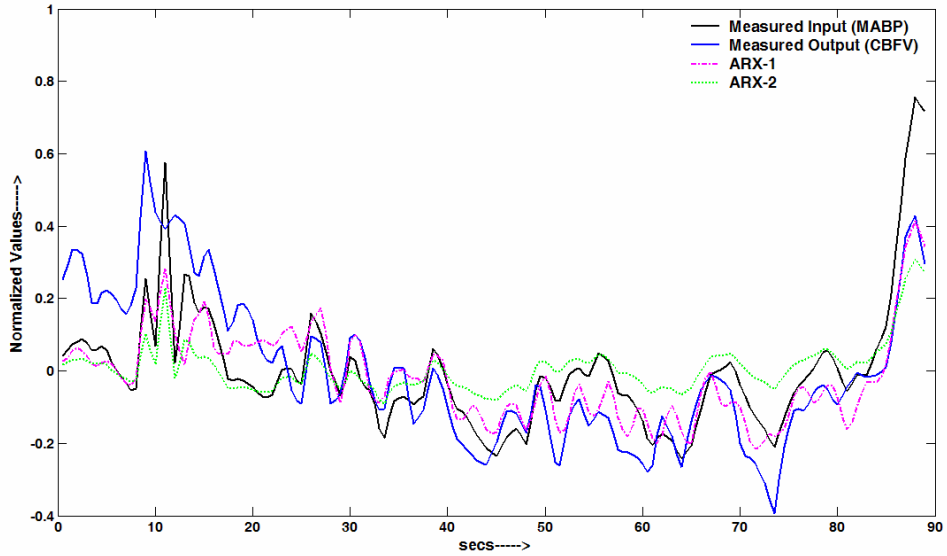

Figure 3.43 Plot of the model outputs with ARX-1 and ARX-2 (1st order model) modeling schemes for SNI data of subject no. 9

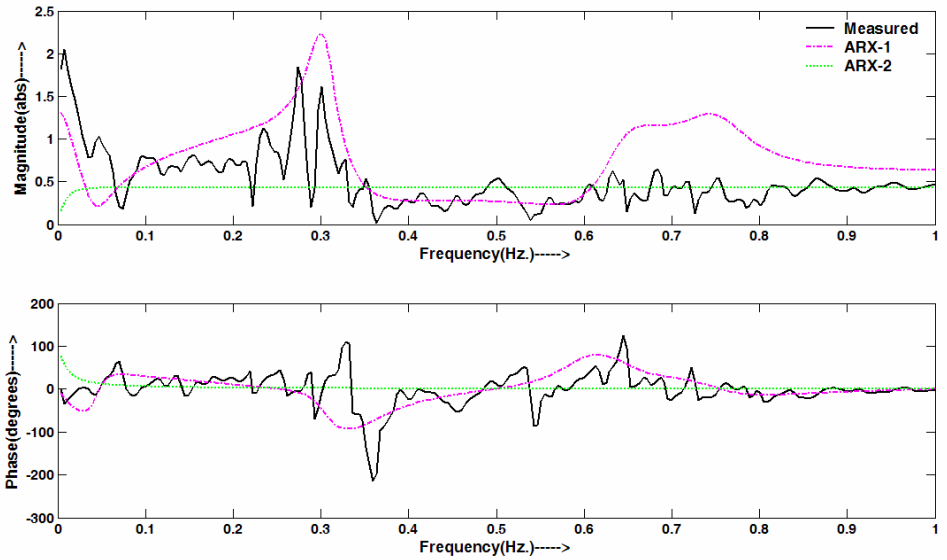

Figure 3.44 Plot of the model frequency responses with ARX-1 and ARX-2 (1st order model) modeling schemes for SNI data of subject no. 9

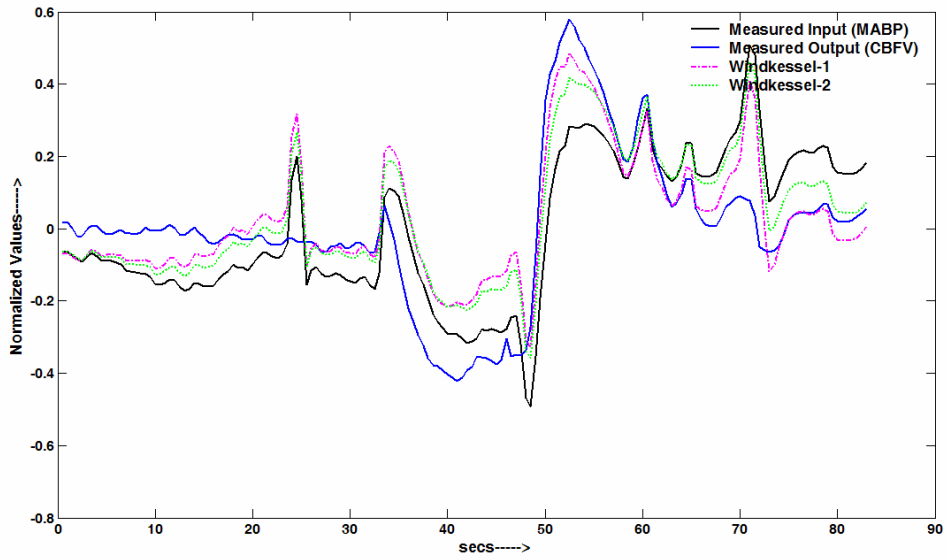

Figure 3.45 Plot of the outputs for Model 2 with Windkessel-1 and Windkessel-2 modeling schemes for VI data of subject no. 3

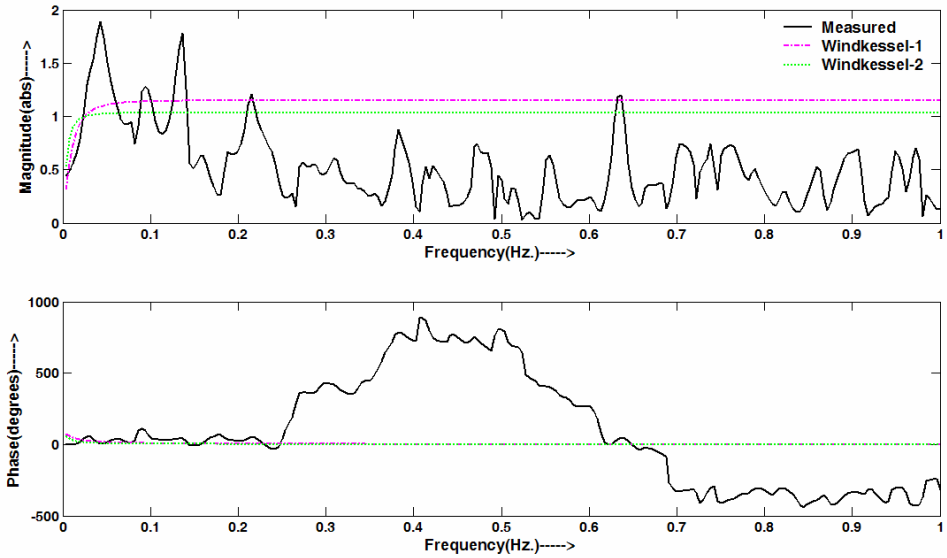

Figure 3.46 Plot of the frequency responses for Model 2 with Windkessel-1 and Windkessel-2 modeling schemes for VI data of subject no. 3

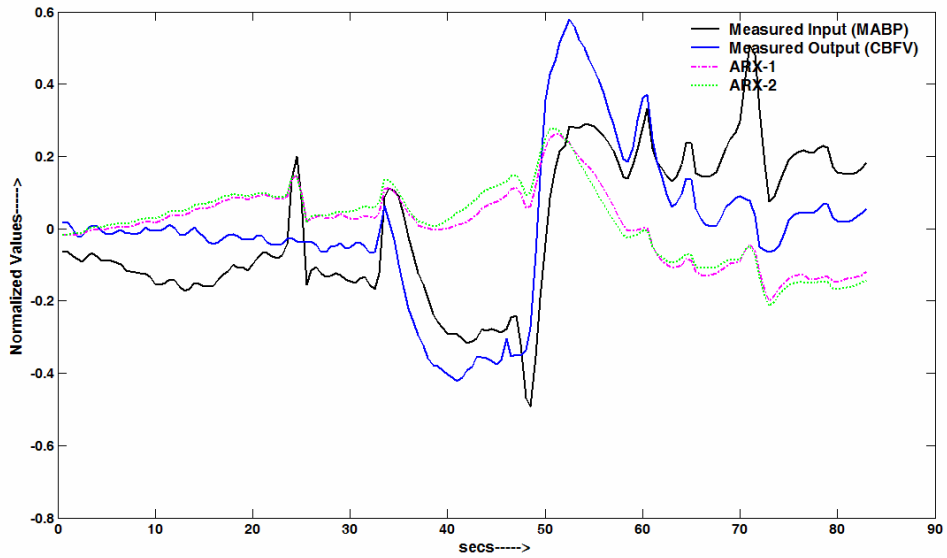

Figure 3.47 Plot of the model outputs with ARX-1 and ARX-2 (2nd order model) modeling schemes for VI data of subject no. 3

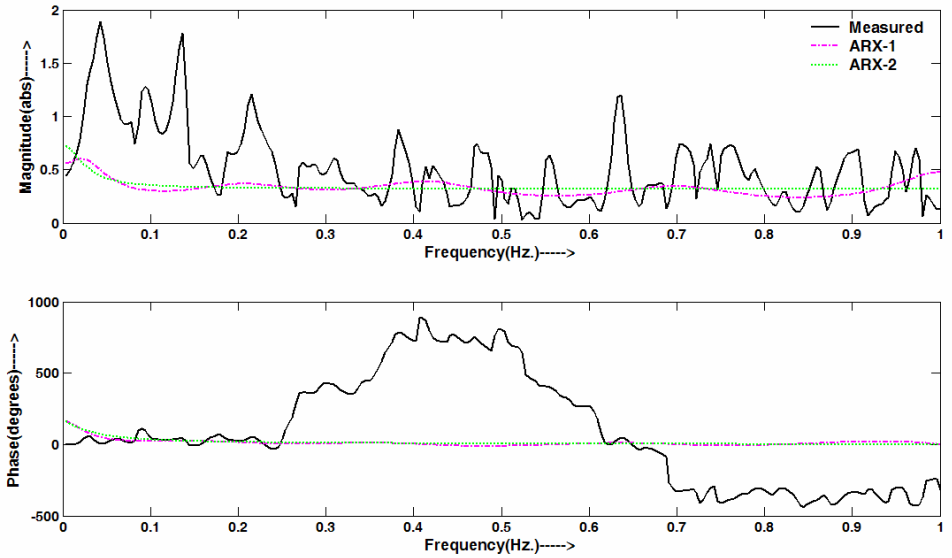

Figure 3.48 Plot of the model frequency responses with ARX-1 and ARX-2 (2nd order model) modeling schemes for VI data of subject no. 3

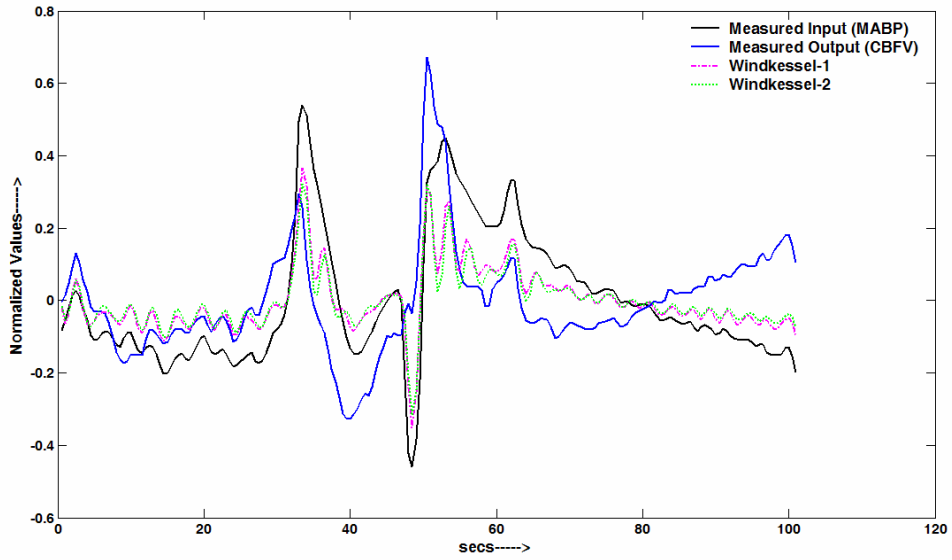

Figure 3.49 Plot of the outputs for Model 3 with Windkessel-1 and Windkessel-2 modeling schemes for VNI data of subject no. 1

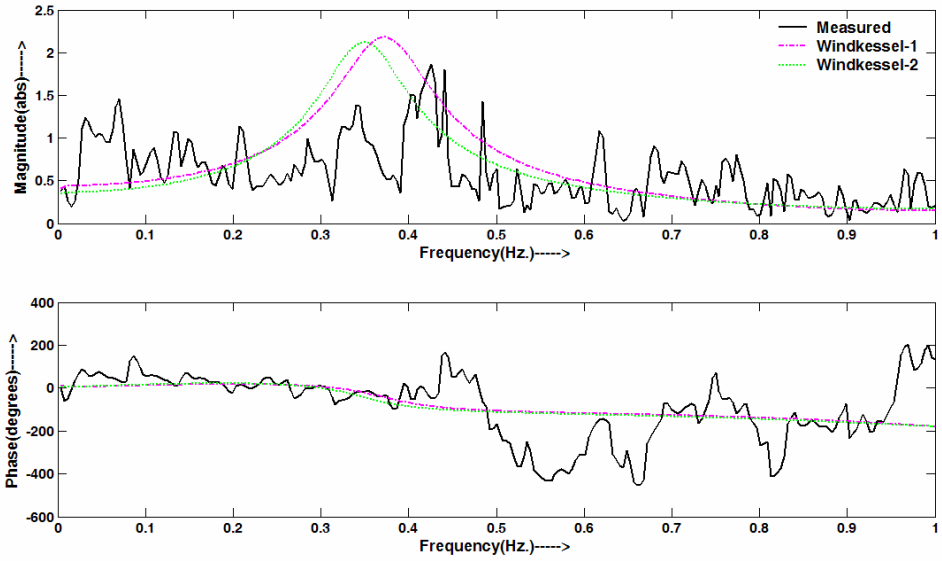

Figure 3.50 Plot of the frequency responses for Model 3 with Windkessel-1 and Windkessel-2 modeling schemes for VNI data of subject no. 1

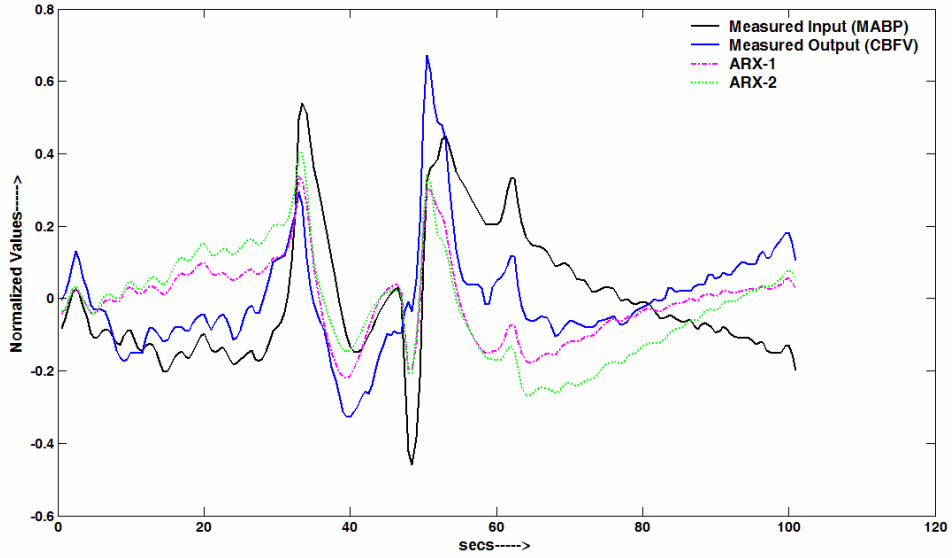

Figure 3.51 Plot of the model outputs with ARX-1 and ARX-2 (3rd order model) modeling schemes for VNI data of subject no. 1

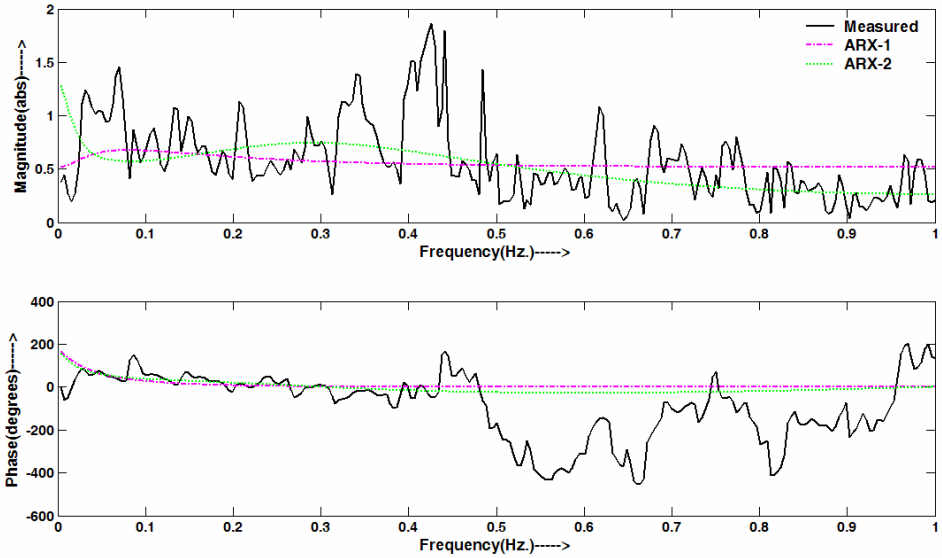

Figure 3.52 Plot of the model frequency responses with ARX-1 and ARX-2 (3rd order model) modeling schemes for VNI data of subject no. 1

Figure 3.53 through Figure 3.56 show plots for SNI data of subject no. 9, employing Model 4 (5-element, 3rd order) as compared to Model 1 (3-element, 1st order) results for the same subject and data condition in Figure 3.41 through Figure 3.44

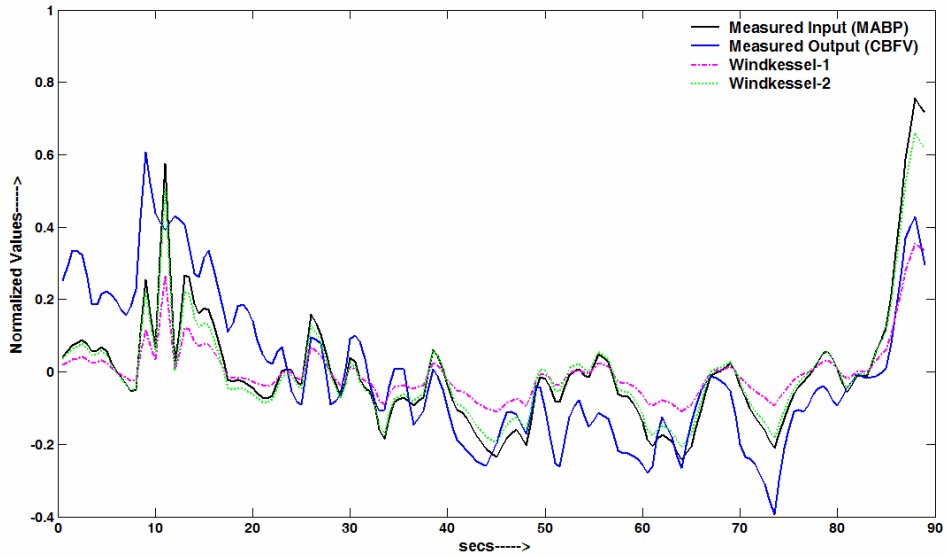

Figure 3.53 Plot of the outputs for Model 4 with Windkessel-1 and Windkessel-2 modeling schemes for SNI data of subject no. 9

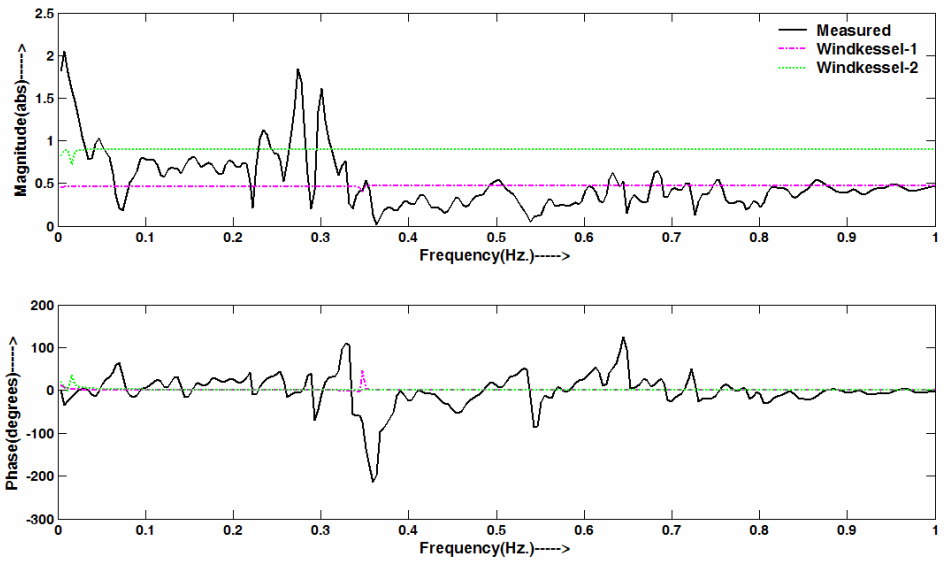

Figure 3.54 Plot of the frequency responses for Model 4 with Windkessel-1 and Windkessel-2 modeling schemes for SNI data of subject no. 9

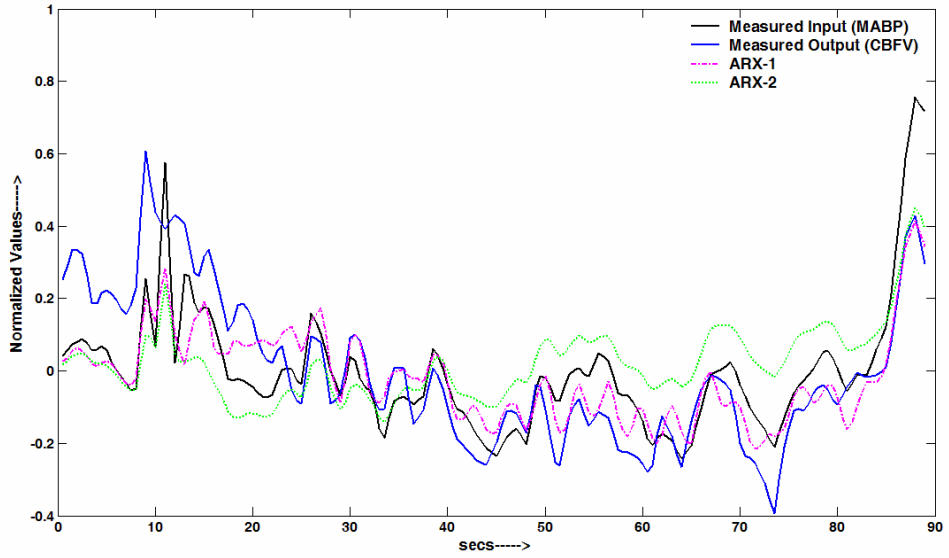

Figure 3.55 Plot of the model outputs with ARX-1 and ARX-2 (3rd order model) modeling schemes for SNI data of subject no. 9

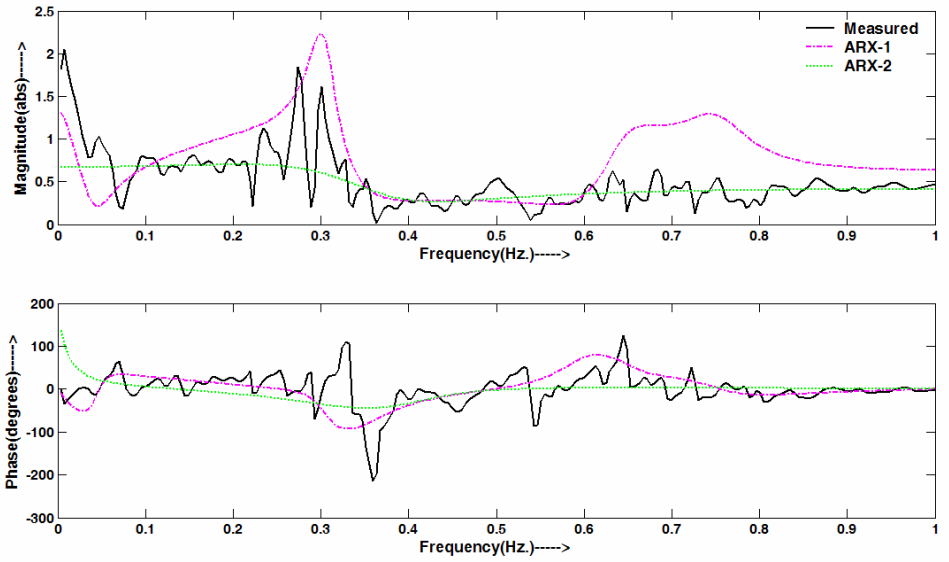

Figure 3.56 Plot of the model frequency responses with ARX-1 and ARX-2 (3rd order model) modeling schemes for SNI data of subject no. 9

Figure 3.57 through Figure 3.60 show plots for VI data of subject no. 3, employing Model 4 (5-element, 3rd order) as compared to Model 2 (5-element, 2nd order) results for the same subject and data condition in Figure 3.47 through Figure 3.50

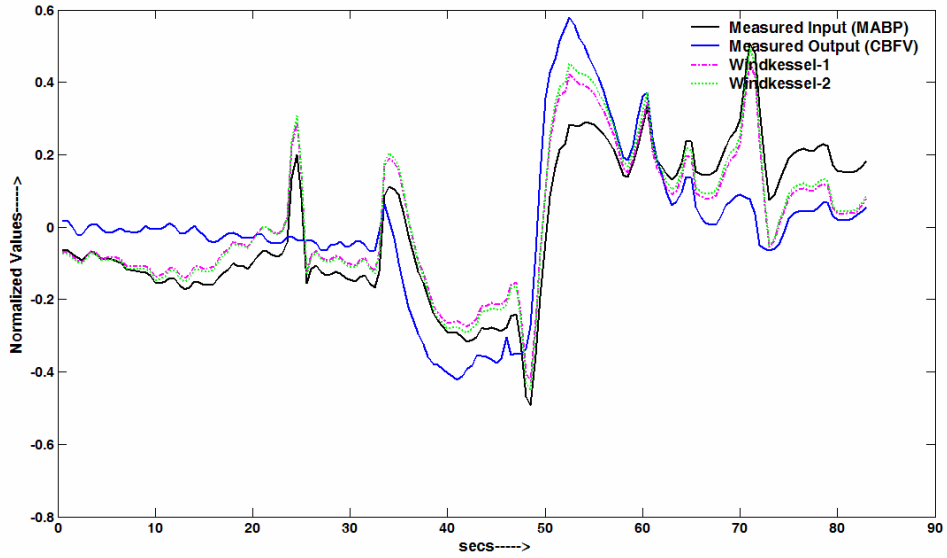

Figure 3.57 Plot of the outputs for Model 4 with Windkessel-1 and Windkessel-2 modeling schemes for VI data of subject no. 3

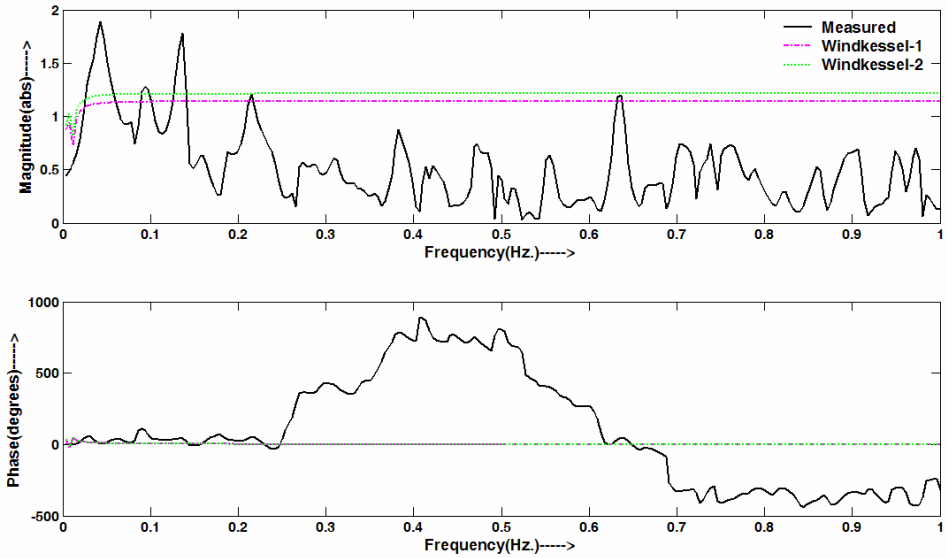

Figure 3.58 Plot of the frequency responses for Model 4 with Windkessel-1 and Windkessel-2 modeling schemes for VI data of subject no. 3

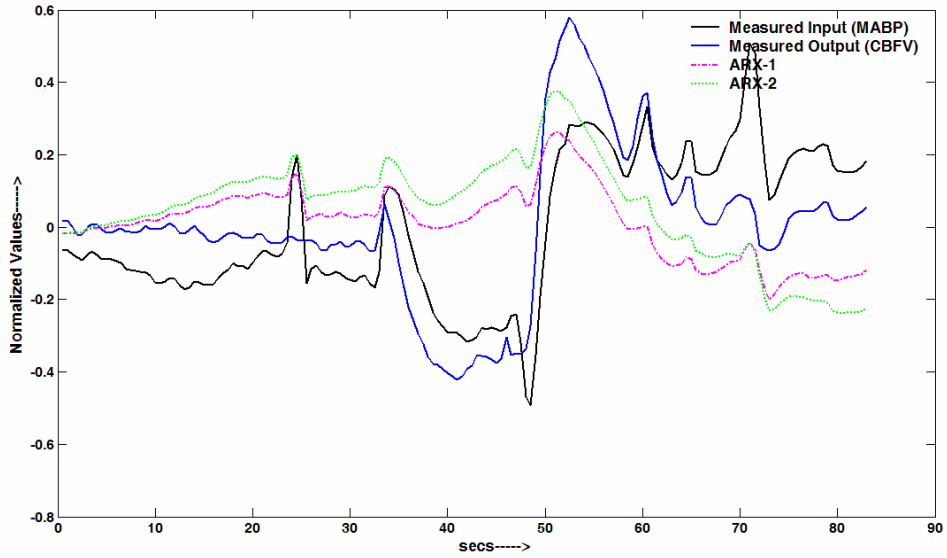

Figure 3.59 Plot of the model outputs with ARX-1 and ARX-2 (3rd order model) modeling schemes for VI data of subject no. 3

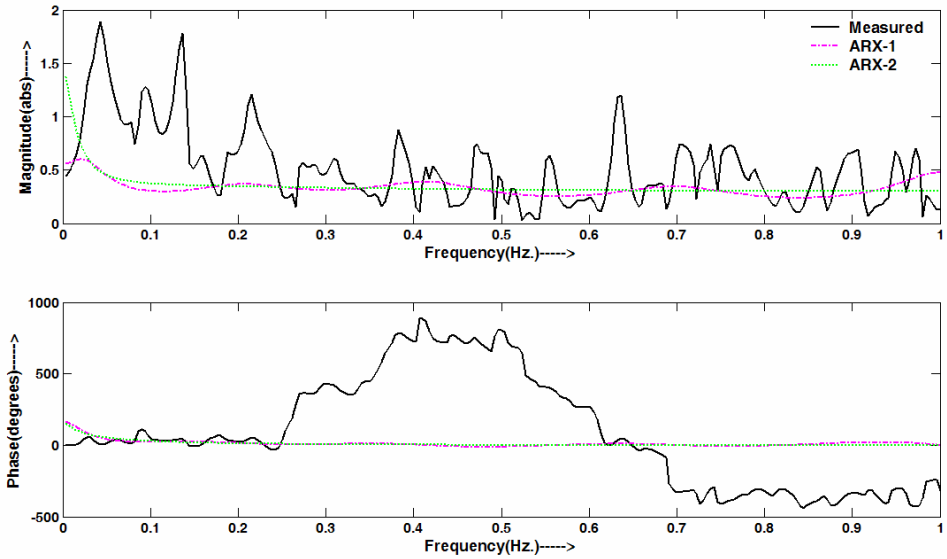

Figure 3.60 Plot of the model frequency responses with ARX-1 and ARX-2 (3rd order model) modeling schemes for VI data of subject no. 3

Figure 3.61 through Figure 3.64 show plots for VI data of subject no. 3, employing Model 5 (4-element, 2nd order) as compared to Model 4 (5-element, 3rd order) results for the same subject and data condition in Figure 3.57 through Figure 3.60

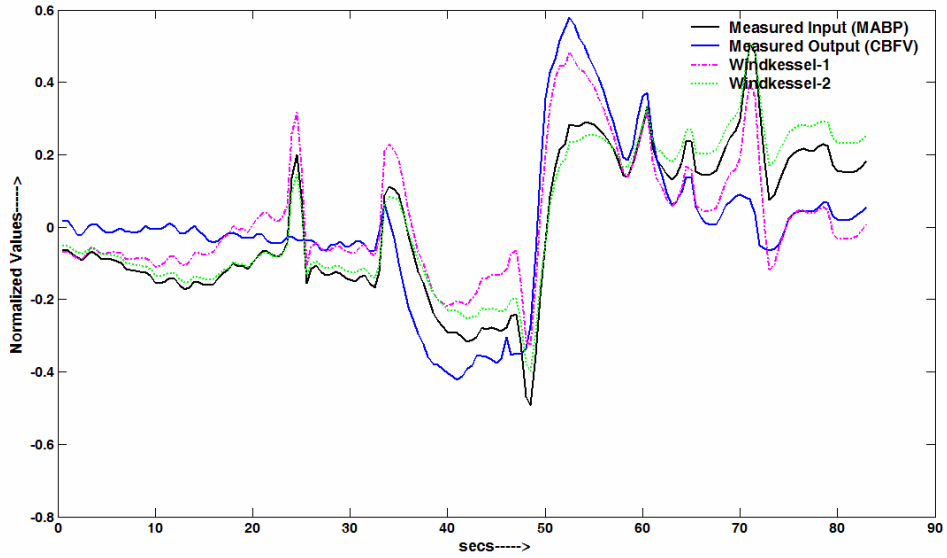

Figure 3.61 Plot of the outputs for Model 5 with Windkessel-1 and Windkessel-2 modeling schemes for VI data of subject no. 3

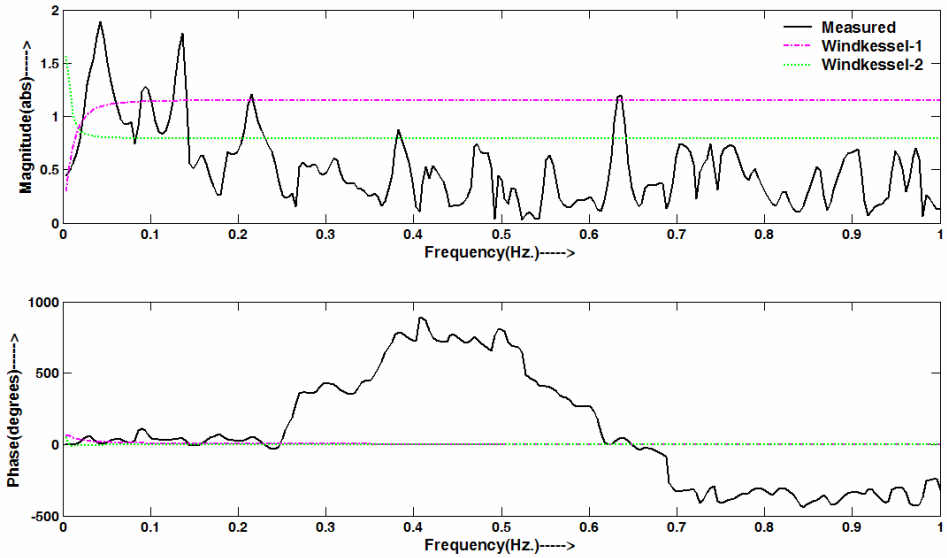

Figure 3.62 Plot of the frequency responses for Model 5 with Windkessel-1 and Windkessel-2 modeling schemes for VI data of subject no. 3

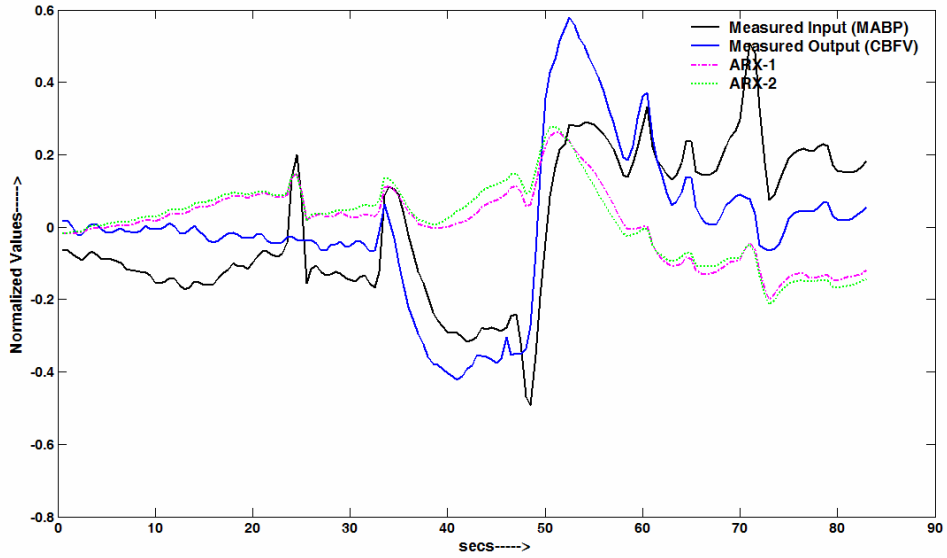

Figure 3.63 Plot of the model outputs with ARX-1 and ARX-2 (2^{nd} order model) modeling schemes for VI data of subject no. 3

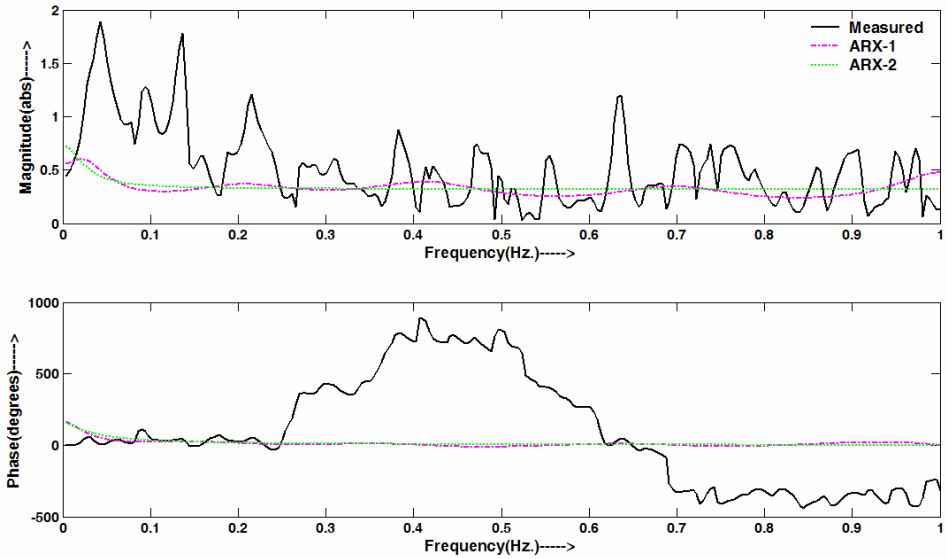

Figure 3.64 Plot of the model frequency responses with ARX-1 and ARX-2 (2^{nd} order model) modeling schemes for VI data of subject no. 3

3.2.2.2 Plots for the Poor Results

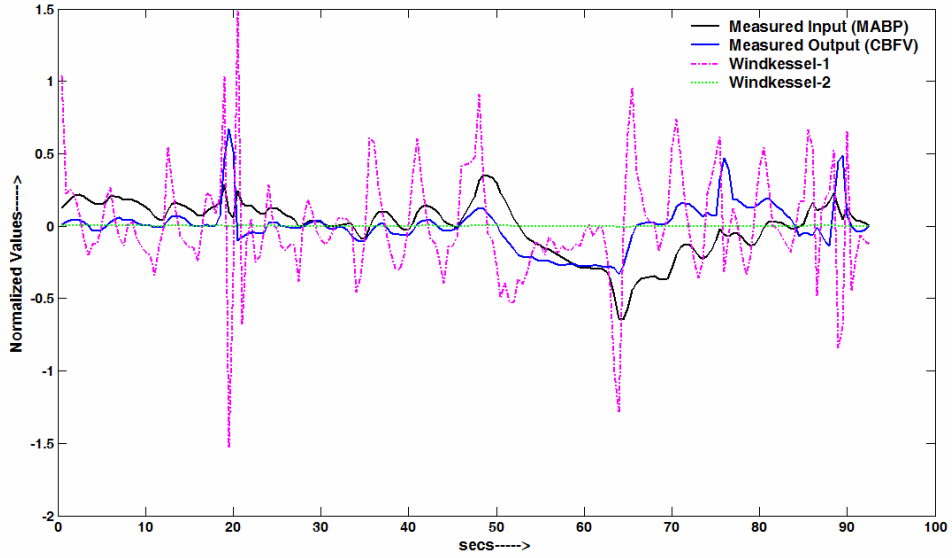

Figure 3.65 Plot of the outputs for Model 1 with Windkessel-1 and Windkessel-2 modeling schemes for VI data of subject no. 2

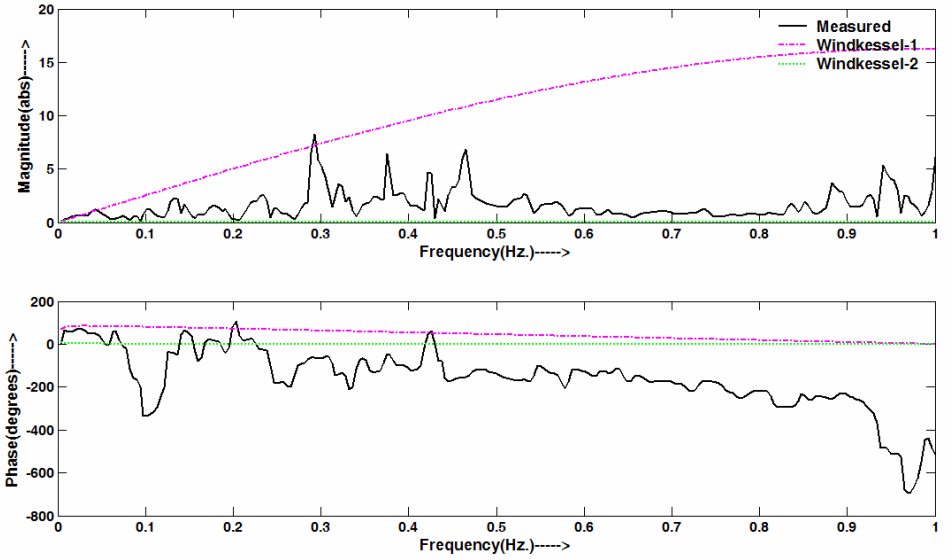

Figure 3.66 Plot of the frequency responses for Model 1 with Windkessel-1 and Windkessel-2 modeling schemes for VI data of subject no. 2

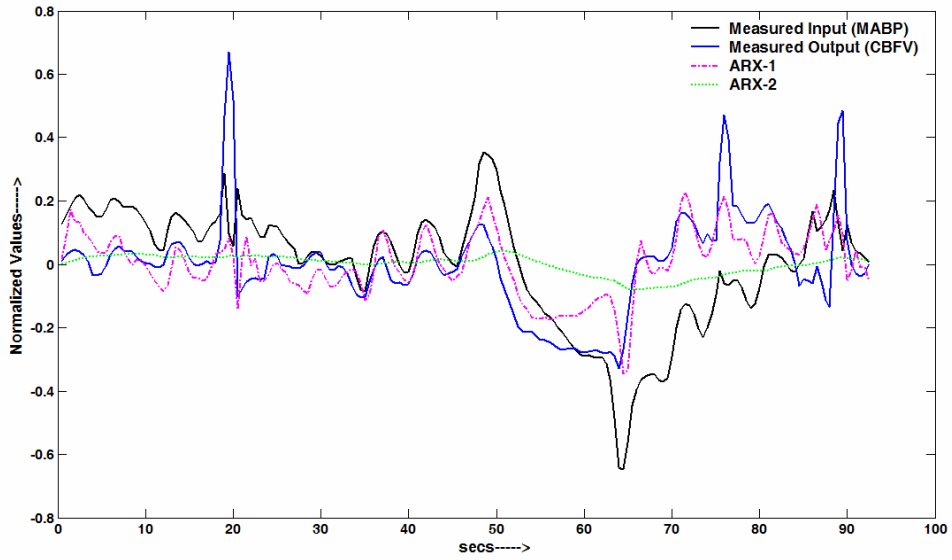

Figure 3.67 Plot of the model outputs with ARX-1 and ARX-2 (1st order model) modeling schemes for VI data of subject no. 2

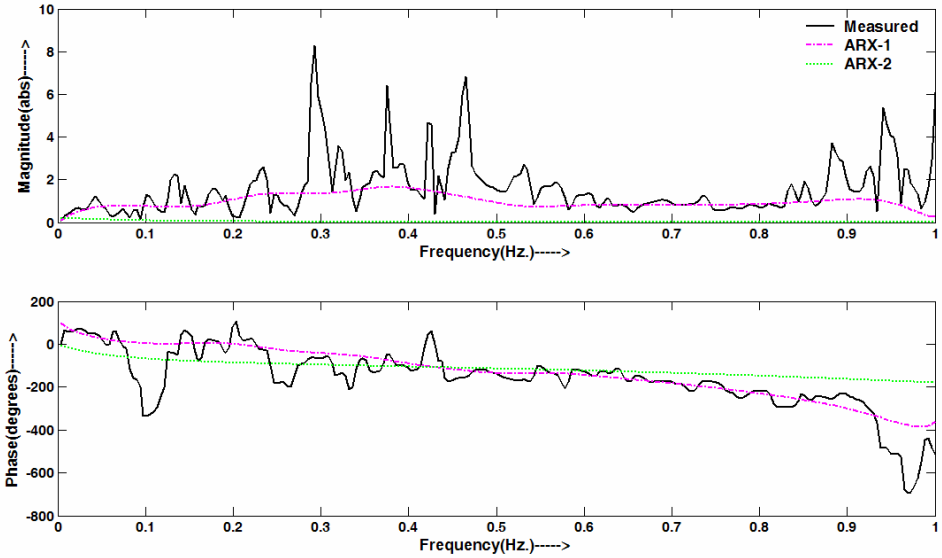

Figure 3.68 Plot of the model frequency responses with ARX-1 and ARX-2 (1st order model) modeling schemes for VI data of subject no. 2

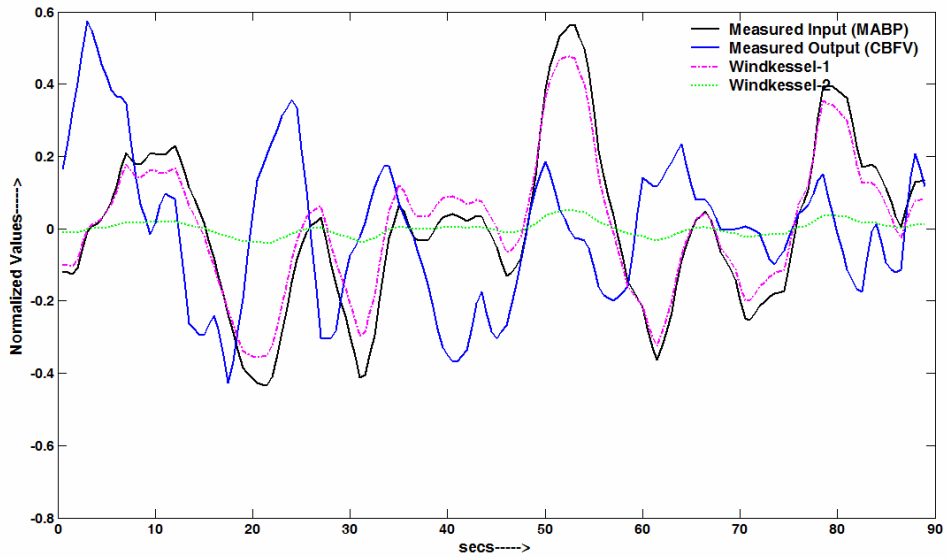

Figure 3.69 Plot of the outputs for Model 2 with Windkessel-1 and Windkessel-2 modeling schemes for SNI data of subject no. 5

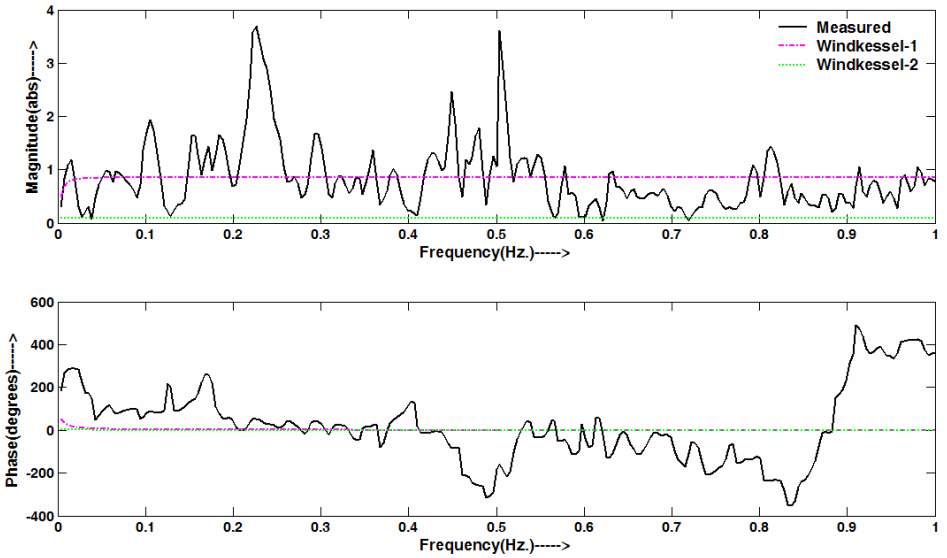

Figure 3.70 Plot of the frequency responses for Model 2 with Windkessel-1 and Windkessel-2 modeling schemes for SNI data of subject no. 5

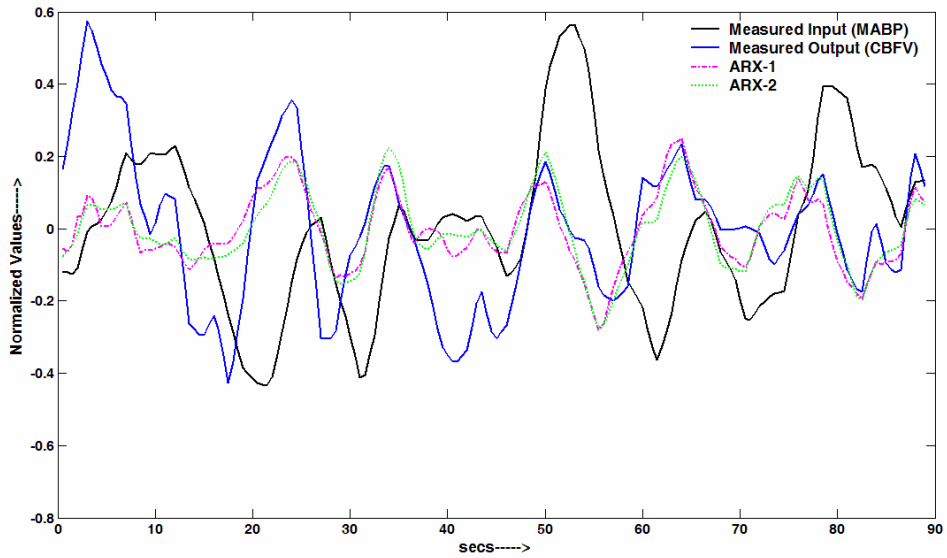

Figure 3.71 Plot of the model outputs with ARX-1 and ARX-2 (2nd order model) modeling schemes for SNI data of subject no. 5

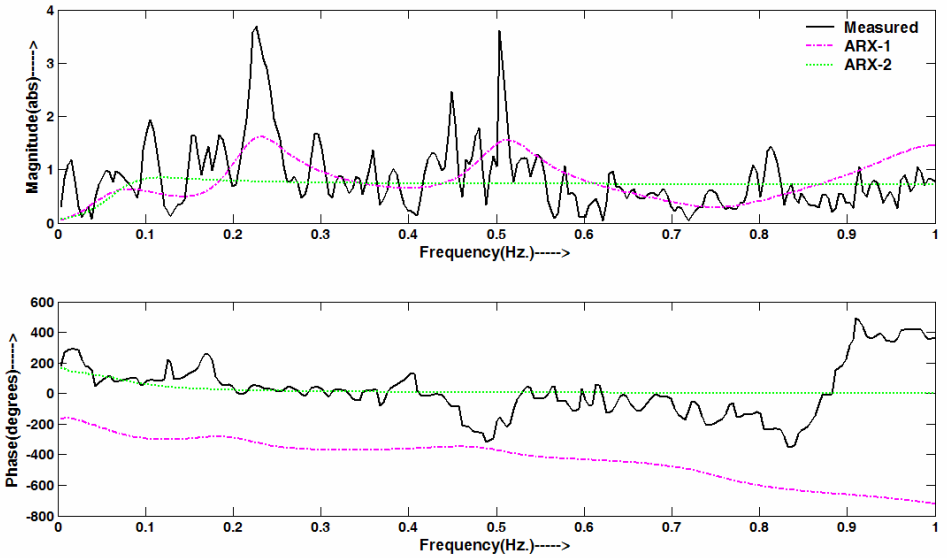

Figure 3.72 Plot of the model frequency responses with ARX-1 and ARX-2 (2nd order model) modeling schemes for SNI data of subject no. 5

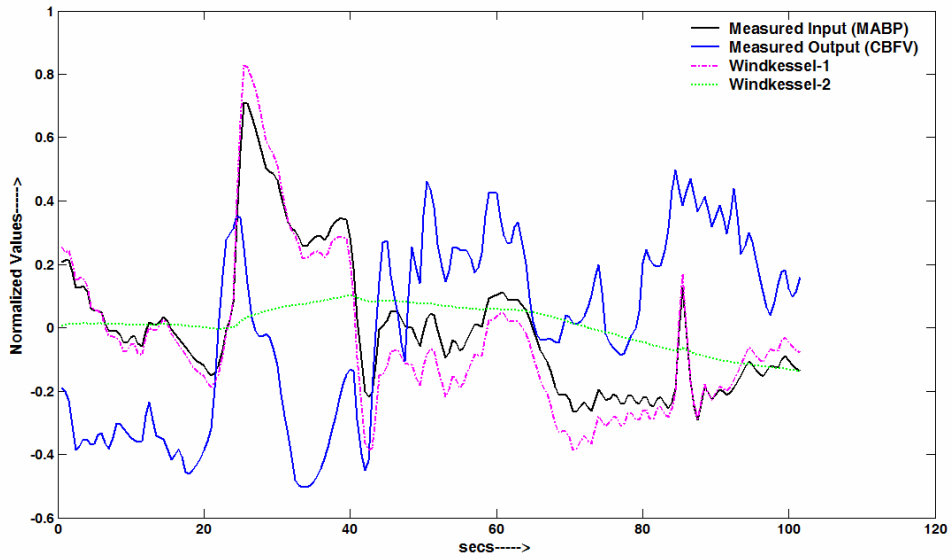

Figure 3.73 Plot of the outputs for Model 3 with Windkessel-1 and Windkessel-2 modeling schemes for VNI data of subject no. 6

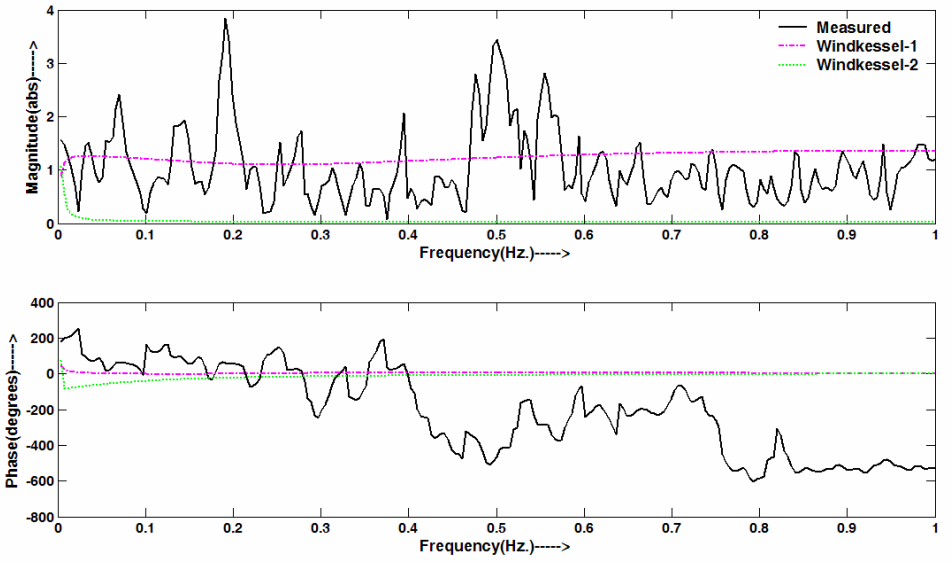

Figure 3.74 Plot of the frequency responses for Model 3 with Windkessel-1 and Windkessel-2 modeling schemes for VNI data of subject no. 6

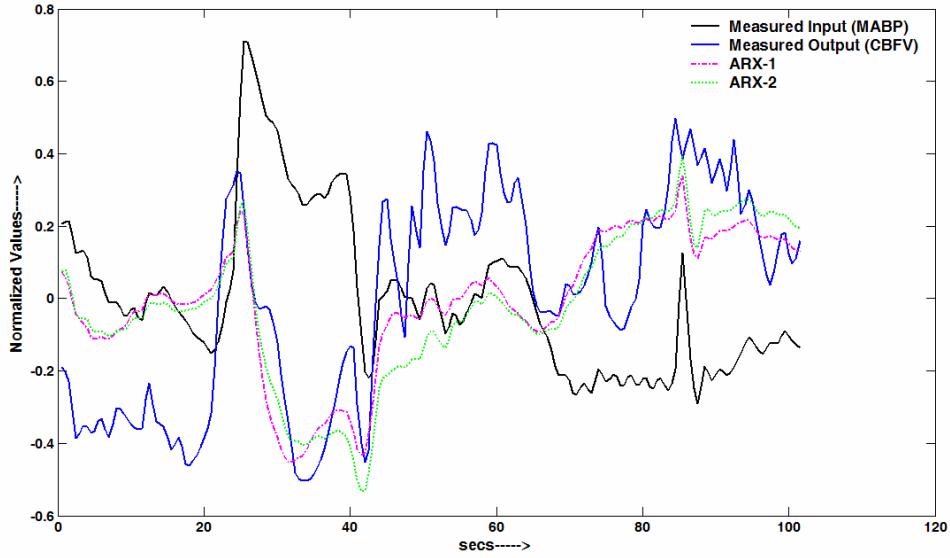

Figure 3.75 Plot of the model outputs with ARX-1 and ARX-2 (3rd order model) modeling schemes for VNI data of subject no. 6

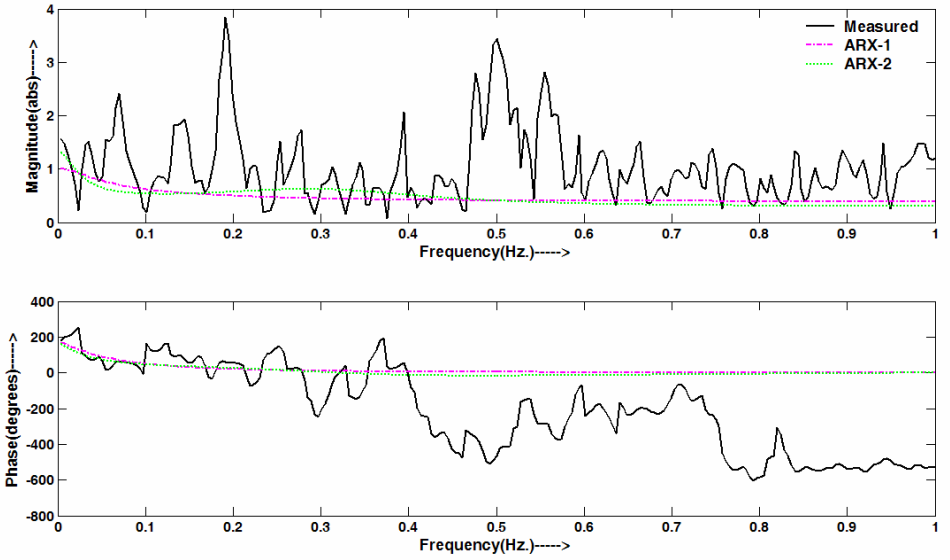

Figure 3.76 Plot of the model frequency responses with ARX-1 and ARX-2 (3rd order model) modeling schemes for VNI data of subject no. 6

Figure 3.77 through Figure 3.80 show plots for SNI data of subject no. 5, employing Model 4 (5-element, 3rd order) as compared to Model 2 (5-element, 2nd order) results for the same subject and data condition in Figure 3.69 through Figure 3.72

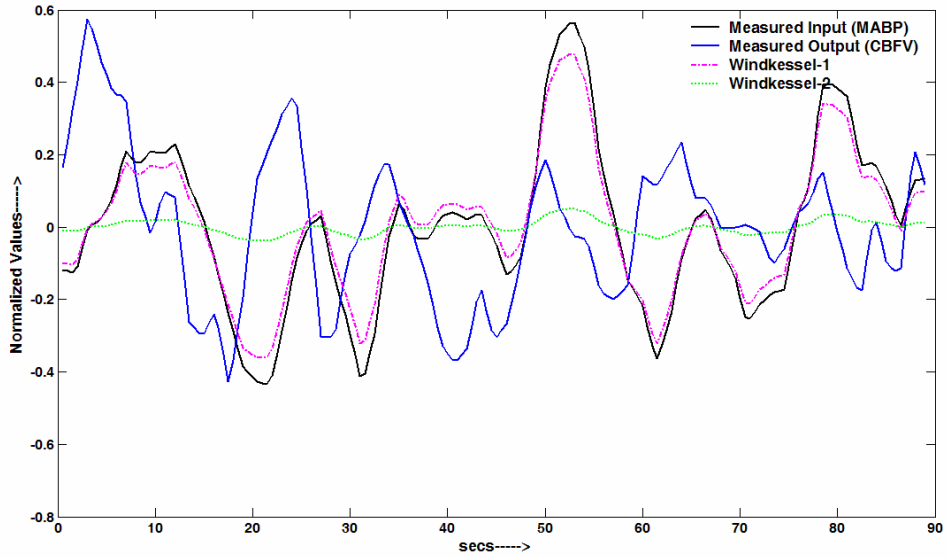

Figure 3.77 Plot of the outputs for Model 4 with Windkessel-1 and Windkessel-2 modeling schemes for SNI data of subject no. 5

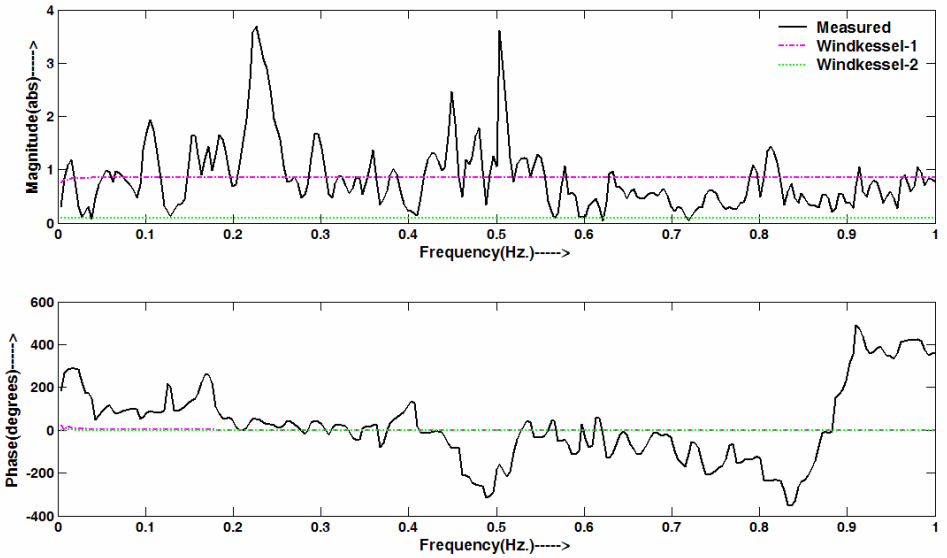

Figure 3.78 Plot of the frequency responses for Model 4 with Windkessel-1 and Windkessel-2 modeling schemes for SNI data of subject no. 5

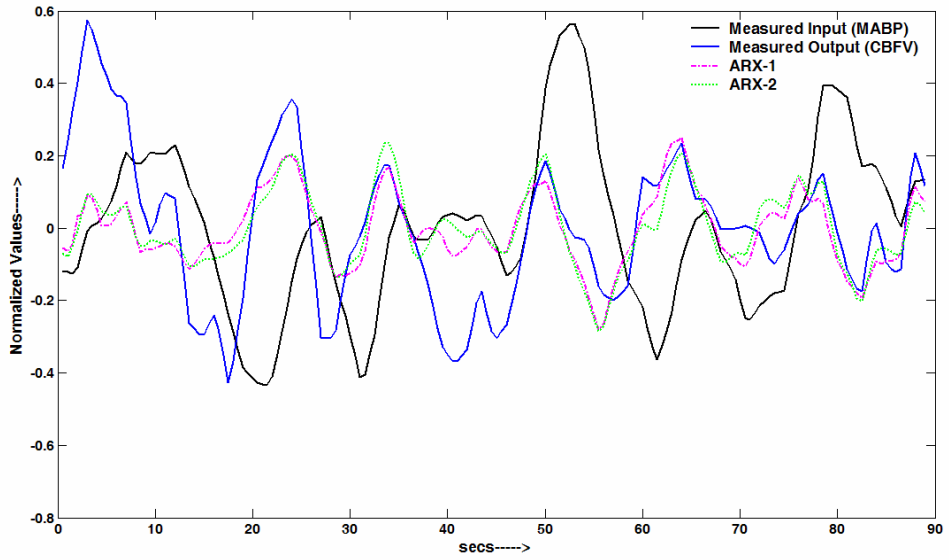

Figure 3.79 Plot of the model outputs with ARX-1 and ARX-2 (3rd order model) modeling schemes for SNI data of subject no. 5

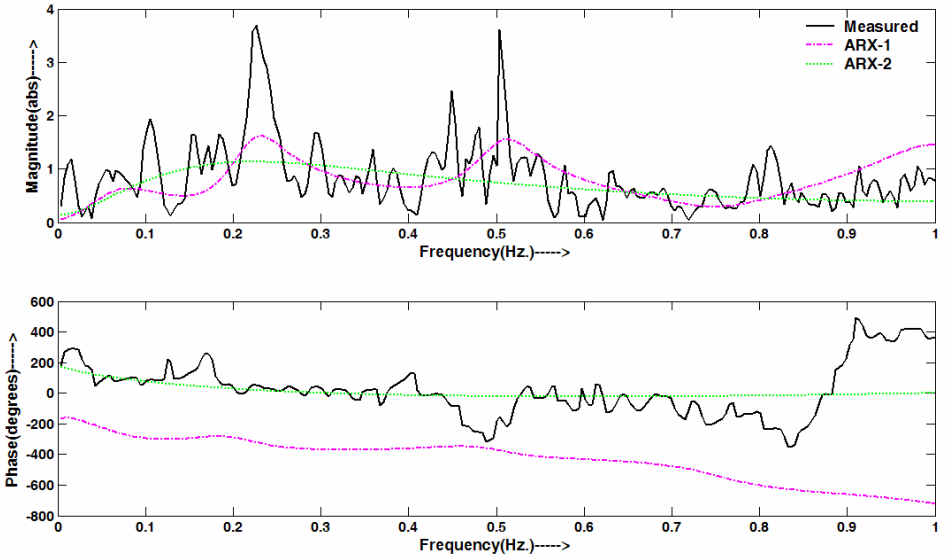

Figure 3.80 Plot of the model frequency responses with ARX-1 and ARX-2 (3rd order model) modeling schemes for SNI data of subject no. 5

Figure 3.81 through Figure 3.84 show plots for VI data of subject no. 2, employing Model 4 (5-element, 3rd order) as compared to Model 1 (3-element, 1st order) results for the same subject and data condition in Figure 3.65 through Figure 3.68

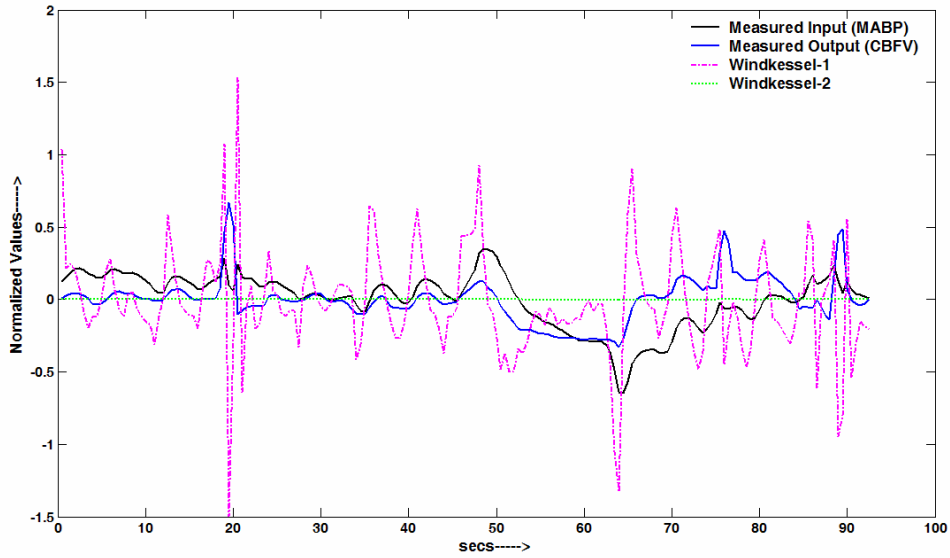

Figure 3.81 Plot of the outputs for Model 4 with Windkessel-1 and Windkessel-2 modeling schemes for VI data of subject no. 2

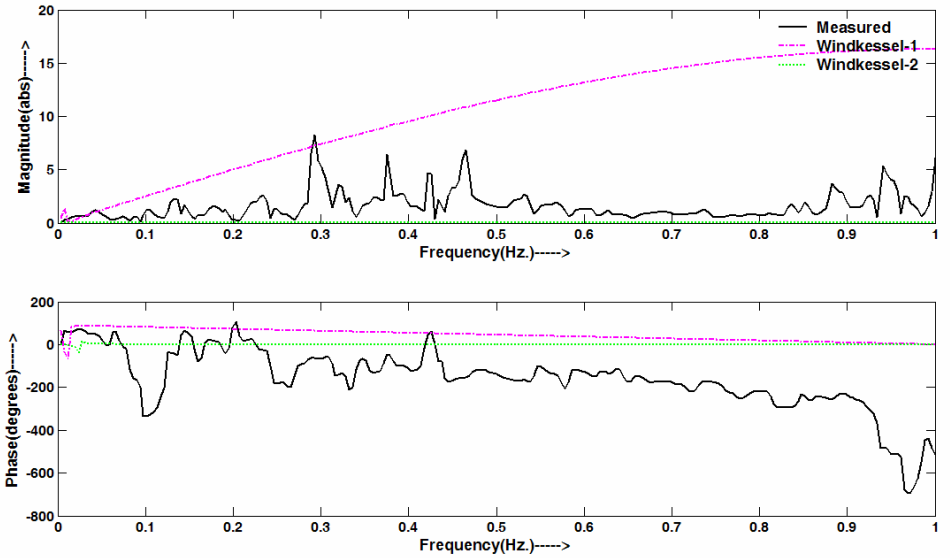

Figure 3.82 Plot of the frequency responses for Model 4 with Windkessel-1 and Windkessel-2 modeling schemes for VI data of subject no. 2

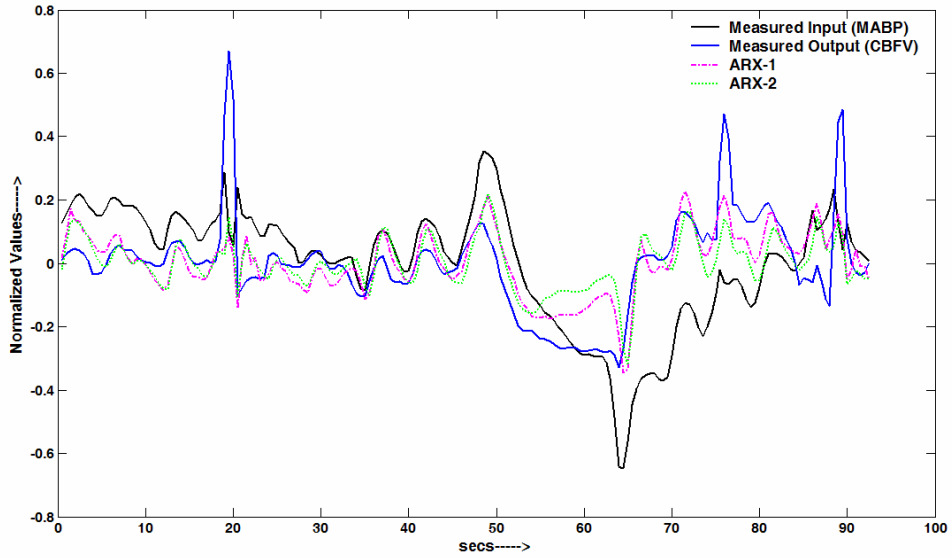

Figure 3.83 Plot of the model outputs with ARX-1 and ARX-2 (3rd order model) modeling schemes for VI data of subject no. 2

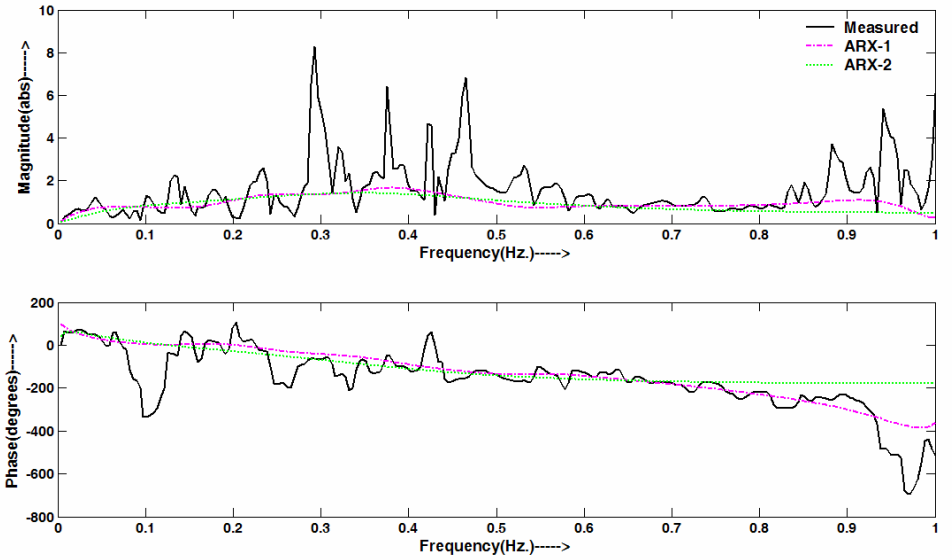

Figure 3.84 Plot of the model frequency responses with ARX-1 and ARX-2 (3rd order model) modeling schemes for VI data of subject no. 2

Figure 3.85 through Figure 3.88 show plots for VNI data of subject no. 6, employing Model 5 (4-element, 2nd order) as compared to Model 3 (5-element, 3rd order) results for the same subject and data condition in Figure 3.73 through Figure 3.76

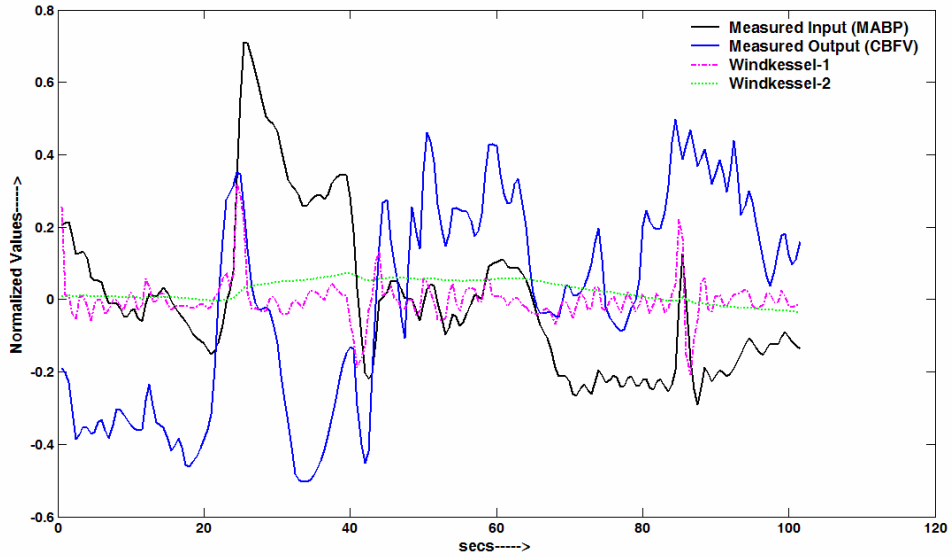

Figure 3.85 Plot of the outputs for Model 5 with Windkessel-1 and Windkessel-2 modeling schemes for VNI data of subject no. 6

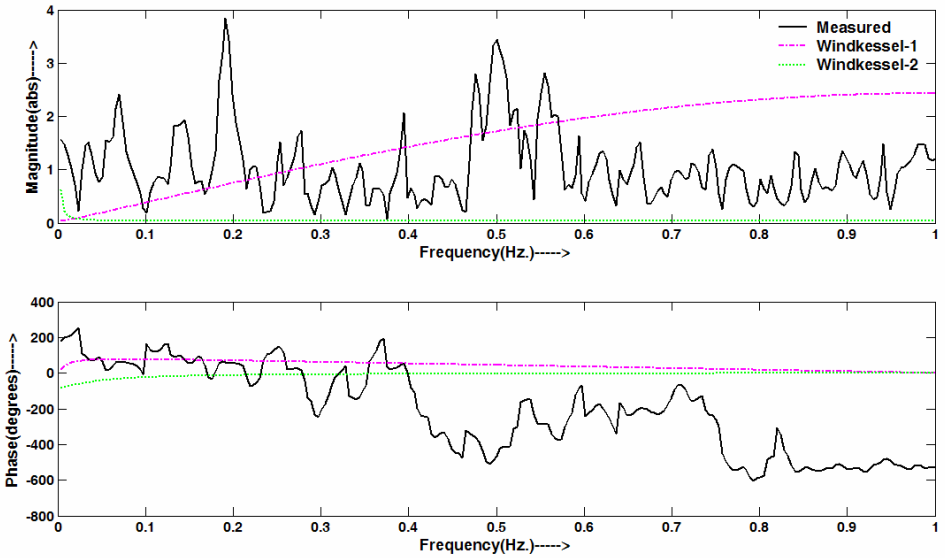

Figure 3.86 Plot of the frequency responses for Model 5 with Windkessel-1 and Windkessel-2 modeling schemes for VNI data of subject no. 6

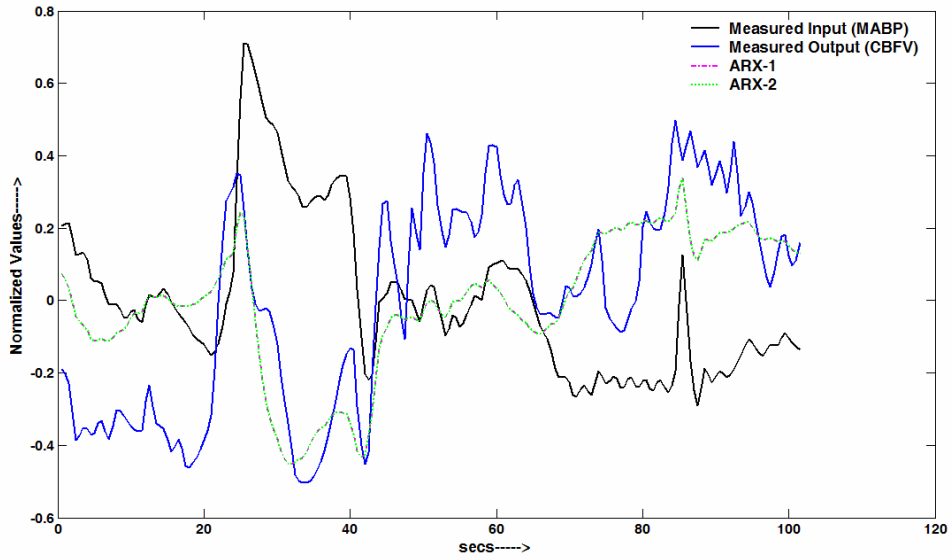

Figure 3.87 Plot of the model outputs with ARX-1 and ARX-2 (2nd order model) modeling schemes for VNI data of subject no. 6

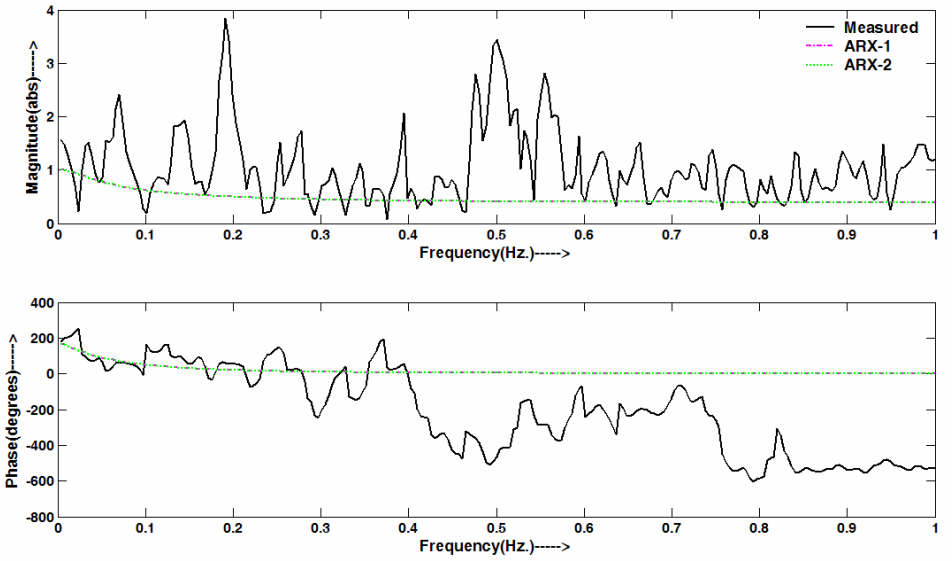

Figure 3.88 Plot of the model frequency responses with ARX-1 and ARX-2 (2nd order model) modeling schemes for VNI data of subject no. 6

Figure 3.89 through Figure 3.92 show plots for VI data of subject no. 2, employing Model 5 (4-element, 2nd order) as compared to Model 4 (5-element, 3rd order) results for the same subject and data condition in Figure 3.81 through Figure 3.84

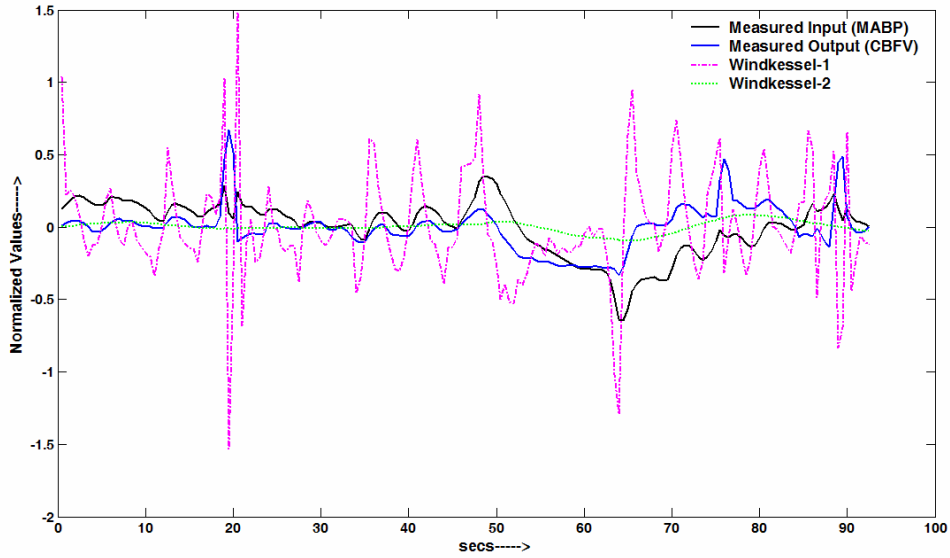

Figure 3.89 Plot of the outputs for Model 5 with Windkessel-1 and Windkessel-2 modeling schemes for VI data of subject no. 2

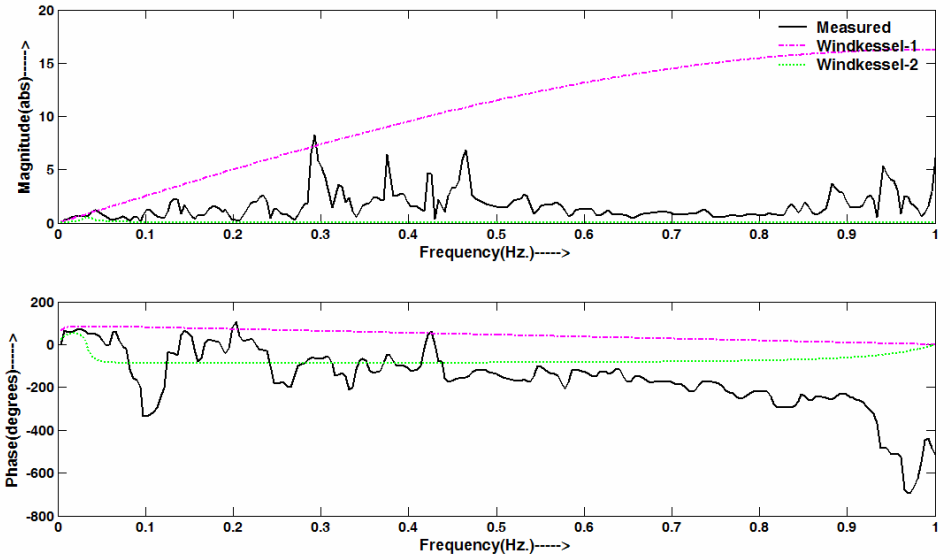

Figure 3.90 Plot of the frequency responses for Model 5 with Windkessel-1 and Windkessel-2 modeling schemes for VI data of subject no. 2

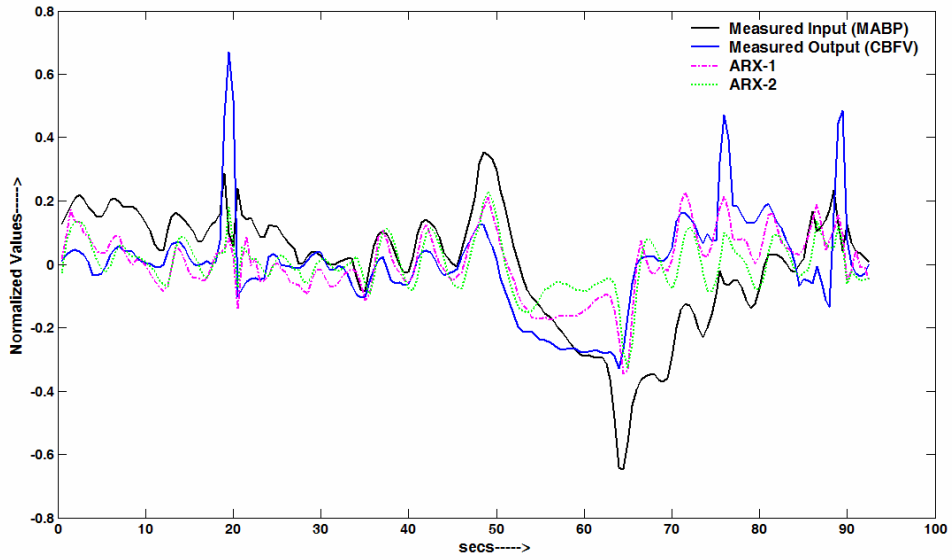

Figure 3.91 Plot of the model outputs with ARX-1 and ARX-2 (2^{nd} order model) modeling schemes for VI data of subject no. 2

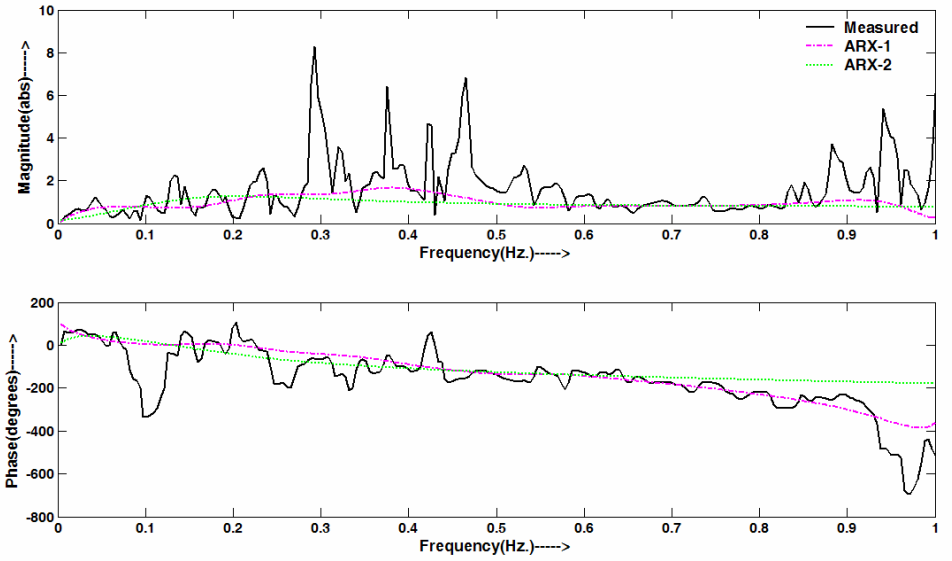

Figure 3.92 Plot of the model frequency responses with ARX-1 and ARX-2 (2^{nd} order model) modeling schemes for VI data of subject no. 2

3.2.2.3 Plots for Windkessel-3 Modeling Scheme

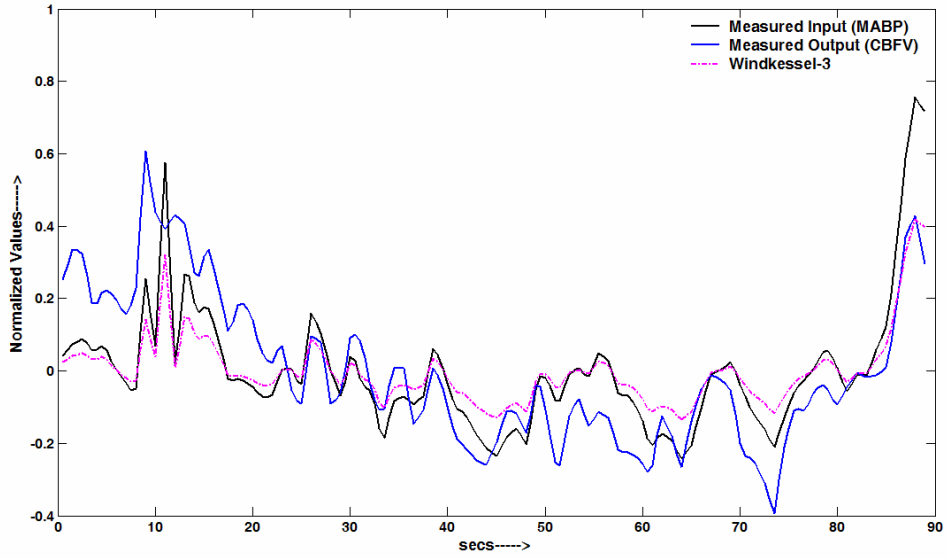

Figure 3.93 Plot of the output for Model 1 with Windkessel-3 modeling scheme for SNI data of subject no. 9

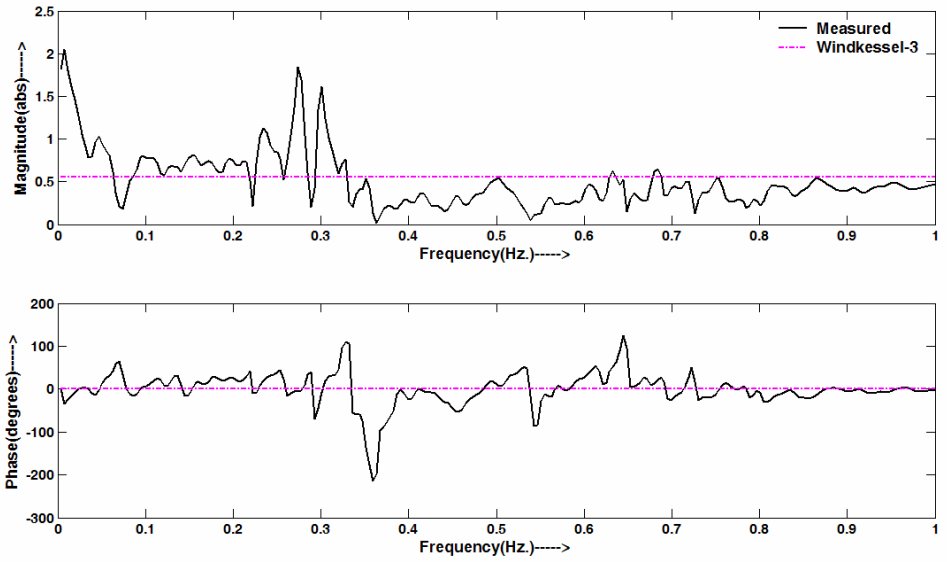

Figure 3.94 Plot of the frequency response for Model 1 with Windkessel-3 modeling scheme for SNI data of subject no. 9

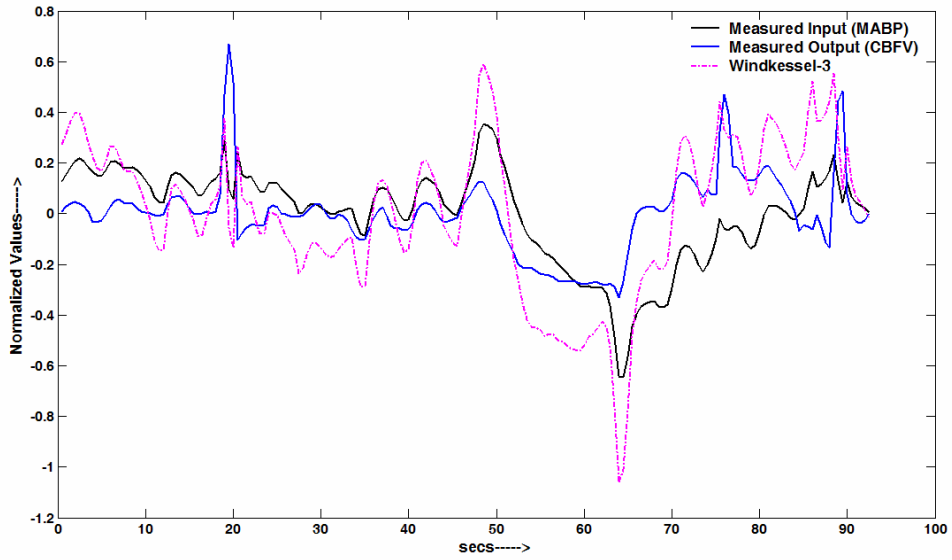

Figure 3.95 Plot of the output for Model 1 with Windkessel-3 modeling scheme for VI data of subject no. 2

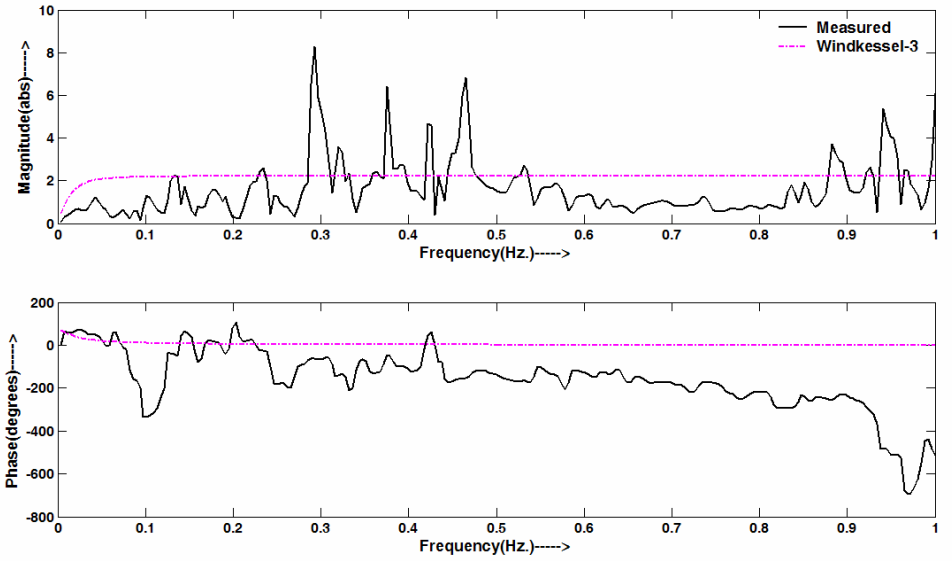

Figure 3.96 Plot of the frequency response for Model 1 with Windkessel-3 modeling scheme for VI data of subject no. 2

3.3 Modeling Results for CPP and CBFV Data

This section presents the results of applying 3-element Windkessel model (Model 1) with Windkessel-1 modeling scheme to CPP and CBFV data taken as the measured input and output respectively, for VNI and VI conditions for all 10 subjects. Table 3.60 shows the MSE values of 10 subjects for the same. Table 3.61 shows the average parameter values for Model 1. Table 3.62 presents the comparison based on t-tests (P_{val}) for the MSE values of 10 subjects for VNI and VI data conditions, between MABP-CBFV and CPP-CBFV results, both analyzed using Windkessel-1 modeling scheme for Model 1. The statistical level of significance for the t-tests was selected to be 0.05. Figure 3.97 illustrates the model output plot and Figure 3.98 shows the frequency response of the model for one subject.

Table 3.60 MSE values for VNI and VI data conditions of CPP-CBFV data of 10 subjects with Windkessel-1 modeling scheme for Model 1

Subject No.	VNI	VI
1	0.0184	0.0162
2	0.0354	0.0495
3	0.0140	0.0358
4	0.0272	0.0288
5	0.0162	0.0226
6	0.0824	0.0171
7	0.0829	0.0160
8	0.0259	0.0291
9	0.0197	0.0096
10	0.0168	0.0217
Average	0.0339	0.0246
STD	0.0265	0.0116

Table 3.61 Average parameter values for VNI and VI data conditions of CPP-CBFV data of 10 subjects with Windkessel-1 modeling scheme for Model 1

	R_1	R_2	C_1
VNI Average	3.2620	10.5894	24.0239
VNI STD	5.8253	7.6332	21.8810
VI Average	2.4657	17.4151	19.9499
VI STD	2.8540	29.5489	19.8028

Table 3.62 Comparison (t-test) of MSE values of 10 subjects for VNI and VI data conditions between MABP-CBFV and CPP-CBFV using Windkessel-1 modeling scheme for Model 1

	VNI	VI
P_{val}	0.607796	0.168638

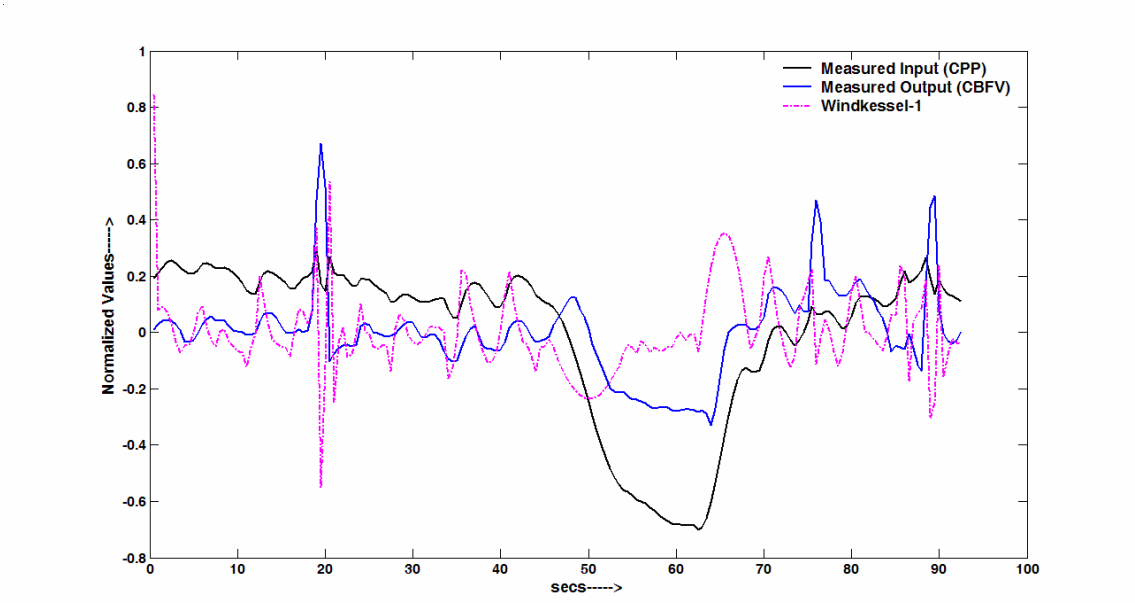

Figure 3.97 Plot of the output for Model 1 with Windkessel-1 modeling scheme for CPP-CBFV VI data of subject no. 2

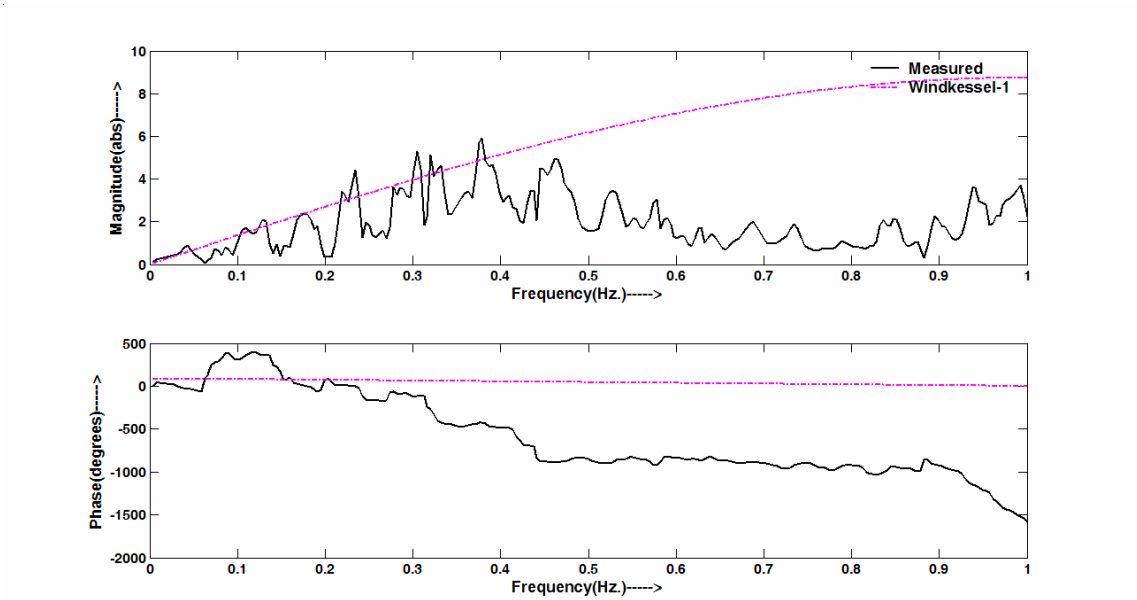

Figure 3.98 Plot of the frequency response for Model 1 with Windkessel-1 modeling scheme for CPP-CBFV VI data of subject no. 2

CHAPTER 4

DISCUSSION AND LIMITATIONS

This section presents the important implications and discussions for the results presented in chapter 3. Limitations to the present study have also been briefly described.

4.1 Discussion for the Results of Testing the Adequacy and Efficacy of 1.5 Minute MABP as Input Stimulus

4.1.1 ARX Models

Results from the present study show that for each of the 10 subjects, MSE values for M_a, M_{e1} and M_{e2} models equal for the 6 minutes study. Also, for each of the four 1.5 minute studies, the MSE values for M_a, M_{e1} and M_{e2} models were equal for a given subject. It should be noted that the models M_a, M_{e1} and M_{e2} for each of the 10 subjects did not necessarily have identical parameters or similar orders, as is reflected in Table 3.4. However, it is noted that the average order for models derived using MABP and PRBS are essentially the same, regardless of what data length (i.e. 6 or 1.5 minute) is used. It can be concluded that beat-to-beat MABP sequence is as effective as PRBS for parametric identification of linear models. Results in Table 3.1 show that MSE values for 1.5 minute duration studies are comparable with that of 6 minutes study. The

t-test results in Table 3.2 and Table 3.3 also suggest that temporal location of the four 1.5 minute sections from the 6 minutes data has no significance. This is based on the observation that for all the cases the P_{val} is greater than the statistical level of significance (0.05). Hence, it is apparent that a segment of 1.5 minute duration of MABP is adequate for parametric system identification of cerebral autoregulation.

4.1.2 Monte-Carlo Simulation for Windkessel Models

This section discusses Windkessel-1 and Windkessel-2 modeling schemes on the basis of Monte-Carlo simulation results (estimated-parameters and MSE values) for the five models for both PRBS and MABP input. Comparing the two modeling techniques, the performance of Windkessel-2 scheme was apparently better than Windkessel-1 scheme, based on the average MSE values and comparison of true-parameters (M_a) and estimated-parameters (M_e). However, results from both schemes point that MABP sequence is as effective and efficient as PRBS for parametric identification of linear models, and also that 1.5 minute duration is adequate for the same.

4.1.2.1 Windkessel-1 Modeling Scheme

Results from the present study show that for Model 1, Model 2 and Model 4, the estimated parameters (M_e) were reasonably close to the parameters obtained for model M_a, using PRBS or MABP as input. This is also reflected in the histograms of true-parameter values and estimated parameter values for the resistance parameter R_1 for each of these three models. For both PRBS and MABP input, the resistance parameter R_1 of Model 3 and Model 5 were poorly estimated, which is reflected in their

corresponding true-parameter value and estimated-parameter value histograms. For the same reason the average MSE values for models 3 and 5 were poor and not comparable to the average MSE values of the other three models, as is shown in Table 3.10 and Table 3.16. However, this being the case for both MABP and PRBS input, the average MSE values for respective models in both cases (Table 3.10 and Table 3.16) are similar and comparable. Noting that both the PRBS and MABP were 1.5 minute duration sequences, it can be concluded that MABP sequence is as good as PRBS for parametric identification of linear models, and also that a duration of 1.5 minute is adequate for the same.

The poor estimates of the true-parameter value of R_1 in case of Model 3 and Model 5 for both PRBS and MABP can be explained from limitation of the Windkessel-1 modeling scheme. The basis of this scheme is the evaluating R_1 from the model transfer function, as explained in section 2.2.3.2. This type of approach of extracting R_1 by applying the limit of frequency ω tending to infinity to the modulus of the transfer function is an approximation, because the actual signal (MABP, CBFV) is the case of this study is sampled at 2 Hz (section 2.1.4). Hence the highest frequency point of the measured impedance curve, Z_m, is at only 1 Hz and not infinity, which may result in poor estimation of resistance parameter R_1, by extracting its value from that point (Equations 2.11, 2.12, and 2.13). This in turn is reflected by higher MSE values for the cases where R_1 is poorly estimated. Furthermore, this approximation technique is affected by presence of noise in the Z_m.

4.1.2.2 Windkessel-2 Modeling Scheme

Results from the present study show that for all the five models, the estimated parameters (M_e) were reasonably close to the true-parameters (M_a), for the PRBS as well as MABP input. This is also reflected in the histograms of true-parameter value and estimated parameter value for the resistance parameter R_1 for each of these three models. For both PRBS and MABP input, the M_a and M_a were exactly the same (up to the fourth place of the decimal) for Model 5, as is reflected in Table 3.21 and Table 3.27 and Figure 3.29, Figure 3.30, Figure 3.39, and Figure 3.40. Also, the average MSE values for the five models for both PRBS and MABP input (Table 3.22 and Table 3.28) are fairly close. Noting that both the PRBS and MABP were 1.5 minute duration sequences, it can be concluded that MABP sequence is as good as PRBS for parametric identification of linear models, and also that a duration of 1.5 minute is adequate for the same.

Apart from establishing the effectiveness and adequacy of 1.5 minute MABP sequence, the Monte-Carlo simulation results play an important role in establishing the effectiveness and accuracy of Windkessel models and modeling schemes. The simulation serves as an exhaustive test for the Windkessel estimation algorithms, testing the estimation techniques on a large number of randomly simulated parameters, with other factors, like the initial estimates for optimization routines, also being random.

4.2 Discussion of the Modeling Results for MABP and CBFV Data

This section discusses and compares the ARX-1, ARX-2, Windkessel-1, Windkessel-2, and Windkessel-3 modeling schemes on the basis of MSE values of 10 subjects for the four data conditions (i.e. SNI, SI, VNI, VI), and plots illustrated in section 3.2.2.

4.2.1 ARX Models

The ARX-1 modeling scheme results in average model orders of 8.5, 6.6, 5.9, and 4.2 for respectively the SNI, SI, VNI, and VI data sets (Table 3.30). It is important to note that for ARX-1 scheme and for 1st, 2nd, and 3rd order models of ARX-2 scheme, for subject no. 9, VI data (1.5 minute) the models produced unstable model outputs, as is reflected by the corresponding MSE values in Table 3.29, Table 3.31, Table 3.33, and Table 3.35. In the same context, the MSE value was lowest for the 1st order model and highest for the 3rd order model. This is also shown in Table 3.30 for ARX-1 scheme, where for subject no. 9, VI case, the best model among 1st to 10th order models turned out to be a 1st order model.

Even though the average MSE values for ARX-1 scheme are lower than 1st, 2nd, and 3rd order models of ARX-2 scheme, the MSE values for ARX-1 scheme (Table 3.29) are close to the MSE values produced by the 1st order model of ARX-2 modeling scheme (Table 3.31), and if the MSE value of the model for subject no. 9, VI case, is ignored for both ARX-1 and ARX-2 scheme, the MSE values are relatively close for ARX-1 scheme and all the three models of ARX-2 scheme. This, combined with the fact that in Table 3.30 one can find a number of models with orders 4 or less, implies

that for ARX estimation, the increase of the model order doesn't improve the MSE value substantially. Moreover, an increase in order and may deteriorate the MSE value, as in VI case of subject no. 9 for the present study.

4.2.2 Windkessel Models

From the results in Appendix B, it is clear that there is no significant difference between the MSE values produced by Windkessel-1, Windkessel-2 and Windkessel-3 modeling schemes for the four data conditions of 10 subjects, for each of the five models. This is based on the t-test comparisons of the three modeling schemes with each other for a given model, which resulted in P_{val} is greater than the statistical level of significance (0.05). However, in terms of the average MSE values of the five models for Windkessel-1 and Windkessel-2 modeling schemes and of Model 1 for Windkessel-3 modeling scheme (section 3.2.1.2), for a given model, Widkessel-2 scheme produced lower average MSE values than Windkessel-1 and Windkessel-3 schemes. It is important to note that within the five models for the four data conditions, the average MSE values were relatively close for all the five models, this being true for both Windkessel-1 and Windkessel-2 scheme. It is also relevant to mention that the average values of the weights W_t and W_f for the four data conditions (Table 3.59), corresponding to Windkessel-3 modeling scheme for Model 1, show that for achieving a lower MSE value in time domain, the algorithm tried to improve frequency domain response of the model to fit it better to the measured one. This inference is based on the result that the average value of weighing-parameter for frequency domain MSE (W_f)

was higher, and almost double the average value of weighing-parameter for the time domain MSE (W_t), for all the four data conditions.

Comparing MSE values for ARX-2 with Windkessel-1 and Windkessel-2 schemes for models with similar order, the results in Appendix B demonstrated significant difference in SNI data condition for Windkessel Model 2, Model 3, Model 4 and Model 5. This is based on the t-test results where P_{val} is smaller than the statistical level of significance (0.05). This is also reflected by the average MSE values for SNI data condition with Windkessel-1 and Windkessel-2 schemes for all the five models, which were higher than the ARX-2 scheme models of similar order for SNI data set. For rest of the ARX-2 scheme comparisons with the three Windkessel schemes, no significant level of difference was observed. Comparing the ARX-1 methodology with the Windkessel schemes, the average MSE values for SNI, SI and VNI data conditions for ARX-1 modeling technique were lower than the corresponding average MSE values of the three Windkessel modeling schemes for all the five models.

4.2.3 Graphical Validation

Section 3.2.2 presented samples of the time-domain output and frequency response plots as good and poor results based on MSE value of the Windkessel-1 methodology in each model and type of data condition. Visually observing the plots for good results in section 3.2.2.1, Figure 3.41 shows that Model 1 for both Windkessel-1 and Windkessel-2 scheme followed the measured output of SNI data for subject no. 9 pretty well. In terms of frequency response, Windkessel-1 scheme matched the measured magnitude response better than Windkessel-2 scheme, and as is expected,

Windkessel-1 scheme magnitude almost meets the measured magnitude response curve at the highest frequency point of 1 Hz. For the same subject and data condition, ARX-1 and ARX-2 plots in Figure 3.43 were also quite comparable to each other, as well as to both of the Windkessel plots in Figure 3.41. But ARX-1 scheme produces a better frequency response comparable to measured one (Figure 3.44), which may be due to higher order models associated with ARX-1 scheme. In Figure 3.45, for VI data of subject no. 3, Model 2 for both the Windkessel schemes produces a good fit of the measured output. For the same subject and data condition, the two ARX schemes in Figure 3.47 did not follow the measured output as well as the Windkessel schemes. It is important to note here that Windkessel schemes had a magnitude response which matched the measured response better at the low frequencies (0.0 – 0.2 Hz), as seen in Figure 3.46, and ARX schemes produced a magnitude response which matched the measured one better at the high frequencies (0.6 – 1.0 Hz), as seen in Figure 3.48. Figure 3.49 shows how the Model 3 for the two Windkessel schemes followed the measured output for VNI data of subject no. 1. For the same subject and data condition, the two ARX schemes in Figure 3.51 followed the low-frequency changes better, including the high peaks and the low dips of the measured output. This is somewhat evident from the comparison of the magnitude responses of Windkessel schemes in Figure 3.50 and ARX schemes in Figure 3.52. Figure 3.53 and Figure 3.55 illustrate the model outputs of Model 4 for Windkessel schemes and of 3^{rd} order model for ARX-2 scheme respectively, for SNI data of subject no. 9. It is worthwhile to note that the responses in both these figures are comparable to the responses of Figure 3.41 and

Figure 3.43, for the same subject and data condition; however the model in the latter case is lower in order and number of elements than the model in the former case, for the ARX-2 and both of the Windkessel schemes. Also, the frequency responses of the two cases are quite similar. A similar observation can be made while comparing the Figure 3.45 with Figure 3.57, and Figure 3.47 with Figure 3.59, for VI data of subject no. 3. Model 5 in Figure 3.61 for VI data of subject no. 3 followed the measured output better in case of Windkessel-1 scheme. The difference in the magnitude response at low frequencies (0.0 – 0.1 Hz) of the two Windkessel schemes in Figure 3.62 is prominent. The two ARX schemes in Figure 3.63 could not perform as good as the Windkessel schemes.

Visually observing the plots for poor results in section 3.2.2.2, Model 1 for both Windkessel schemes in Figure 3.65 failed to follow the measured output for VI data of subject no. 2. Also, the model frequency responses for same in Figure 3.66 did not match the measured response. For the same subject and data condition, ARX-1 modeling scheme in Figure 3.67 produced a better result, which also is evident from the frequency response of ARX-1 model in Figure 3.68. Figure 3.69 shows that Model 2 for Windkessel-1 scheme had a comparatively better result than Windkessel-2 scheme, for SNI data of subject no. 5; this can also be seen in the magnitude response of Windkessel-1 scheme in Figure 3.70. For the same subject and data condition, both ARX-1 and ARX-2 modeling scheme in Figure 3.71 produced a superior result than Windkessel schemes. A similar observation can be made for the Windkessel results for Model 3 in Figure 3.73 and ARX results in Figure 3.75, for VNI data of subject no. 6.

Figure 3.77 and Figure 3.79 for SNI data of subject no. 5 shows that going to a higher order and higher element model did not produce any improvements in the model fit to the measured data, as compared to Figure 3.69 and Figure 3.71 respectively for the same subject and data condition. Likewise, a similar observation can be made while comparing the Windkessel results for Model 4 for VI data of subject no. 2 in Figure 3.81 and for Model 1 in Figure 3.65, for the same subject and data condition. Figure 3.85 shows that Model 5 for Windkessel-1 scheme had a comparatively better result than Windkessel-2 scheme, for VNI data of subject no. 6. For the same subject and data condition, both ARX-1 and ARX-2 modeling scheme in Figure 3.87 produced a superior result than Windkessel schemes. Figure 3.89 for VI data of subject no. 2 shows no improvements for Model 5 with Windkessel schemes, as compared to Figure 3.65 and Figure 3.81. Again, both ARX schemes in Figure 3.91 produced better results for the same subject and data condition. Plot for Model 1 with Windkessel-3 modeling scheme in Figure 3.93 has no significant difference as compared to Windkessel-1 and Windkessel-2 schemes in Figure 3.41 and Figure 3.53. However, Model 1 with Windkessel-3 scheme in Figure 3.95 for VI data of subject no. 2 shows significant improvement when compared to Figure 3.65, Figure 3.81 and Figure 3.89.

From the MSE value comparisons and discussion of the plots, it is clear that in Windkessel schemes, Windkessel-1 modeling scheme is superior to Windkeseel-2 modeling scheme. The apparent reason for which is the magnitude response in case on Windkessel-1 scheme which is forced to the match the measured magnitude response curve, Z_m, by extracting the resistance parameter R_1 form Z_m and fixing its value by not

optimizing it. For results with Model 1, Windkessel-3 scheme seems promising in terms of graphical validation results, but the average MSE values for the four data conditions in this scheme is larger than Windkessel-1 and Windkessel-2 schemes for Model 1. Comparing the five Windkessel models, there was no significant difference in the MSE values for both Windkessel-1 and Windkessel-2 schemes (Appendix B). In the plots for good results where the model response followed the measured output closely, for the same subject and data condition higher element models produced no significant improvement. This was also the case when the model output did not follow the measured output well. The two ARX schemes are comparable to each other in terms of average MSE values and the proximity of the model output to the measured output, but are better than the Windkessel schemes in both the MSE results and the proximity of the model output to the measured output, ignoring the case for VI data of subject no. 9, where both the ARX schemes produced unstable models.

Comparing MSE values and parameter values of the data conditions with and without infusion (i.e. SNI vs. SI, VNI vs. VI) for the five Windkessel models with Windkessel-1 modeling scheme (Appendix B), it can be seen that there was no significant difference observed. Also, the comparison results of MSE values and parameter values of the data conditions with and without infusion for 1st order model with ARX-1 modeling scheme showed a lack of significance for most of the *p* values (Appendix B). The statistical level of significance for all of these results was taken as 0.05. These outcomes show that the blockade of autonomic neural activity by drug infusion in the measured data could not be reproduced by the models in their MSE and

parameter values of the models, even though the effect of blockade can be observed in the spontaneous (SNI, SI) as well as Valsalva maneuver (VNI, VI) conditions of the measured data (Figures 2.1 through 2.4) in terms of MABP and CBFV values and the four recognized Valsalva maneuver phases (section 2.1.3). This indicates that ganglion blockade did not have a noteworthy effect on the MSE and parameter values of the ARX and Windkessel models.

4.3 Discussion of the Modeling Results for CPP and CBFV Data

Table 3.60 presents the MSE values associated with Windlkessel-1 scheme of Model 1 for CPP-CBFV VNI and VI data of 10 subjects. Comparing the average MSE values with the corresponding average MSE values for MABP-CBFV data in Table 3.37, there was a slight deterioration in the average MSE value for VNI case of CPP-CBFV data, but the VI case showed improvement. However, results for the comparison (t-test) of CPP-CBFV and MABP-CBFV in Table 3.62 show a P_{val} greater than 0.05 for VNI and VI, indicating no significant level of difference for the two cases. Plot in Figure 3.97 for VI data of subject no. 2 shows no significant improvement when compared to Figure 3.65, Figure 3.81 and Figure 3.89. These results weaken the conjecture of using CPP-CBFV data for linear modeling of cerebral autoregulation to yield better results as compared to using MABP-CBFV data.

4.4 Limitations

All of the modeling methods discussed in the present study rely on the assumption that the dynamic autoregulatory mechanism can be approximated by a linear system, ignoring several nonlinearities, like those related to fluid flow. It has been assumed that the MABP and CBFV are correlated without taking into account any phase lag or feedback action between them. Another presumption is that the middle cerebral artery (MCA), where CBFV is measured, does not change its diameter. This presumption was important to this study as the TCD technique used measures velocity of blood flow in the MCA, rather than the volumetric or mass flow rate of blood in MCA. Also, regarding the measurement of MABP in finger using photoplethysmography technique, the arterial pressure waveforms in the finger may be different from that in the MCA due to pressure wave reflection and amplification in the peripheral vascular bed. With respect to the CPP-CBFV data, the estimation of CPP was done from the MABP data, whereas, to assess changes in CPP, MABP should be measured simultaneously with ICP and/or CVP. With respect to results from the present study, an important limitation is that for Windkessel models, different parameter values associated with the resistive (R), capacitive (C) and inductive (L) elements could result into similar and comparable MSE values. This indicates that these model parameters are not distinctive and unique.

CHAPTER 5

CONCLUSION AND DIRECTIONS FOR FUTURE WORK

5.1 Conclusions

The present study is focused on employing single input single output linear lumped parametric models (ARX and Windkessel) to beat-to-beat mean arterial blood pressure (MABP) considered as input to the model, and cerebral blood flow velocity (CBFV) considered as output of the model. For some models and modeling methodologies, the data consisted of cerebral perfusion pressure (CPP, estimated from MABP) and CBFV. The measurement of the data from the subjects was done while the subjects were performing Valsalva maneuver with and without the use of trimethaphan for ganglion blockade, the infusion of which essentially removes the autonomic neural activity. The main objective of this study was to examine the relative performance and limitations of the above mentioned linear modeling options and to demonstrate newer modeling methodologies for them. Another purpose of this study was to examine and establish the efficacy of beat-to-beat blood pressure time sequence in serving as an input stimulus, and to investigate the use of a short data segment of 1.5 minute changes in MABP for obtaining linear model estimation of cerebral autoregulation.

Results from chapter 3 and their discussion in chapter 4 suggest that linear system method for parametric identification of pressure-flow relationship of cerebral circulation is feasible. The models used for the present study had very simple and basic mechanisms and structures, but were still able to reproduce the measured data. Even though the modeling methodologies for the study were not restricted to lower order systems, and examined even 10^{th} ordered systems in case of ARX models and higher element models in case of Windkessel models, results indicate that lower order ARX models (1^{st}, 2^{nd}, and 3^{rd} order models for ARX-2 scheme) and 3-element Windkessel model (Model 1) may be adequate. Among the ARX and Windkessel methodologies, ARX modeling schemes produced superior results. Windkessel-1 modeling scheme turns out to be better than Windkeseel-2 modeling scheme. Also, for results with Model 1, Windkessel-3 scheme seems promising in terms of graphical validation results. The results of using CPP-CBFV data did not prove to be better than MABP-CBFV data results, for Model 1 with Windkessel-1 scheme. Comparing MSE values and parameter values of the data conditions with and without infusion (i.e. SNI vs. SI, VNI vs. VI) for the five Windkessel models with Windkessel-1 modeling scheme and for 1^{st} order model with ARX-1 modeling scheme, it can be seen that the ganglion blockade did not have a significant effect on the MSE and parameter values of the ARX and Windkessel models.

From the results of testing the adequacy and efficacy of 1.5 minute MABP as input stimulus by ARX models, it can be concluded that a data segment of 1.5 minute duration of changes in MABP is adequate for parametric system identification of

cerebral circulation. This conclusion is strengthened by the results for Monte-Carlo simulations of Windkessel models using Windkessel-1 and Windkessel-2 schemes with MABP and PRBS as inputs. Hence it is clear that a segment of 1.5 minute duration of MABP is effective and adequate for estimating linear models of cerebral autoregulation.

5.2 Directions for Future Work

Even though the various modeling methodologies employed in the present study were able to model the cerebral circulation data in conjunction with Valsalva maneuver for ganglion blockade, all of them were linear parametric modeling techniques. Hence it would be of interest for future investigation to determine if other modeling techniques involving non-parametric techniques, non-linear analysis or neural network modeling can improve the time-domain and frequency-domain response of the models. Also, the present study was limited to applying Windkessel-3 modeling scheme to Model 1 using CPP-CBFV data. Future work can involve applying this scheme to other models as well. Some other important points to be considered for future investigation of the MABP-CBFV data include analyzing the coherence levels of input and output, and residual analysis of the data and model to examine a feedback relationship between MABP and CBFV. Also, it would be of immense interest to quantitatively analyze the results for the parameters of various models in the present study to extract clinical findings and implications from them. This may be useful for identifying patients at risk for cerebrovascular events. Clearly, more number of subjects will be required for this type of study.

APPENDIX A

DATA ANALYSIS ALGORITHMS AND PROGRAMS

A1 Program Used for ARX-1 Modeling Scheme described in Section 2.2.1.1

```
% estimation of model for system order from 1 to 10, and then selection of
% best model on the basis of MSE
subname =
{'Brian','Dak','Danial','Danny','Fennig','Janet','Ronnie','Sandra','Steve','Vineet'}
;  % subject files
addfix={'abpcbfv_sni','abpcbfv_si','abpcbfv_vni','abpcbfv_vi'}; % data
condition
subcase_vni=[1,1,1,2,1,2,2,2,2,3];
subcase_vi= [3,3,1,4,4,1,2,4,3,3];
h=waitbar(0,'Please wait.....')
for ct=1:4
   for vr1 =  1:10
      waitbar(((10*(ct-1))+vr1)/40,h);
      vr2=char(strcat(subname(vr1),addfix(ct)));
      if (ct==3)
         vr2=strcat(vr2,num2str(subcase_vni(vr1)));
      end
      if (ct==4)
         vr2=strcat(vr2,num2str(subcase_vi(vr1)));
      end
      a1=load (strcat(vr2,'rsmp.m'),'-ascii');
      u1=dtrend(a1(:,2));
      u1_=u1./(max(u1)-min(u1)); % MABP
      v2=0;
      for var1=1:length(a1(:,1))
         v2(var1,1)=0.1257*a1(var1,1);
      end
      v1=dtrend(v2);
      v2_=v1./(max(v1)-min(v1)); % CBFV
      z1 = [v2_ u1_];
      par=0;
      ctr=0;
      for no = 2:11 % numerator order
         for do = 1:10 % denominator order
            if (no-1) <= do
               ctr=ctr+1;
               th2=arx(z1,[do,no,0]); % ARX identification
               th1=sett(th2,0.5);
               [NUM,DEN] = TH2TF(th1,1);
               tmp3=zeros(1,22);
```

A1 *Continued.*

```
                for tmp4=1:length(NUM)
                tmp3(1,tmp4+(11-length(NUM)))=NUM(1,tmp4);
              end
              for tmp4=1:length(DEN)
                tmp3(1,tmp4+(22-length(DEN)))=DEN(1,tmp4);
              end
              par(ctr,1:22)=tmp3;
            end
          end
        end
      % calculation of MSE values for model for system order from 1 to 10 for
      the subject for selection of best model
        ctr=0;
        mse=0;
        tmp5=par;
        for no = 2:11
          for do = 1:10
            if (no-1) <= do
              ctr=ctr+1;
              n(1,1:11)=tmp5(ctr,1:11);
              d(1,1:11)=tmp5(ctr,12:22);
              tmp1=0;
              for tmp2=1:length(u1_)
                tmp1(tmp2,1)=tmp2*0.5;
              end
              P1=[tmp1 u1_];  % input to the simulink model
              Timespan=[0.5 length(u1_)/2];
              sim('ARX_analysis',Timespan);
              msetime=(sum((v2_(1:length(v2_),1)-
             v1_(1:length(v1_),1)).^2))/length(v1_);
              mse(ctr,1)=msetime;
            end
          end
        end
        mse1=min(mse);
        par1=tmp5(find(mse==mse1),:);
        save(strcat(vr2,'_ARX.m'),'par1','-ascii');
    end
end
close(h);
```

A2 Program Used for Monte-Carlo Simulation of Model 1 for Windkessel-1 Modeling Scheme with MABP (SNI) as Input described in Section 2.2.3.2 and Section 2.3.2

```
% Monte Carlo Simulation
subname =
{'Brian','Dak','Danial','Danny','Fennig','Janet','Ronnie','Sandra','Steve','Vineet'}
;  % subject files
rand('state',0);
h=waitbar(0,'Simulation in progress.....')
for itr=1:1:1000 % 1000 trial simulation
  waitbar(itr/1000)
  randm3=rand(1,1);
  vr1=round((randm3*9)+1); % random selection of subject SNI data
  between subjects 1-10
  vr2=char(strcat(subname(vr1),'abpcbfv_sni'));
  a1=load (strcat(vr2,'rsmp.m'),'-ascii');
  u1=dtrend(a1(:,2));
  u1_=u1./(max(u1)-min(u1)); % MABP
  tmp1=0;
  for tmp2=1:length(u1_)
     tmp1(tmp2,1)=tmp2*0.5;
  end
  P1=[tmp1 u1_];  % input to the simulink model
  Timespan=[0.5 length(u1_)/2];
  randm1=rand(3,1);
  Rs=(randm1(1,1)*7)+7; % parameter R1
  Rp=(randm1(2,1)*5)+3; % parameter R2
  Cap=(randm1(3,1)*4)+1; % parameter C1
  a=(Cap*Rs*Rp);
  b=(Rs+Rp);
  c=(Cap*Rp);
  sim('mcarlo_sim',Timespan);
  w=hanning(512);
  Syx=xcorr(v1_,u1_);
  Sxx=xcorr(u1_);
  Pmu1 = psd(Sxx,512,2,w,256);
  Pmv1 = psd(Syx,512,2,w,256);
  Suf=0;
  Svf=0;
```

A2 *Continued.*

```
    for k=1:length(Pmu1)
        Suf(k,1)=(Pmu1(k,1))^0.5;
        Svf(k,1)=(Pmv1(k,1))^0.5;
    end
    Z1m1 = Svf./Suf;
    for var1=1:256
        fr(var1,1)=2*(var1/512); % Fs = 2 Hz
    end
    Z1m=Z1m1(1:256,1); % measured impedance
    randm2=rand(2,1);
    % frequency-domain optimization
    Rs1a = 1/Z1m(256,1); % extraction of R1 from Z1m
    options=optimset('MaxFunEvals',1000000,'MaxIter',1000000,'TolFun',1.e-
    10,'TolCon',1.e-1,'TolX',1.e-10);
    x1=0;
    x1=fminimax(@optfun_olufsen3,[(randm2(1,1)*5)+3,(randm2(2,1)*4)+1]
    ,[],[],[],[],[3,1],[8,5],[],options,Z1m,Rs1a);
    x1(1,3)=x1(1,2);
    x1(1,2)=x1(1,1);
    x1(1,1)=Rs1a;
    % time-domain optimization
    options=optimset('MaxFunEvals',1000000,'MaxIter',1000000,'TolFun',1.e-
    10,'TolCon',1.e-1,'TolX',1.e-10);
    x=0;
    x=fminimax(@optfun_subjects4,[x1(1,2),x1(1,3)],[],[],[],[],[3,1],[8,5],[],
    options,u1_,v1_,Rs1a);
    y2=idsim(u1_,thc2thd(poly2th(1,[1/Rs1a 1/(x(1,2)*x(1,1)*Rs1a)],1,1,[1
    (x(1,1)+Rs1a)/(x(1,2)*x(1,1)*Rs1a)],1,0),0.5));
    mse1(itr,1)= (sum((y2(1:length(y2),1)-
    v1_(1:length(v1_),1)).^2))/length(v1_);     % storing the MSE value for
    time domain
    param1(itr,1)= Rs; % storing the true parameters for respective run
    param1(itr,2)= Rp;
    param1(itr,3)= Cap;
    param2(itr,1)= Rs1a; % storing the estimated parameters for respective
    run
    param2(itr,2)= x(1,1);
    param2(itr,3)= x(1,2);
end
close(h)
```

A2 *Continued.*

```
save true_parameters.m param1 -ascii
save estimated_parameters.m param2 -ascii
save mse_timedomain.m mse1 -ascii
save mse_freqdomain.m mse2 -ascii
% function used for frequency-domain optimization
%x1(1)=R2
%x1(2)=C1
function f = optfun_olufsen3(x1,Z1m,Rs1a)
for k=1:256
   w(k,1)=2*(k/512);
   Zw(k,1)=abs((1+i*(w(k,1)*x1(2)*x1(1)))/(x1(1)+Rs1a+i*(w(k,1)*x1(2)*
   Rs1a*x1(1))));
end
f = sum((Zw(1:256,1)-Z1m(1:256,1)).^2);
% function used for time-domain optimization
%x(1)=R2
%x(2)=C1
function f = optfun_subjects4(x,u1_,v1_,Rs1a)
y1=idsim(u1_,c2d(poly2th(1,[1/Rs1a 1/(x(2)*x(1)*Rs1a)],1,1,
[1 (x(1)+Rs1a)/(x(2)*x(1)*Rs1a)],1,0),0.5));
f = sum(((y1(1:length(y1),1)-v1_(1:length(v1_),1)).^2));
```

A3 Program Used for Monte-Carlo Simulation of Model 1 for Windkessel-2 Modeling Scheme with MABP (SNI) as Input described in Section 2.2.3.3 and Section 2.3.2

```
%Monte Carlo Simulation
subname =
{'Brian','Dak','Danial','Danny','Fennig','Janet','Ronnie','Sandra','Steve','Vineet'}
;  % subject files
rand('state',0);
h=waitbar(0,'Simulation in progress.....')
for itr=1:1:1000 % 1000 trial simulation
  waitbar(itr/1000)
  randm3=rand(1,1);
  vr1=round((randm3*9)+1); % random selection of subject SNI data
  vr2=char(strcat(subname(vr1),'abpcbfv_sni'));
  a1=load (strcat(vr2,'rsmp.m'),'-ascii');
```

A3 *Continued.*

```
u1=dtrend(a1(:,2));
u1_=u1./(max(u1)-min(u1)); % MABP
tmp1=0;
for tmp2=1:length(u1_)
   tmp1(tmp2,1)=tmp2*0.5;
end
P1=[tmp1 u1_];  % input to the simulink model
Timespan=[0.5 length(u1_)/2];
randm1=rand(3,1);
Rs=(randm1(1,1)*7)+7; % parameter R1
Rp=(randm1(2,1)*5)+3; % parameter R2
Cap=(randm1(3,1)*4)+1; % parameter C1
a=(Cap*Rs*Rp);
b=(Rs+Rp);
c=(Cap*Rp);
sim('mcarlo_sim',Timespan);
w=hanning(512);
Syx=xcorr(v1_,u1_);
Sxx=xcorr(u1_);
Pmu1 = psd(Sxx,512,2,w,256);
Pmv1 = psd(Syx,512,2,w,256);
Suf=0;
Svf=0;
for k=1:length(Pmu1)
  Suf(k,1)=(Pmu1(k,1))^0.5;
  Svf(k,1)=(Pmv1(k,1))^0.5;
end
Z1m1 = Svf./Suf;
for var1=1:256
  fr(var1,1)=2*(var1/512); % Fs = 2 Hz
end
Z1m=Z1m1(1:256,1); % measured impedance
randm2=rand(2,1);
% frequency-domain optimization
Rs1a = 1/Z1m(256,1); % extraction of R1 from Z1m
options=optimset('MaxFunEvals',1000000,'MaxIter',1000000,'TolFun',
1.e-10,'TolCon',1.e-1,'TolX',1.e-10);
x1=0;
```

A3 *Continued.*

```
  x1=fminimax(@optfun_olufsen3_2,[(randm2(1,1)*5)+3,(randm2(2,1)*4)+1]
  ,[],[],[],[],[],[3,1],[8,5],[],options,Z1m,Rs1a);
   x1(1,3)=x1(1,2);
   x1(1,2)=x1(1,1);
   x1(1,1)=Rs1a;
   % time-domain optimization
   options=optimset('MaxFunEvals',1000000,'MaxIter',1000000,'TolFun',
   1.e-  10,'TolCon',1.e-1,'TolX',1.e-10);
   x=0;
   x=fminimax(@optfun_subjects4_2,[x1(1,1),x1(1,2),x1(1,3)],[],[],[],[],
   [7,3,1],[14,8,5],[],options,u1_,v1_);
   y2=idsim(u1_,thc2thd(poly2th(1,[1/x(1,1) 1/(x(1,3)*x(1,2)*x(1,1))],1,1,[1
   (x(1,2)+x(1,1))/(x(1,3)*x(1,2)*x(1,1))],1,0),0.5));
   mse1(itr,1)= (sum((y2(1:length(y2),1)-
   v1_(1:length(v1_),1)).^2))/length(v1_);     % storing the MSE value for time
   domain
   param1(itr,1)= Rs; % storing the true parameters for respective run
   param1(itr,2)= Rp;
   param1(itr,3)= Cap;
   param2(itr,1)= x(1,1);  % storing the estimated parameters for respective run
   param2(itr,2)= x(1,2);
   param2(itr,3)= x(1,3);
end
close(h)
save true_parameters.m param1 -ascii
save estimated_parameters.m param2 -ascii
save mse_timedomain.m mse1 -ascii
save mse_freqdomain.m mse2 –ascii
% function used for frequency-domainoptimization
%x1(1)=R2
%x1(2)=C1
function f = optfun_olufsen3_2(x1,Z1m,Rs1a)
for k=1:256
    w(k,1)=2*(k/512);
    Zw(k,1)=abs((1+i*(w(k,1)*x1(2)*x1(1)))/(x1(1)+Rs1a+i*(w(k,1)*x1(2)*
    Rs1a*x1(1))));
end
f = sum((Zw(1:256,1)-Z1m(1:256,1)).^2);
```

A3 *Continued.*

```
% function used for time-domain optimization
%x(1)=R1
%x(2)=R2
%x(3)=C1
function f = optfun_subjects4_2(x,u1_,v1_)
y1=idsim(u1_,c2d(poly2th(1,[1/x(1) 1/(x(3)*x(2)*x(1))],1,1,
[1 (x(2)+x(1))/(x(3)*x(2)*x(1))],1,0),0.5));
f = sum(((y1(1:length(y1),1)-v1_(1:length(v1_),1)).^2));
```

A4 Program Used for Model 1 with Windkessel-3 Modeling Scheme described in Section 2.2.3.4

```
 subname =
{'Brian','Dak','Danial','Danny','Fennig','Janet','Ronnie','Sandra','Steve','Vineet'}
;  % subject files
addfix={'abpcbfv_sni','abpcbfv_si','abpcbfv_vni','abpcbfv_vi'};
subcase_vni=[1,1,1,2,1,2,2,2,2,3];
subcase_vi= [3,3,1,4,4,1,2,4,3,3];
h=waitbar(0,'Please wait.....')
for ct = 1:4
   for vr1 = 1:10
      waitbar(((10*(ct-1))+vr1)/40,h);
      vr2=char(strcat(subname(vr1),addfix(ct)));
      if (ct==3)
         vr2=strcat(vr2,num2str(subcase_vni(vr1)));
      end
      if (ct==4)
         vr2=strcat(vr2,num2str(subcase_vi(vr1)));
      end
      a1=load (strcat(vr2,'rsmp.m'),'-ascii');
      u1=dtrend(a1(:,2));
      u1_=u1./(max(u1)-min(u1)); % MABP
      v2=0;
      for var1=1:length(a1(:,1))
         v2(var1,1)=0.1257*a1(var1,1);
      end
      v1=dtrend(v2);
      v1_=v1./(max(v1)-min(v1)); % CBFV
```

A4 *Continued.*

```
w=hanning(512);
Syx=xcorr(v1_,u1_);
Sxx=xcorr(u1_);
Pmu1 = psd(Sxx,512,2,w,256);
Pmv1 = psd(Syx,512,2,w,256);
Suf=0;
Svf=0;
for k=1:length(Pmu1)
   Suf(k,1)=(Pmu1(k,1))^0.5;
   Svf(k,1)=(Pmv1(k,1))^0.5;
end
Z1m1 = Svf./Suf;
for var1=1:256
   fr(var1,1)=2*(var1/512); % Fs = 2 Hz
end
Z1m=Z1m1(1:256,1); % measured impedance
ctr=1;
for wgtime = 0.1:0.1:0.9 % weighting parameter for time MSE
   wgfreq = 1-wgtime; % weighing parameter for frequency MSE
   options=optimset('MaxFunEvals',1000000,'MaxIter',1000000,
   'TolFun',1.e-1,'TolCon',1.e-1,'TolX',1.e-1);
   x=0;
   x=fgoalattain(@freqtime_fun1,[10.6,5.4,3.3],[0,0],
   [wgtime,wgfreq],[],[],[],[],[0.01,0.01,0.01],[100,100,100],[],
   options,u1_,v1_,Z1m);
   y2=idsim(u1_,thc2thd(poly2th(1,[1/x(1,1) /(x(1,3)*x(1,2)*x(1,1))],1,1,
   [1 (x(1,2)+x(1,1))/(x(1,3)*x(1,2)*x(1,1))],1,0),0.5));
   mse_tmp1= (sum((y2(1:length(y2),1)-
   v1_(1:length(v1_),1)).^2))/length(v1_);
   if (ctr == 1)
      mse_tmp2 = mse_tmp1;
      wg1=[wgtime,wgfreq];
      par=[x(1,1) x(1,2) x(1,3)];
   elseif (mse_tmp1 < mse_tmp2)
      mse_tmp2 = mse_tmp1;
      wg1=[wgtime,wgfreq];
      par=[x(1,1) x(1,2) x(1,3)];
   end
```

A4 *Continued.*

```
          ctr=ctr+1;
        end
        x=par;
        y2=idsim(u1_,thc2thd(poly2th(1,[1/x(1,1) 1/(x(1,3)*x(1,2)*x(1,1))],1,1,
        [1 (x(1,2)+x(1,1))/(x(1,3)*x(1,2)*x(1,1))],1,0),0.5));
         mse1=(sum((y2(1:length(y2),1)-v1_(1:length(v1_),1)).^2))/length(v1_);
         % storing the MSE value for time domain
        wg(((ct-1)*10)+vr1,:)=wg1; % storing the weights
        save(strcat(vr2,'_par.m'),'par','-ascii');
        save(strcat(vr2,'_msetimefreq.m'),'mse1','mse2','-ascii');
    end
end
save('weights_1.m','wg','-ascii');
close(h);
% function used for optimization
%x(1)=R1
%x(2)=R2
%x(3)=C1
function f = freqtime_fun1(x,u1_,v1_,Z1m)
for k=1:256
    w(k,1) = 2*(k/512);
    Zw(k,1) = abs((1+i*(w(k,1)*x(3)*x(2)))/(x(2)+x(1)
      +i*(w(k,1)*x(3)*x(1)*x(2))));
end
y1 = idsim(u1_,c2d(poly2th(1,[1/x(1) 1/(x(3)*x(2)*x(1))],1,1,[1
(x(2)+x(1))/(x(3)*x(2)*x(1))],1,0),0.5));
f = [sum(((y1(1:length(y1),1)-v1_(1:length(v1_),1)).^2)),
sum((Zw(1:256,1)-Z1m(1:256,1)).^2)];
```

APPENDIX B

COMPARISON OF MSE AND PARAMETER VALUES

Table B1 Comparison (t-test) of MSE values of 10 subjects for four data conditions between ARX-2 (1st order model) and Windkessel-1 (Model 1) modeling schemes

	SNI	SI	VNI	VI
P_{val}	0.795561	0.846517	0.528716	0.171701

Table B2 Comparison (t-test) of MSE values of 10 subjects for four data conditions between ARX-2 (2nd order model) and Windkessel-1 (Model 2) modeling schemes

	SNI	SI	VNI	VI
P_{val}	0.035873	0.380281	0.226517	0.343361

Table B3 Comparison (t-test) of MSE values of 10 subjects for four data conditions between ARX-2 (3rd order model) and Windkessel-1 (Model 3) modeling schemes

	SNI	SI	VNI	VI
P_{val}	0.043953	0.423494	0.371526	0.343403

Table B4 Comparison (t-test) of MSE values of 10 subjects for four data conditions between ARX-2 (3rd order model) and Windkessel-1 (Model 4) modeling schemes

	SNI	SI	VNI	VI
P_{val}	0.043953	0.423494	0.371526	0.343403

Table B5 Comparison (t-test) of MSE values of 10 subjects for four data conditions between ARX-2 (2nd order model) and Windkessel-1 (Model 5) modeling schemes

	SNI	SI	VNI	VI
P_{val}	0.009435	0.338753	0.303466	0.343577

Table B6 Comparison (t-test) of MSE values of 10 subjects for four data conditions between ARX-2 (1st order model) and Windkessel-2 (Model 1) modeling schemes

	SNI	SI	VNI	VI
P_{val}	0.882653	0.493889	0.537134	0.168465

Table B7 Comparison (t-test) of MSE values of 10 subjects for four data conditions between ARX-2 (2nd order model) and Windkessel-2 (Model 2) modeling schemes

	SNI	SI	VNI	VI
P_{val}	0.017622	0.926783	0.37839	0.342751

Table B8 Comparison (t-test) of MSE values of 10 subjects for four data conditions between ARX-2 (3rd order model) and Windkessel-2 (Model 3) modeling schemes

	SNI	SI	VNI	VI
P_{val}	0.093488	0.876214	0.658093	0.343373

Table B9 Comparison (t-test) of MSE values of 10 subjects for four data conditions between ARX-2 (3rd order model) and Windkessel-2 (Model 4) modeling schemes

	SNI	SI	VNI	VI
P_{val}	0.074718	0.928205	0.821422	0.343388

Table B10 Comparison (t-test) of MSE values of 10 subjects for four data conditions between ARX-2 (2nd order model) and Windkessel-2 (Model 5) modeling schemes

	SNI	SI	VNI	VI
P_{val}	0.036894	0.544073	0.494593	0.342687

Table B11 Comparison (t-test) of MSE values of 10 subjects for four data conditions between Windkessel-1 and Windkessel-2 modeling schemes for Model 1

	SNI	SI	VNI	VI
P_{val}	0.68782	0.464833	0.981423	0.805173

Table B12 Comparison (t-test) of MSE values of 10 subjects for four data conditions between Windkessel-1 and Windkessel-2 modeling schemes for Model 2

	SNI	SI	VNI	VI
P_{val}	0.649444	0.425047	0.856225	0.38808

Table B13 Comparison (t-test) of MSE values of 10 subjects for four data conditions between Windkessel-1 and Windkessel-2 modeling schemes for Model 3

	SNI	SI	VNI	VI
P_{val}	0.286579	0.48866	0.541137	0.416529

Table B14 Comparison (t-test) of MSE values of 10 subjects for four data conditions between Windkessel-1 and Windkessel-2 modeling schemes for Model 4

	SNI	SI	VNI	VI
P_{val}	0.193247	0.393005	0.815817	0.542089

Table B15 Comparison (t-test) of MSE values of 10 subjects for four data conditions between Windkessel-1 and Windkessel-2 modeling schemes for Model 5

	SNI	SI	VNI	VI
P_{val}	0.169342	0.691807	0.864143	0.359314

Table B16 Comparison (t-test) of MSE values of 10 subjects for four data conditions between ARX-2 (1^{st} order model) and Windkessel-3 (Model 1) modeling schemes

	SNI	SI	VNI	VI
P_{val}	0.297809	0.719612	0.95119	0.171572

Table B17 Comparison (t-test) of MSE values of 10 subjects for four data conditions between Windkessel-1 and Windkessel-3 modeling schemes for Model 1

	SNI	SI	VNI	VI
P_{val}	0.413835	0.87383	0.509365	0.996521

Table B18 Comparison (t-test) of MSE values of 10 subjects for four data conditions between Windkessel-2 and Windkessel-3 modeling schemes for Model 1

	SNI	SI	VNI	VI
P_{val}	0.24869	0.396462	0.516817	0.664909

Table B19 Comparison (t-test) of MSE values of 10 subjects between infusion and no-infusion data conditions for Model 1 with Windkessel-1 modeling scheme

	SNI-SI	VNI-VI
P_{val}	0.763949	0.288703

Table B20 Comparison (t-test) of R_1 parameter values of 10 subjects between infusion and no-infusion data conditions for Model 1 with Windkessel-1 modeling scheme

	SNI-SI	VNI-VI
P_{val}	0.393828	0.288282

Table B21 Comparison (t-test) of R_2 parameter values of 10 subjects between infusion and no-infusion data conditions for Model 1 with Windkessel-1 modeling scheme

	SNI-SI	VNI-VI
P_{val}	0.757161	0.656618

Table B22 Comparison (t-test) of C_1 parameter values of 10 subjects between infusion and no-infusion data conditions for Model 1 with Windkessel-1 modeling scheme

	SNI-SI	VNI-VI
P_{val}	0.69311	0.681824

Table B23 Comparison (t-test) of MSE values of 10 subjects between infusion and no-infusion data conditions for Model 2 with Windkessel-1 modeling scheme

	SNI-SI	VNI-VI
P_{val}	0.730341	0.325159

Table B24 Comparison (t-test) of R_1 parameter values of 10 subjects between infusion and no-infusion data conditions for Model 2 with Windkessel-1 modeling scheme

	SNI-SI	VNI-VI
P_{val}	0.393828	0.288282

Table B25 Comparison (t-test) of R_2 parameter values of 10 subjects between infusion and no-infusion data conditions for Model 2 with Windkessel-1 modeling scheme

	SNI-SI	VNI-VI
P_{val}	0.978729	0.153842

Table B26 Comparison (t-test) of R_3 parameter values of 10 subjects between infusion and no-infusion data conditions for Model 2 with Windkessel-1 modeling scheme

	SNI-SI	VNI-VI
P_{val}	0.978581	0.153842

Table B27 Comparison (t-test) of C_1 parameter values of 10 subjects between infusion and no-infusion data conditions for Model 2 with Windkessel-1 modeling scheme

	SNI-SI	VNI-VI
P_{val}	0.430827	0.727742

Table B28 Comparison (t-test) of C_2 parameter values of 10 subjects between infusion and no-infusion data conditions for Model 2 with Windkessel-1 modeling scheme

	SNI-SI	VNI-VI
P_{val}	0.430826	0.727007

Table B29 Comparison (t-test) of MSE values of 10 subjects between infusion and no-infusion data conditions for Model 3 with Windkessel-1 modeling scheme

	SNI-SI	VNI-VI
P_{val}	0.938366	0.802229

Table B30 Comparison (t-test) of R_1 parameter values of 10 subjects between infusion and no-infusion data conditions for Model 3 with Windkessel-1 modeling scheme

	SNI-SI	VNI-VI
P_{val}	0.393828	0.288282

Table B31 Comparison (t-test) of R_2 parameter values of 10 subjects between infusion and no-infusion data conditions for Model 3 with Windkessel-1 modeling scheme

	SNI-SI	VNI-VI
P_{val}	0.568589	0.390295

Table B32 Comparison (t-test) of C_1 parameter values of 10 subjects between infusion and no-infusion data conditions for Model 3 with Windkessel-1 modeling scheme

	SNI-SI	VNI-VI
P_{val}	0.764379	0.964158

Table B33 Comparison (t-test) of C_2 parameter values of 10 subjects between infusion and no-infusion data conditions for Model 3 with Windkessel-1 modeling scheme

	SNI-SI	VNI-VI
P_{val}	0.304284	0.620317

Table B34 Comparison (t-test) of L_1 parameter values of 10 subjects between infusion and no-infusion data conditions for Model 3 with Windkessel-1 modeling scheme

	SNI-SI	VNI-VI
P_{val}	0.550687	0.455087

Table B35 Comparison (t-test) of MSE values of 10 subjects between infusion and no-infusion data conditions for Model 4 with Windkessel-1 modeling scheme

	SNI-SI	VNI-VI
P_{val}	0.855139	0.204928

Table B36 Comparison (t-test) of R_1 parameter values of 10 subjects between infusion and no-infusion data conditions for Model 4 with Windkessel-1 modeling scheme

	SNI-SI	VNI-VI
P_{val}	0.393828	0.288282

Table B37 Comparison (t-test) of R_2 parameter values of 10 subjects between infusion and no-infusion data conditions for Model 4 with Windkessel-1 modeling scheme

	SNI-SI	VNI-VI
P_{val}	0.257989	0.691529

Table B38 Comparison (t-test) of C_1 parameter values of 10 subjects between infusion and no-infusion data conditions for Model 4 with Windkessel-1 modeling scheme

	SNI-SI	VNI-VI
P_{val}	0.491042	0.52144

Table B39 Comparison (t-test) of C_2 parameter values of 10 subjects between infusion and no-infusion data conditions for Model 4 with Windkessel-1 modeling scheme

	SNI-SI	VNI-VI
P_{val}	0.310584	0.074284

Table B40 Comparison (t-test) of L_1 parameter values of 10 subjects between infusion and no-infusion data conditions for Model 4 with Windkessel-1 modeling scheme

	SNI-SI	VNI-VI
P_{val}	0.992003	0.834781

Table B41 Comparison (t-test) of MSE values of 10 subjects between infusion and no-infusion data conditions for Model 5 with Windkessel-1 modeling scheme

	SNI-SI	VNI-VI
P_{val}	0.12183	0.326871

Table B42 Comparison (t-test) of R_1 parameter values of 10 subjects between infusion and no-infusion data conditions for Model 5 with Windkessel-1 modeling scheme

	SNI-SI	VNI-VI
P_{val}	0.393828	0.288282

Table B43 Comparison (t-test) of R_2 parameter values of 10 subjects between infusion and no-infusion data conditions for Model 5 with Windkessel-1 modeling scheme

	SNI-SI	VNI-VI
P_{val}	0.408513	0.710861

Table B44 Comparison (t-test) of C_1 parameter values of 10 subjects between infusion and no-infusion data conditions for Model 5 with Windkessel-1 modeling scheme

	SNI-SI	VNI-VI
P_{val}	0.634658	0.7375

Table B45 Comparison (t-test) of L_1 parameter values of 10 subjects between infusion and no-infusion data conditions for Model 5 with Windkessel-1 modeling scheme

	SNI-SI	VNI-VI
P_{val}	0.269113	0.104187

Table B46 Comparison (t-test) of MSE values of 10 subjects between infusion and no-infusion data conditions for 1st order model with ARX-2 modeling scheme

	SNI-SI	VNI-VI
P_{val}	0.617352	0.163342

Table B47 Comparison (t-test) of a_1 parameter values of 10 subjects between infusion and no-infusion data conditions for 1st order model with ARX-2 modeling scheme

	SNI-SI	VNI-VI
P_{val}	0.583461	0.203746

Table B48 Comparison (t-test) of b_0 parameter values of 10 subjects between infusion and no-infusion data conditions for 1st order model with ARX-2 modeling scheme

	SNI-SI	VNI-VI
P_{val}	0.157702	0.01745

Table B49 Comparison (t-test) of b_1 parameter values of 10 subjects between infusion and no-infusion data conditions for 1st order model with ARX-2 modeling scheme

	SNI-SI	VNI-VI
P_{val}	0.090033	0.034714

REFERENCES

1. Ljung L., "System Identification: Theory for the User", 2nd Edition, Upper Saddle River, NJ: Prentice Hall PTR, 1999.
2. MATLAB User Manual (Release 13) ver. 6.5, 2002.
3. Stuart Ira Fox, "Human Physiology", 6th Edition, McGraw-Hill, 1999.
4. Carter GC, Knapp CH, Nuttall AH, "Statistics of the Estimate of the Magnitude-Coherence Function", IEEE Transactions on Audio and Electro Acoustics, Vol. 21, no. 4, pp 388-389, 1973.
5. Carter GC, Knapp CH, Nuttall AH, "Estimation of the Magnitude-Squared Coherence Function via Overlapped Fast Fourier Transform Processing", IEEE Transactions on Audio and Electro Acoustics, Vol. 21, no. 4, pp 337-343, 1973.
6. Diehl RR, Linden D, Lücke D, Berlit P, "Phase Relationship between Cerebral Blood Flow Velocity and Blood Pressure: A Clinical Test of Autoregulation", Stroke 26: 1801-1804. 1995.
7. Panerai RB, Chacon M, Pereira R, Evans DH, "Neural Networks Modeling of Dynamic Cerebral Autoregulation Assessment and Comparison with Established Methods", Medical Engineering and Physics Vol. 26, pp 43-52, 2004.

8. Panerai RB, Dawson SL, Chacon Potter JF, “Linear and Non-linear Analysis of Human Dynamic Cerebral Autoregulation”, American Journal of Physiology, Heart Circulation Physiology, Vol. 277, pp 1089-1099, 1999.
9. Panerai RB, Eames PJ, Potter JF, “Variability of Time-domain Indices of Dynamic Cerebral Autoregulation”, Physiol. Meas. 24 (2003) 367-381.
10. Panerai RB, “Assessment of Cerebral Pressure Autoregulation in Humans – A Review of Measurement Methods”, Physiol. Meas. 19 (1998) 305-338.
11. Behbehani K, Zhang R, Peng Q, and Levine BD, “Parametric and Non-Parametric Modeling of Spontaneous Cerebral Blood Flow Velocity Variations”, Biomedical Engineering Society 2001 Annual Fall Meeting, Oct. 4-7, 2001, Annals of Biomedical Engineering Vol. 29, Supplement 1, page S-79
12. Zhang R, Zuckerman JH, Giller CA, Levine BD, “Transfer Function Analysis of Dynamic Cerebral Autoregulation in Humans”, American Journal of Physiology, Vol. 274. Heart Circulation Physiology, 43, pp 233-241, 1998.
13. Zhang R, Zuckerman JH, Iwasaki K, Wilson TE, Crandall GC, Levine BD, “Autonomic Neural Control of Dynamic Cerebral Autoregulation in Humans”, Circulation. 2002; 106:1814-1820.
14. Zhang R, Behbehani K, Crandall CG, Zuckerman JH, Levine BD, “Dynamic Regulation of Heart Rate during Acute Hypotension: New Insight into Baroreflex Function”, American Journal of Physiology, Heart Circulation Physiology, Vol. 280, pp 407-419, 2001.

15. Aaslid R, Lash SR, Bardy GH, Gild WH, Newell DW, “Dynamic Pressure-Flow Velocity Relationships in Human Cerebral Circulation”, Stroke 2003;34:1645-1649.
16. Olufsen M, Tran H, Ottesen J, “Modeling Cerebral Blood Flow Control during Posture Change from Sitting to Standing”, Journal of Cardiovascular Engineering, Vol. $, No. 1, March 2004.
17. Olufsen M, “On Deriving Lumped Models for Blood Flow and Pressure in the Systemic Arteries”, Mathematical Biosciences and Engineering, Vol. 1, No. 1, June 2004.
18. Zhang R, Crandall CG, Levine BD, “Cerebral Hemodynamics During Valsalva Maneuver: Insights from Ganglion Blockade”, Stroke 2004;35:843-847.
19. Zhang R, Iwasaki K, Zuckerman J, Behbehani K, Crandall CG, Levine BD, “Mechanism of Blood Pressure and R-R Variability: Insights from Ganglion Blockade in Humans”, Journal of Physiology, 543.1, pp.337-348,2002.
20. Zhang R, Zuckerman J, Levine BD, “Deterioration of Cerebral Autoregulation during Orthostatic Stress: Insights from the Frequency Domain”, Journal of Applied Physiology, 1998.
21. Olufsen M, Nadim A, Lipsitz L, “Autoregulation of Cerebral Blood Flow”, IEEE Transactions on Biomedical Engineering, 2000.
22. Akaike H, “A New Look at the Statistical Model Identification”, IEEE Transactions on Automatic Control, December 1974.

23. Ursino M, Lodi CA, “A Simple Mathematical Model of the Interaction between Intracranial Pressure and Cerebral Hemodynamics”, Journal of Applied Physiology, 1997.
24. Ursino M, Giulioni M, Lodi CA, “Relationships among Cerebral Perfusion Pressure, Autoregulation, and Transcranial Doppler Waveform: A Modeling Study”, Journal of Neurosurgery, Vol. 89:255-266, 1998.
25. Dawson SL, Panerai RB, Potter JF, “Critical Closing Pressure Explains Cerebral Hemodynamics during Valsalva Maneuver”, Journal of Applied Physiology, 1999.
26. Greenfield JC, Rembert JC, Tindall GT, “Transient Changes in Cerebral Vascular Resistance during the Valsalva Maneuver in Man”, Stroke Vol. 15, No. 1, 1984.
27. Christini DJ, Bennett FM, Lutchen KR, Ahmed HM, Hausdroff JM, Oriol N, “Application of Linear and Nonlinear Time Series Modeling to Heat Rate Dynamics Analysis”, IEEE transactions on Biomedical Engineering, Vol. 42, No. 4, April 1995.
28. Tiecks FP, Douville C, Byrd S, Lam AM, Newell DW, “Evaluation of Impaired Cerebral Autoregulation by the Valsalva Maneuver”, Stroke 1996;27:1177-1182.
29. Pott F, Van Lieshout JJ, Ide K, Madsen P, Secher NH, “Middle Cerebral Artery Blood Velocity during a Valsalva Maneuver in the Standing Position”, Journal of Applied Physiology, 88:1545-1550,2000.

30. Tiecks FP, lam AM, Matta BF, Strebel S, Douville C, Newell Dw, “Effects of the Valsalva Maneuver on Cerebral Circulation in Healthy Adults”, Stroke, 1995;26:1386-1392.
31. Ling RYS, Clark JW, Srinivasan R, Cole JS, Pruett RC, “An Identification Scheme for the Determination of Systemic Arterial Load Parameters”, Technical Report #7507, Department of Electrical Engineering, Rice University, Houston Texas, U.S.A, April 1975.
32. Mandeville JB, Marota JJ, Ayata C, Zaharchuk G, Moskowitz MA, Rosen BR, Weisskoff RM, “Evidence of Cerebrovascular Postarteriole Windkessel with delayed Compliance”, Journal of Cerebral Blood Flow and Metabolism, 19:679-689, 1999.
33. Segers P, Brimioulle S, Stergiopulos N, Westerhof N, Naeije R, Maggiorini M, Verdonck P, “Pulmonary Arterial Compliance in Dogs and Pigs: The Three-Element Windkessel Model revisited”, Journal of Applied Physiology, 1999.
34. Grant BJB, Paradowski J, “Characterization of Pulmonary Arterial Input Impedance with Lumped Parameter Models”, Journal of Applied Physiology, 1987.
35. Fogliardi R, Donfrancesco MD, Burattini R, “Comparison of Linear and Nonlinear Formulations of the Three-Element Windkessel Models”, Journal of Applied Physiology, 1996.

36. Zhang S, Finkelstein SM, Cohn JN, “Verification of the Modified Windkessel Model of the Arterial Vasculature”, IEEE transactions on Biomedical Engineering, 1992.
37. Manning TS, Shykoff BE, Izzo JL, “Validity and Reliability of Diastolic Pulse Contour Analysis (Windkessel Model) in Humans”, Hypertension, 2002; 39:963-968.
38. Stergiopulos N, Westerhof BE, Westerhof N, “Total Arterial Inertance as the Fourth Element of the Windkessel Model”, Journal of Applied Physiology, 1999.
39. Crabtree V, Smith PR, “Physiological Models of the Human Vasculature and Photoplethysmography”, Electronic Systems and Control Division Research, 2003.
40. McvVeigh GE, Hamilton PK, Morgan DR, “Evaluation of Mechanical Arterial Properties: Clinical, Experimental and Therapeutic Aspects”, Clinical Science, 2002, 102:51-67.
41. Reinhard M, Roth M, Muller T, Czosnyka M, Timmer J, Hetzel A, “Cerebral Autoregulation in Carotid Artery Occlusive Disease Assessed From Spontaneous Blood Pressure Fluctuations by the Correlation Coefficient Index”, Stroke, 2003;34:2138-2144.

42. Novak V, Yang ACC, Lepicovsky L, Goldberger AL, Lipsitz LA, Peng CK, "Multimodal Pressure-Flow Method to Assess Dynamics of Cerebral Autoregulation in Stroke and Hypertension", BioMedical Engineering OnLine 2004, 3:39.
43. Kuo TBJ, Chern CM, Sheng WY, Wong WJ, Hu HH, "Frequency Domain Analysis of Cerebral Blood Flow Velocity and Its Correlation with Arterial Blood Pressure", Journal of Cerebral blood Flow and Metabolism, 1998;18:311-318.
44. Mathew AM, "Parametric Analysis of Cerebral Autoregulation", Project Report, Joint Biomedical Engineering Program, University of Texas at Arlington and University of Texas Southwestern Medical Center at Dallas, December 2003.

BIOGRAPHICAL INFORMATION

Piyush Gehalot was born in Dewas, a small town in Central India, on the 28th of May, 1980. He received his degree in Bachelor of Engineering in Electronics and Instrumentation Engineering from Institute of Engineering and Technology (I.E.T.), Indore, in May 2002. He then decided to pursue his graduate studies in the area of Biomedical Engineering at the University of Texas at Arlington, specializing in the track of Bioinstrumentation and Human Performance. His current research interests are in the area of Physiological System Modeling and Identification, Biomedical Signal Processing, Process Control and Image Processing. He looks forward to pursue his career in Biomedical Engineering research and development.